NASA CONTRACTOR REPORT

NASA CR-831

ANALYSIS AND DESIGN OF SPACE VEHICLE FLIGHT CONTROL SYSTEMS

VOLUME XII - ATTITUDE CONTROL IN SPACE

by Arthur L. Greensite

Prepared by
GENERAL DYNAMICS CORPORATION
San Diego, Calif.
for George C. Marshall Space Flight Center

NATIONAL AERONAUTICS AND SPACE ADMINISTRATION • WASHINGTON, D. C. • AUGUST 1967

NASA CR-831

ANALYSIS AND DESIGN OF SPACE VEHICLE FLIGHT CONTROL SYSTEMS

VOLUME XII - ATTITUDE CONTROL IN SPACE

By Arthur L. Greensite

Issued by Originator as GDC-DDE67-001

Prepared under Contract No. NAS 8-11494 by
GENERAL DYNAMICS CONVAIR
A DIVISION OF GENERAL DYNAMICS CORPORATION
San Diego, Calif.

for George C. Marshall Space Flight Center

NATIONAL AERONAUTICS AND SPACE ADMINISTRATION

For sale by the Clearinghouse for Federal Scientific and Technical Information
Springfield, Virginia 22151 – CFSTI price $3.00

FOREWORD

This report was prepared under NASA Contract NAS 8-11494 and is one of a series intended to illustrate methods used for the design and analysis of space vehicle flight control systems. Below is a complete list of the reports in the series:

Volume I	Short Period Dynamics
Volume II	Trajectory Equations
Volume III	Linear Systems
Volume IV	Nonlinear Systems
Volume V	Sensitivity Theory
Volume VI	Stochastic Effects
Volume VII	Attitude Control During Launch
Volume VIII	Rendezvous and Docking
Volume IX	Optimization Methods
Volume X	Man in the Loop
Volume XI	Component Dynamics
Volume XII	Attitude Control in Space
Volume XIII	Adaptive Control
Volume XIV	Load Relief
Volume XV	Elastic Body Equations
Volume XVI	Abort

The work was conducted under the direction of Clyde D. Baker, Billy G. Davis and Fred W. Swift, Aero-Astro Dynamics Laboratory, George C. Marshall Space Flight Center. The General Dynamics Convair program was conducted under the direction of Arthur L. Greensite.

TABLE OF CONTENTS

TABLE OF CONTENTS, Contd.

LIST OF ILLUSTRATIONS

LIST OF ILLUSTRATIONS, Contd.

LIST OF ILLUSTRATIONS, Contd.

LIST OF TABLES

1. STATEMENT OF THE PROBLEM

In its broadest sense, attitude control of a vehicle in space is sometimes taken to include vehicles on lunar or interplanetary trajectories as well as in planetary (earth) orbit. The present monograph is concerned exclusively with the attitude-control problem for a satellite in earth orbit. Attention is focused in particular on the analysis and synthesis of attitude control systems which satisfy well-defined objectives.

Satellite missions may be classified in various ways. One possible breakdown is the following:

a. Function
    1. communication and weather satellites
    2. orbiting telescopes
    3. manned space stations
b. Vehicle Configuration
    1. geometric shape
    2. elastic compliance
    3. spinning or nonspinning
    4. internal moving parts
c. Pointing Accurary
    1. fine; 0.05 - 0.10 degree
    2. moderate; 0.10 - 1.0 degree
    3. coarse; 1-5 degree
d. Control Philosophy
    1. active or passive
    2. single or multiple axis
    3. maneuvering capability
e. Actuators
    1. momentum exchange
    2. reaction (mass expulsion) devices

f. Sensors

1. inertial
2. sun and stellar trackers
3. horizon scanning

Once the mission function is established, the overall features of the vehicle configuration may be defined and this, together with the pointing accuracy required, serves to provide the basic information leading to control system synthesis. A system in which long lifetime and high reliability are paramount considerations would seem to dictate the use of a passive control system. However, for high pointing accuracy, the use of active controllers is mandatory. Furthermore, a lightweight structure is an obviously desirable goal, but this could compromise the control system stability. Many tradeoffs exist and no general rules can be given. Each system must be studied with regard to its own particular features and objectives. The decision process carries right on down to the lowest level. For example, if passive control has been decided upon, is it more advantageous to use gravity-gradient, earth magnetic, or radiation pressure techniques? If active techniques are used, is gyrotorquer control superior to flywheel control? Using gyrotorquer control, is a back-to-back configuration better than a single gyro unit? When using flywheels, is a bigger flywheel and lower speed preferable to a smaller flywheel at higher speed for a given momentum capability? The list is very large and considerable controversy still exists in many areas.

The aim of this monograph is to provide as unified a framework as possible for the analysis and synthesis of the attitude control system. While the details and objectives of specific systems will vary, there is nevertheless a common conceptual basis for mathematical treatment. This forms the main theme of the monograph.

2. STATE OF THE ART

The attitude control problem for a satellite in orbit differs in many essential respects from that of a body flying within the atmosphere. First of all, there are no aerodynamic forces available for stabilization and, second, in free fall it is not easy to establish a local vertical for reference — a condition which is taken for granted in terrestrial applications. Furthermore, for a satellite, the aims of attitude control are different from those of a body in the atmosphere. The purpose is not to change the path of the vehicle (this is already determined by the free-fall ballistic trajectory). Rather, attitude control is required generally to permit particular operations to be performed. In other words, prescribed attitude is to be maintained irrespective of the flight path in inertial space.

The first meaningful study of the problem was made by Esnault-Pelterie [52] in 1930 — at about the same time science fiction writers began to treat the theme. Except for a trickle of published papers, the problem was not further studied in any depth until Roberson and his co-workers began a detailed investigation in 1952, the results of which were published in 1960.[51] Because of the fact that by that time, a variety of satellite missions were already being envisioned, the number of published studies on the problem soon reached the proportions of a flood.

The satellite attitude control problem may be studied from two distinct, though related points of view: 1) developing the necessary theory and 2) designing the required hardware. On the theoretical side, several basic schemes for controlling the attitude of a body in inertial space suggested themselves. In the first place, it was long known that a spinning body will tend to maintain its attitude in force-free space. Furthermore, the principle of conservation of angular momentum led to the "momentum exchange" idea whereby, in the absence of externally applied torques, if one part of a closed system increased its momentum by a prescribed amount, the rest of the system "lost" an equal amount of momentum. An early implementation of this concept was the flywheel controller.[13] Similar devices acting on this principle are the gyrotorquer [6] and the integrating gyro.[53] Units of this type contain moving parts and require power, so that without supervision and maintenance, these are satisfactory only for short-lifetime missions. As a result so-called passive means of controlling attitude were investigated; these depend mainly on some sort of judicious interaction with the ambient environment. Schemes of this type employ gravity gradient, [54] the earth's magnetic field, [44] and/or solar radiation pressure. [55]

In order to control attitude, some means of sensing it must be provided. Some obvious choices are rate and displacement gyros, which are, however, useful only for short-duration missions, because of gyro drift. For accuracy and long duration, celestial line-of-sight devices have been developed, including star trackers [56] and

sun trackers.[36] The local vertical may be determined by specially designed horizon scanners.[57] A magnetometer [50] may be used in conjunction with magnetic attitude control.

At the present time, various satellites have already been launched or will be placed in orbit in the near future which are characterized by attitude control systems of varying degrees of sophistication.

Nimbus uses flywheels for three-axis vehicle control, with cold gas for removing initial rates and for flywheel desaturations. Horizon sensors give two-axis reference to the local vertical, and gyrocompassing provides yaw information. Sun sensors also provide auxiliary yaw information and solar array drive control.

The Orbiting Astronomical Observatory (OAO) has flywheels and cold gas similar to Nimbus. In addition, three iron-core coils provide magnetic torquing for flywheel desaturation. A second set of "coarse" flywheels is provided to give slewing control, starting them from rest and counting revolutions to determine the angle traversed, and stopping them at the desired position. Six star trackers give attitude reference information to ± 30 arc seconds. For finer control, control signals accurate to ± 0.1 arc seconds will be provided by the payload.

The Orbiting Solar Observatory (OSO) consists of a main body that is spin-stabilized and a non-spinning "sail." Nitrogen jets in the rotating section produce precessing torques to maintain the spin axis within 3 degrees of normal to the sun line. The sail is servoed about the spin axis to maintain continuous sun orientation; a second servo provides fine pointing of the instruments about the axis orthogonal to the sun line and the spin axis. This gives a two-axis pointing accuracy of 1 arc minute. A passive damper in the stabilized sail provides nutation damping.

The Advanced Orbiting Solar Observatory (AOSO) is a flywheel-stabilized vehicle with two axes referenced to the sun and the third to Canopus. Pointing anywhere within a 10-degree square centered on the sun is required, with accuracy of 5 arc seconds within a center 40 arc minute square. Flywheel desaturation is accomplished with cold gas jets.

The Orbiting Geophysical Observatory (OGO) has three-axis flywheel controls. Two axes are earth-referenced using IR sensors. Sun sensors control the third vehicle axis and the solar paddle drive. A separate control using a gyro in a gyrocompassing mode rotates an experiment package relative to the vehicle to maintain approximate velocity vector orientation. Argon gas is used for the mass-expulsion system.

Advanced Syncom is a spin-stabilized vehicle with its own axial "apogee motor" to adjust orbit eccentricity, period, and epoch. After this is accomplished the attitude control system performs the following tasks: 1) spin axis precession

normal to orbit plane, 2) maintenance of proper spin rpm, 3) station keeping, and 4) orbit inclination maintenance. This is accomplished by four hypergolic jets: two radial and two "axial" with a variable cant angle. Onboard sensors consist only of sun sensors. Spin maintenance is self-contained. All other functions are accomplished via ground command of the jets, pulsing each revolution or firing continuously as required. The antenna beam is derotated by suitably energizing the elements of the phased array.

The Applications Technology Satellite (ATS) is passively stabilized to the orbit plane and the local vertical. Four extendable rods in an "X" configuration give a stable configuration to gravity gradient and orbital rate rotation. Two additional rods are coupled to the vehicle, with a choice of either eddy current or hysteresis damping of the relative motion. It is one of the purposes of the mission to evaluate the relative merits of different dampers.

While many types of satellites have been proven to be operationally feasible, there remain a multitude of problems to be resolved on future configurations. In many cases, only the actual flight will establish either the severity of the problem or whether indeed there is any cause for concern at all. There is still some question regarding the effect of extraneous torque disturbances. It should be mentioned that the time profile of these disturbances is important as well as their magnitude. This is particularly true when the disturbances are cyclic.

Solar pressure exerts a secular torque in interplanetary trajectories and in some earth orbits. In most orbiting cases, solar pressure produces a cyclic torque not only because of the changing orientation of the vehicle, but also because of the day-night cycle.

Magnetic effects are likewise cyclic. Gravity-gradient torques may be either cyclic or secular depending on the vehicle's orientation.

Momentum of onboard equipment can arise from scanning sensors, tape recorders or other payload devices, and positioning drives such as for orienting antennas, solar panels, or directional payload sensors. In many cases the momentum due to servoed members can be cancelled by designing the drive motor and gear train to have momentum equal to that of the driven member but opposite in sign.

During low-level thrusting such as for station keeping of a synchronous satellite, the normal control system may be used to control the vehicle. Major perturbations in this case may arise from a shift of the vehicle c.g. and from fuel sloshing.

Release and pushoff of a landing capsule can produce sizable disturbances.

One of the most difficult perturbations to evaluate is the effect of crew motions within a manned vehicle. The disturbances that a man can produce in a given activity can be determined. The more difficult thing to determine is the disturbance that he will produce under orbital conditions while executing the same tasks. Likewise, the frequency or sequence of performing the various activities cannot be predicted with certainty.

Reset or desaturation of flywheels and gyros is a premeditated perturbation on the vehicle. Where precise attitude control is required it may be necessary to interlock the reset function with the data-taking cycle so as to ensure that a star picture, for instance, in OAO will not be blurred.

Particle impacts on the vehicle are generally considered to be a low-probability source of important vehicle perturbations.

Various other problems are expected to persist for some time. As noted earlier, only test data obtained under actual operating conditions will resolve most of them.

To date no direct way has been found of measuring the direction of the velocity vector in orbit. Gyrocompassing is reasonably satisfactory; however, its performance depends on an earth-oriented vehicle posture, with roll and pitch control properly operating.

Overall, the sun's brightness is an asset for optical devices rather than a hindrance. However, with some present types of devices solar impingement on surfaces in the field-of-view of the sensor can seriously affect sensor operation for sun angles as great as 90 deg from the boresight axis of the device. Even for sensors of types insensitive to sun interference (star trackers have been built that can track Polaris from the earth's surface in daylight) the sun may be on a direct line from the spacecraft to the earth or other object which it is desired to track.

Exhaust plumes from hot gas thrusters or cold gas nozzles alike have considerable divergence. As a result they present problems of contamination, temperature, erosion, or corrosion resulting from impingement of the plume on vehicle and optical surfaces. Satisfactory location of the nozzles may be difficult without sacrificing moment arm, resulting in increased fuel consumption. Where a large surface such as a solar panel moves through the plume, undesired vehicle torques may result.

As indicated earlier, gyro torquing rates and drift rates are expected to present a problem to the attitude control system designer.

Unmonitored operation of gyros and platforms is thus limited to short intervals. Likewise, lifetime of the gyro and power consumption are continuing problems. The continuing interest in unconventional gyros confirms this.

High accuracy in gimbal pickoffs is difficult to achieve. For applications like star trackers, even a pickoff with complex circuitry may add errors as great as those of the tracker itself.

In addition to hardware problems, the analytical aspects of attitude control assume awesome proportions for certain advanced configurations.

The effect of deployed masses nonrigidly coupled to the vehicle greatly complicate the problem, as does the consideration of structural elasticity effects. Computer simulation is not a simple answer. Programs of this sort take time to build, and problems that now exist can exceed the capacity of presently available computers.

In a more straightforward problem of vehicle stabilization when the vehicle reaches its operating orientation, it has been found that the only way to assure that it will stabilize from a given range of initial conditions is to run analog simulations covering the full range of all initial conditions. This can occupy weeks of computer runs and is necessitated by the fact that isolated combinations are found, from which stabilization is not possible.

Other problems peculiar to this field continually arise, such as the thermal deflection of a long extendable gravity-gradient rod, due to solar heating on one side.

In addition to the technical difficulties of simulating space conditions for testing attitude control systems (or even obtaining verification of key parameters) there is a major problem of facility availability, schedule problems, and in some cases a major increase in cost in carrying out the tests that are needed.

Air-bearing simulators, analog simulation, and the various partial tests that are feasible must be carried out with great care. Otherwise there may be surprises when the entire vehicle is assembled or, worse yet, after launch.

Reliability is of concern at both ends of the scale. For few-of-a-kind complex vehicles the cost of an unsuccessful launch or premature failure grows as the vehicles grow. On the other hand, operational systems, such as weather or communications satellites may require keeping spares in orbit to minimize outages. Thus, for even simple vehicles the savings for increased reliability are large.

Not only is achievement of reliability difficult; verifying that it has been achieved is also difficult.

In the way of future trends, it may be trite to mention the fact that sensors in general will be improved in performance and life. It is of interest to consider trends that can be expected.

Imaging tubes are ready for new uses, such as planet tracking, star field reference sensing, and planet limb sensing. The availability of ruggedized image orthicons will increase the number of special sensing tasks that can be accomplished. Image dissectors should also be used more often.

Unconventional gyros will no doubt begin to come into use, but the most significant developments will probably be the increased life of "present" types of gyros.

New IR horizon sensors will continue to appear, with improvements in detector elements and more advanced logic for ignoring cloud temperature variations. An important advance will be the better determination of the nature of the horizon as seen from a satellite. One of the results of detector developments will be the development of new types of passive sensors using detector mosaics.

More sophisticated optical correlation techniques will probably find application in attitude reference devices and tracking sensors. These may also be associated with lasers.

Momentum transfer devices will no doubt become more common and may include most of the devices now under development. Electric and nuclear thrusting devices are likely to come into use more slowly. There will probably be some interest in fluid logic devices for control system use.

Improved system techniques — on-off control logic, adaptive techniques, etc. — will improve the performance available with present kinds of expulsive actuators and also accommodate the microthrust engines which will be coming into use.

Passive techniques will also find greater application. Used in conjunction with active systems, they may permit the active control to go dormant during a long interplanetary cruise, or put the vehicle in trim to the summation of external forces. Performance of passive systems also will improve, increasing the types of missions for which they are satisfactory.

3. RECOMMENDED PROCEDURES

There are five main categories which demand attention in the design of an attitude control system for a satellite vehicle. These are:

1. Choice of reference axes
2. Development of equations of motion
3. Selection of sensors
4. Selection of actuators
5. Evaluation of disturbance torques

With the exception of item 3, all of these questions are treated in the sections which follow.* An attempt is made to present a unified point of view and a general framework within which a variety of specialized missions may be analyzed. The discussion emphasizes analytical tools and conceptual control philosophies, rather than the relative merits of competitive design techniques. However, necessary design data is presented where appropriate (Subsection 3.5), and the results of various numerical studies are summarized in Subsection 3.6.

3.1 COORDINATE REFERENCE FRAMES

Upon superficial examination, it would appear that the selection of appropriate reference frames for a satellite vehicle is rather straightforward. That such a view is deceptive can be made evident by consideration of two simple examples. First, consider the case of a reference frame which is aligned with the local vertical. This is a natural choice for a satellite vehicle which has a principal axis about which the moment of inertia is smaller than either of the other two principal moments of inertia. The gravity-gradient torque will tend to align this "long" axis with the gravity-gradient vector. However, with this choice of reference frame the gravity gradient at the satellite does not have a constant angular velocity in inertial space as the satellite moves along its orbit. This is true even for a circular orbit if the oblate-body effects of the planet are considered. Thus, control torques would have to be applied to give the satellite the necessary angular acceleration to keep up with the accelerating reference.

An even more awkward situation is encountered when the satellite contains internally moving parts. In this case, the equations of motion will include time-varying moments of inertia. From an analytical point of view this is a distressing state of

*A comprehensive treatment of the properties and selection of sensors for satellite attitude control is contained in Ref. 22. A brief discussion of these is presented in Appendix E.

affairs. Furthermore, the spurious torques thus introduced will require the application of control forces to maintain attitude. A thoughtful examination of this condition often leads to the choice of a reference frame which is reasonably optimal with respect to one or both of these factors. However, such a choice must, of necessity, be a compromise between conflicting requirements. These ideas will be clarified in the subsequent sections.

We define first a body coordinate system which is represented by the right hand unit vector triad ($\bar{i}_b$, $\bar{j}_b$, $\bar{k}_b$) whose origin is O. This body axis system will be assumed fixed to the satellite vehicle. We will also define a reference coordinate system represented by the right hand unit vector triad ($\bar{i}_r$, $\bar{j}_r$, $\bar{k}_r$) whose origin is coincident with that of the body coordinate system. The relative orientation between these two systems is described by three Euler angles, (ψ, θ, φ) as follows:

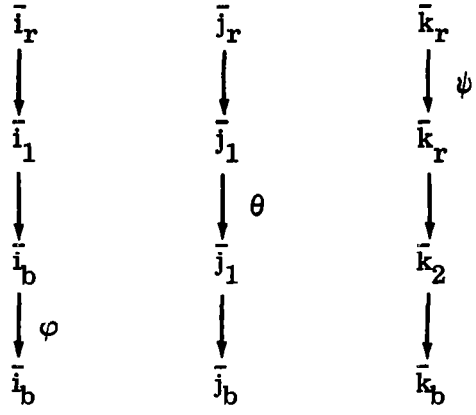

In words, the reference axis system is rotated about the $\bar{k}_r$ axis by a positive* amount, ψ, thereby defining a new axis system ($\bar{i}_1$, $\bar{j}_1$, $\bar{k}_r$). This is followed by a positive rotation about axis $\bar{j}_1$ of an amount, θ, and finally by a positive rotation of amount, φ, about axis $\bar{i}_b$. At the end of this rotation sequence, the reference frame is coincident with the body frame. The sequence is illustrated graphically in Fig. 1. From this we find that the components of a vector, $\bar{\rho}$, in the two frames are related by

$$\begin{bmatrix} x_b \\ y_b \\ z_b \end{bmatrix} = C_b^r \begin{bmatrix} x_r \\ y_r \\ z_r \end{bmatrix} \tag{1}$$

*In the sense of the right-hand rule.

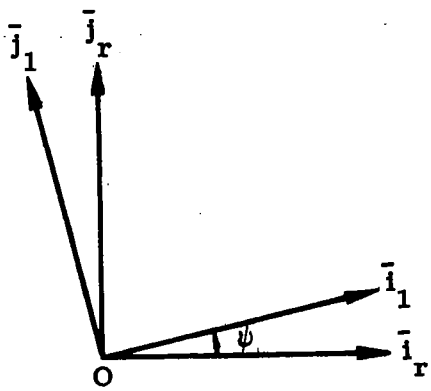

$$\begin{bmatrix} x_1 \\ y_1 \\ z_r \end{bmatrix} = \begin{bmatrix} c\psi & s\psi & 0 \\ -s\psi & c\psi & 0 \\ 0 & 0 & 1 \end{bmatrix} \begin{bmatrix} x_r \\ y_r \\ z_r \end{bmatrix}$$

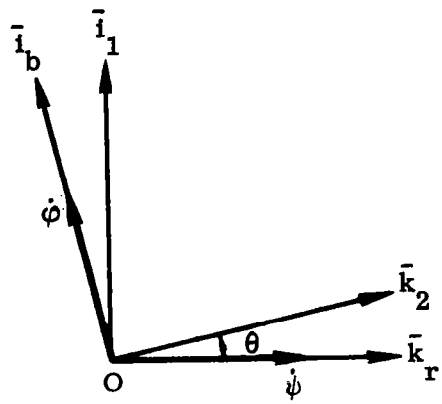

$$\begin{bmatrix} x_b \\ y_1 \\ z_2 \end{bmatrix} = \begin{bmatrix} c\theta & 0 & -s\theta \\ 0 & 1 & 0 \\ s\theta & 0 & c\theta \end{bmatrix} \begin{bmatrix} x_1 \\ y_1 \\ z_r \end{bmatrix}$$

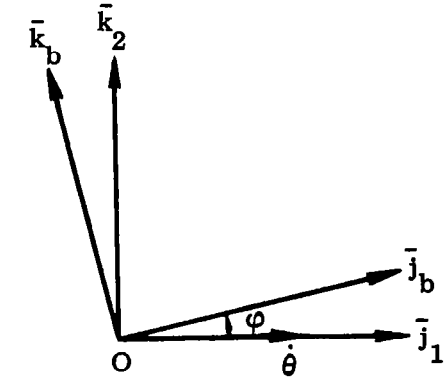

$$\begin{bmatrix} x_b \\ y_b \\ z_b \end{bmatrix} = \begin{bmatrix} 1 & 0 & 0 \\ 0 & c\varphi & s\varphi \\ 0 & -s\varphi & c\varphi \end{bmatrix} \begin{bmatrix} x_b \\ y_1 \\ z_2 \end{bmatrix}$$

(See footnote, p. 12)

Figure 1. Euler Angle Rotation Sequence

where

$$\bar{\rho} = x_b \bar{i}_b + y_b \bar{j}_b + z_b \bar{k}_b$$

$$= x_r \bar{i}_r + y_r \bar{j}_r + z_r \bar{k}_r$$

and C_b^r is the rotation matrix.*

$$C_b^r = \begin{bmatrix} c\theta c\psi & c\theta s\psi & -s\theta \\ s\varphi s\theta c\psi - c\varphi s\psi & s\varphi s\theta s\psi + c\varphi c\psi & s\varphi c\theta \\ c\varphi s\theta c\psi + s\varphi s\psi & c\varphi s\theta s\psi - s\varphi c\psi & c\varphi c\theta \end{bmatrix} \tag{2}$$

This is obtained by matrix multiplication of the three matrices shown in Fig. 1.

Note that

$$(C_b^r)^{-1} = (C_b^r)^T \equiv C_r^b \tag{3}$$

which is merely a statement of the fact that rotation matrices are orthogonal.

It should be emphasized that, in general, a change in the sequence of rotations will yield a different value for the rotation matrix. Only when the angles ψ, θ, and φ are assumed small is the sequence of performing the rotations immaterial.

The angular velocity of the body frame with respect to the reference frame is now written as

$$\bar{\omega}_b = p\bar{i}_b + q\bar{j}_b + r\bar{k}_b \tag{4}$$

where, by inspection of Fig. 1 (resolving the components of $\dot{\varphi}$, $\dot{\theta}$, and $\dot{\psi}$ along the indicated axes)

$$p = \dot{\varphi} - \dot{\psi}\sin\theta \tag{5}$$

$$q = \dot{\theta}\cos\varphi + \dot{\psi}\cos\theta\sin\varphi \tag{6}$$

$$r = \dot{\psi}\cos\theta\cos\varphi - \dot{\theta}\sin\varphi \tag{7}$$

These equations may be solved for $\dot{\varphi}$, $\dot{\theta}$, and $\dot{\psi}$ as follows:

$$\dot{\varphi} = p + (q\sin\varphi + r\cos\varphi)\tan\theta \tag{8}$$

*Hereafter, whenever convenient, we will write $s\theta$ for $\sin\theta$ and $c\theta$ for $\cos\theta$, etc.

$$\dot{\theta} = q\cos\varphi - r\sin\varphi \tag{9}$$

$$\dot{\psi} = (q\sin\varphi + r\cos\varphi)\sec\theta \tag{10}$$

The angular velocity of the reference coordinate frame with respect to inertial space will be denoted by $\bar{\omega}_r$. It is not necessary at this time to specify the precise orientation of the reference coordinate system with respect to the inertial frame. This can be done in many ways, and each particular problem will generally suggest the most convenient format. It is now possible to proceed with the development of the basic equations of motion of a satellite vehicle.

3.2 LAWS OF MOTION

The equations which describe the attitude motion of a satellite vehicle may be derived in a manner analogous to the classical problem of deriving the motion of a rigid body about a fixed point.[4] For the satellite, however, the situation is complicated by: 1) the fact that the body is not rigid (there are elements in the body which have motion relative to each other), 2) the point about which the motion is to be described is not fixed, and 3) there are a variety of extraneous forces which must be taken into account.

Various special cases of this general problem will be treated in the following subsections. These comprise the systems of greatest practical interest at the present time.

3.2.1 Rigid Body with Momentum-Exchange Devices

One of the most useful and practical means for controlling the attitude of an orbiting satellite vehicle is by momentum-exchange devices. The fundamental principle involved is that for any vehicle, the total external torque is equal to the rate of change of the total angular momentum of the vehicle. Thus, in the absence of any external torque, if the angular momentum of any part of the vehicle (the control element) is changed by some means, the angular momentum of the remainder of the vehicle will change by an equal and opposite amount. The change in angular momentum of the control element may be accomplished either by varying the speed of a flywheel (whose axis of rotation is fixed with respect to the vehicle), or by tilting the spin axis of a rotating flywheel with respect to the vehicle. The first method is usually called flywheel control while the second is called gyrotorquer control. Generally the gyrotorquer (also called control moment gyro) rotor has a constant speed of rotation.

Many configurations are possible utilizing these control philosophies. In order to exhibit the basic performance characteristics, we will consider a single-degree-of-freedom gyro located within the vehicle, as shown in Fig. 2. The body axis system is here denoted by (X_b, Y_b, Z_b). A gimbal coordinate system is fixed to the gyro gimbal (not the rotor) and is denoted by (X_G, Y_G, Z_G). The origins of the two

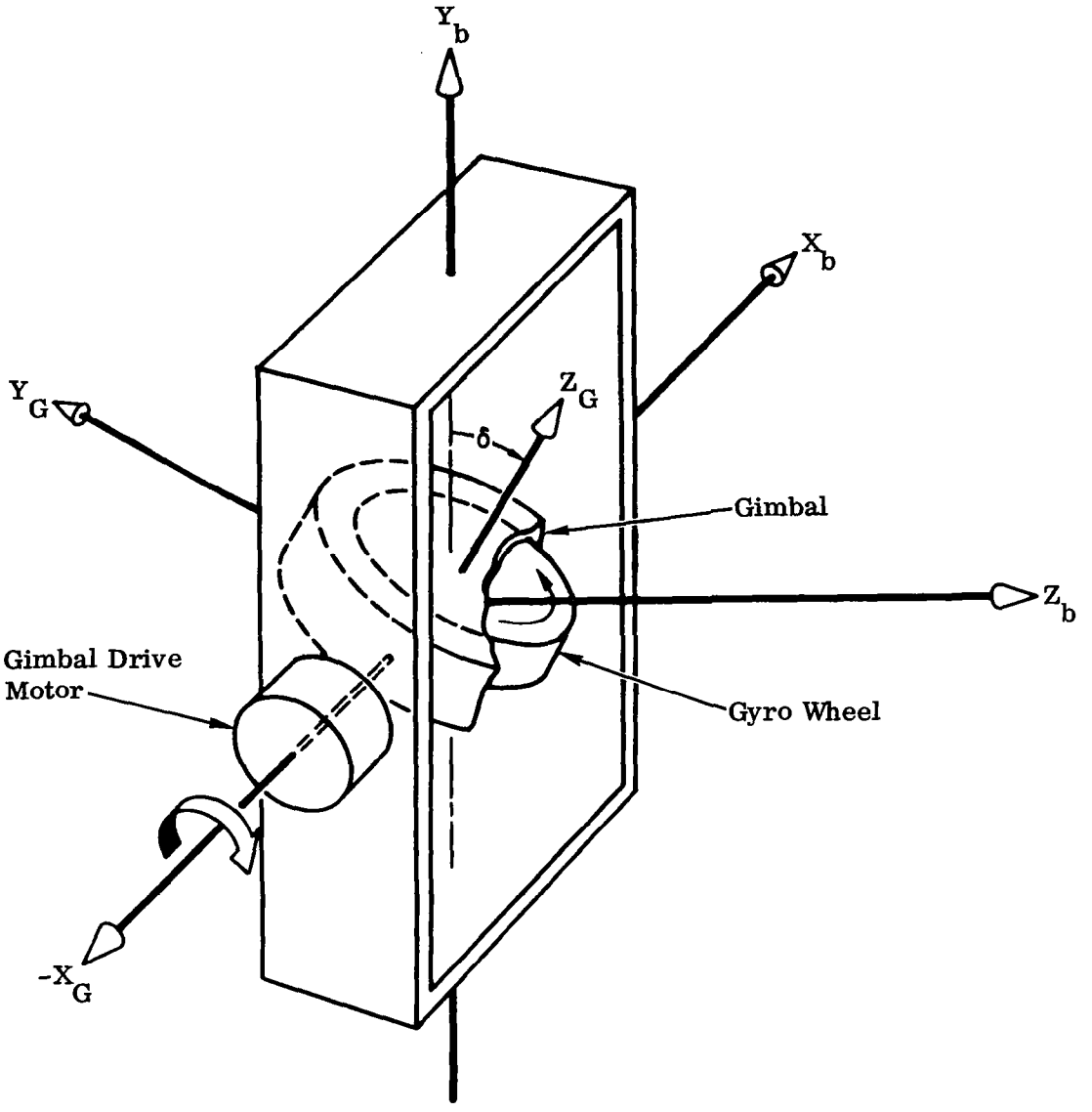

Figure 2. Configuration for Single-Degree-of-Freedom Gyro

coordinate frames are coincident, and, for simplicity, we assume that the gyro and vehicle mass centers are also at this origin. It is further assumed that the respective coordinate axes for each system are also the principal inertial axes for the vehicle and gyro respectively.

In dealing with a multiple gyro (or flywheel) system, it is convenient to have a uniform designation for the spin axis of each rotor. Therefore, we will always take the spin axis to be coincident with the Z_G axis, and with the vector direction of spin positive in the direction of positive Z_G (in the sense of the right-hand rule). The gyro degree of freedom (gimbal rotation) is represented by the angle, δ, which is taken to be positive when rotated about X_G in a positive sense.*

For the case shown in Fig. 2, the components of a vector in the body and gimbal coordinate frames are related by

$$\begin{bmatrix} x_G \\ y_G \\ z_G \end{bmatrix} = C_G^b \begin{bmatrix} x_b \\ y_b \\ z_b \end{bmatrix} \tag{11}$$

where

$$\bar{\rho} = x_G \bar{i}_G + y_G \bar{j}_G + z_G \bar{k}_G$$

$$= x_b \bar{i}_b + y_b \bar{j}_b + z_b \bar{k}_b$$

and where the rotation matrix is given by

$$C_G^b = \begin{bmatrix} 1 & 0 & 0 \\ 0 & s\delta & -c\delta \\ 0 & c\delta & s\delta \end{bmatrix} \tag{12}$$

Now the total angular momentum of the system about point O is

$$\bar{H} = \bar{H}_b + \bar{H}_g \tag{13}$$

Here

$$\bar{H}_b = I \cdot (\bar{\omega}_b + \bar{\omega}_r) \tag{14}$$

*Also in the sense of the right-hand rule.

$$\bar{H}_g = J \cdot (\bar{\omega}_g + \bar{\omega}_G + \bar{\omega}_b + \bar{\omega}_r) \tag{15}$$

$\omega_g \equiv$ angular velocity of gyro frame with respect to gimbal frame

$\omega_G \equiv$ angular velocity of gimbal frame with respect to body frame

where the second expression is obtained from Eq. (A16) of Appendix A. The quantity I is the inertia dyadic of the vehicle and may be written explicitly as

$$I = I_x \bar{i}_b \bar{i}_b + I_y \bar{j}_b \bar{j}_b + I_z \bar{k}_b \bar{k}_b \tag{16}$$

and J is the inertia dyadic of the rotor defined by Eq. (A11). There are no product-of-inertia terms since it was assumed that the body axes coincide with the principal inertial axes of the vehicle.

We may write Eq. (13) as

$$\bar{H} = (I + J) \cdot (\bar{\omega}_b + \bar{\omega}_r) + J \cdot (\bar{\omega}_g + \bar{\omega}_G)$$

In practical applications, $J \ll I$. Therefore, we may write the angular momentum as

$$\bar{H} = I \cdot (\bar{\omega}_b + \bar{\omega}_r) + J \cdot (\bar{\omega}_g + \bar{\omega}_G) \tag{17}$$

The equation of motion of the system is obtained by equating the external torques to the time derivative of the above expression, viz.

$$\frac{d}{dt}\left[I \cdot (\bar{\omega}_b + \bar{\omega}_r)\right] + \frac{d}{dt}\left[J \cdot (\bar{\omega}_g + \bar{\omega}_G)\right] = \bar{L} \tag{18}$$

In order to apply this equation for design purposes, it is necessary to expand it in some convenient fashion. This requires some care; we will therefore proceed in an organized fashion. We have first of all

$$\frac{d}{dt}\left[I \cdot (\bar{\omega}_b + \bar{\omega}_r)\right] = I \cdot \left[\left(\frac{\delta \bar{\omega}_b}{\delta t}\right)_b + \left(\frac{\delta \bar{\omega}_r}{\delta t}\right)_b\right]$$

$$+ (\bar{\omega}_r + \bar{\omega}_b) \times \left[I \cdot (\bar{\omega}_r + \bar{\omega}_b)\right] \tag{19}$$

Now the inertia dyadic, I, is expressed in components relative to the body frame as is the angular velocity vector, $\bar{\omega}_b$.* If, for sake of discussion, we assume that the

*See Eqs. (4) and (16).

vehicle is in a circular orbit such that the $\bar{i}_r$ axis is tangent to the orbital path and in the direction of travel (and with the $\bar{i}_r \bar{k}_r$ plane in the orbital plane), then the angular velocity of the reference frame with respect to inertial space is given by

$$\bar{\omega}_r = -\omega_o \bar{j}_r \tag{20}$$

By virtue of the relations, (1) - (3), we may express this in terms of its components in the body frame as follows

$$\bar{\omega}_r = -\omega_o c\theta s\psi \bar{i}_b - \omega_o(s\varphi s\theta s\psi + c\varphi c\psi)\bar{j}_b - \omega_o(c\varphi s\theta s\psi - s\varphi c\psi)\bar{k}_b \tag{21}$$

If the angles ψ, θ, φ, as well as the angular rate, ω_o, are assumed small, then the above expression reduces to

$$\bar{\omega}_r = -\omega_o \bar{j}_b \tag{22}$$

Using Eqs. (4), (16), and (22) to expand the right-hand side of Eq. (19), the latter becomes

$$\begin{aligned}\frac{d}{dt}\left[I \cdot (\bar{\omega}_b + \bar{\omega}_r)\right] = &\left[I_x \dot{p} + (q - \omega_o) r (I_z - I_y)\right]\bar{i}_b \\ &+ \left[I_y \dot{q} + pr(I_x - I_z)\right]\bar{j}_b \\ &+ \left[I_z \dot{r} + p(q - \omega_o)(I_y - I_x)\right]\bar{k}_b\end{aligned} \tag{23}$$

assuming that $\dot{\omega}_o = 0$. Note that when $\bar{\omega}_r$ is identically zero, we obtain the classical Euler equations of motion for a rigid body about a fixed point.

We now focus our attention on the second term on the left-hand side of Eq. (18). The expansion of this term will be conducted with reference to the situation depicted in Fig. 2. Applying the rule for the time derivative in the case of a rotating coordinate reference frame, we find

$$\begin{aligned}\frac{d}{dt}\left[J \cdot (\bar{\omega}_g + \bar{\omega}_G)\right] = &J \cdot \left[\left(\frac{\delta \bar{\omega}_g}{\delta t}\right)_G + \left(\frac{\delta \bar{\omega}_G}{\delta t}\right)_G\right] \\ &+ (\bar{\omega}_G + \bar{\omega}_b + \bar{\omega}_r) \times \left[J \cdot (\bar{\omega}_g + \bar{\omega}_G)\right]\end{aligned} \tag{24}$$

*Note that in this case $\bar{k}_r$ is pointed toward the earth's center.

In this case, it is convenient to express all vectors in terms of their components in the gimbal coordinate system. From Fig. 2, it is immediately apparent that*

$$\bar{\omega}_g = \Omega_y \bar{k}_G \tag{25}$$

$$\bar{\omega}_G = \dot{\delta}_y \bar{i}_G \tag{26}$$

Also, by virtue of the relations

$$\begin{bmatrix} x_G \\ y_G \\ z_G \end{bmatrix} = C_G^b \begin{bmatrix} x_b \\ y_b \\ z_b \end{bmatrix}$$

and

$$\begin{bmatrix} x_G \\ y_G \\ z_G \end{bmatrix} = C_G^b C_b^r \begin{bmatrix} x_r \\ y_r \\ z_r \end{bmatrix}$$

which follow from Eqs. (1) and (11), we find that $\bar{\omega}_b$ and $\bar{\omega}_r$ may be written as

$$\bar{\omega}_b = p\bar{i}_G + (qs\delta - rc\delta)\bar{j}_G + (qc\delta + rs\delta)\bar{k}_G \tag{27}$$

$$\bar{\omega}_r = -\omega_o\left[\ell_2 \bar{i}_G + (m_2 s\delta - n_2 c\delta)\bar{j}_G + (m_2 c\delta + n_2 s\delta)\bar{k}_G\right] \tag{28}$$

where for brevity, we have defined the quantities

$$\ell_2 = c\theta s\psi$$

$$m_2 = s\varphi s\theta s\psi + c\varphi c\psi$$

$$n_2 = c\varphi s\theta s\psi - s\varphi c\psi$$

*The set of gimbal-gyro parameters (Ω, δ, A, C) will hereafter contain the subscript x, y, or z to indicate that (in the steady state) the spin axis is along X_b, Y_b, or Z_b.

It is now a straightforward procedure to expand the right-hand side of Eq. (24). The end result is

$$\frac{d}{dt}\left[J \cdot (\bar{\omega}_g + \bar{\omega}_G)\right] = \left\{C_y\Omega_y\left[qs\delta_y - rc\delta_y - \omega_o(m_2 s\delta_y - n_2 c\delta_y)\right] + A_y\ddot{\delta}_y\right\}\bar{i}_G + \left\{A_y\dot{\delta}_y\left[qc\delta_y + rs\delta_y - \omega_o(m_2 c\delta_y + n_2 s\delta_y)\right] - C_y\Omega_y(\dot{\delta}_y + p - \omega_o\ell_2)\right\}\bar{j}_G + \left\{C_y\dot{\Omega}_y - A_y\dot{\delta}_y\left[qs\delta_y - rc\delta_y - \omega_o(m_2 s\delta_y - n_2 c\delta_y)\right]\right\}\bar{k}_G \qquad (29)$$

We now assume that the quantities ψ, θ, φ, and ω_o are small. In this event, the above expression reduces to

$$\frac{d}{dt}\left[J \cdot (\bar{\omega}_g + \bar{\omega}_G)\right] = \left[A_y\ddot{\delta}_y + C_y\Omega_y(qs\delta_y - rc\delta_y - \omega_o s\delta_y)\right]\bar{i}_G + \left[A_y\dot{\delta}_y(qc\delta_y + rs\delta_y - \omega_o c\delta_y - C_y\Omega_y(\dot{\delta}_y + p)\right]\bar{j}_G + \left[C_y\dot{\Omega}_y - A_y\dot{\delta}_y(qs\delta_y - rc\delta_y - \omega_o s\delta_y)\right]\bar{k}_G \qquad (30)$$

Now by transforming to components in the body frame via (11), we find

$$\frac{d}{dt}\left[J \cdot (\bar{\omega}_g + \bar{\omega}_G)\right] = \left[A_y\ddot{\delta}_y + C_y\Omega_y(qs\delta_y - rc\delta_y - \omega_o s\delta_y)\right]\bar{i}_b + \left[C_y\dot{\Omega}_y c\delta_y - c_y\Omega_y(\dot{\delta}_y + p)s\delta_y + A_y\dot{\delta}_y r\right]\bar{j}_b$$

$$+ \left[C_y \dot{\Omega}_y s\delta_y + C_y \Omega_y (\dot{\delta}_y + p) c\delta_y - A_y \dot{\delta}_y (q - \omega_o) \right] \bar{k}_b$$

$$\equiv -\bar{M}_y \tag{31}$$

This equation, together with (23) when combined with (18), gives the equation of motion of the vehicle with one gyro-gimbal unit mounted as shown in Fig. 2. The control is obtained by varying δ_y or Ω_y in some prescribed fashion.

For application to practical systems requiring three-axis attitude control, various gyro-gimbal configurations may be used. We will here consider two special cases:

1. Twin Gyrotorquer Unit on each body axis.
2. Flywheel Unit on each body axis.

The configuration for a twin gyrotorquer unit on the Y_b axis is shown in Fig. 3. The two gyro gimbals are geared together so as to be precessed by one motor. When facing each other, the gyros will be spinning in opposite directions. The lower gyro in Fig. 3 will have a rate of change of angular momentum given by Eq. (31), while for the upper gyro, it is apparent that its rate of change of angular momentum is given by Eq. (31) with the quantities δ_y, $\dot{\delta}_y$, $\ddot{\delta}_y$, Ω_y, $\dot{\Omega}_y$ replaced by $-\delta_y$, $-\dot{\delta}_y$, $-\ddot{\delta}_y$, $-\Omega_y$, $-\dot{\Omega}_y$, respectively. Adding these two expressions gives for the gyrotorquer unit

$$-\bar{M}_y = \left[2 C_y \Omega_y (q - \omega_o) \sin\delta_y \right] \bar{i}_b - \left[2 C_y \Omega_y p \sin\delta_y \right] \bar{j}_b$$
$$+ 2 C_y \left[\dot{\Omega}_y \sin\delta_y + \Omega_y \dot{\delta}_y \cos\delta_y \right] \bar{k}_b \tag{32}$$

With identical units placed on the other two body axes, it is readily found that the expression for the rate of change of angular momentum — obtained by expanding an equation of the form (31) about these body axes — is given by

$$-\bar{M}_x = -\left[2 C_x \Omega_x r \sin\delta_x \right] \bar{i}_b + 2 C_x \left[\dot{\Omega}_x \sin\delta_x + \Omega_x \dot{\delta}_x \cos\delta_x \right] \bar{j}_b$$
$$+ \left[2 C_x \Omega_x (p - \omega_o) \sin\delta_x \right] \bar{k}_b \tag{33}$$

$$-\bar{M}_z = 2 C_z \left[\dot{\Omega}_z \sin\delta_z + \Omega_z \dot{\delta}_z \cos\delta_z \right] \bar{i}_b$$
$$+ \left[2 C_z \Omega_z (r - \omega_o) \sin\delta_z \right] \bar{j}_b - \left[2 C_z \Omega_z q \sin\delta_z \right] \bar{k}_b \tag{34}$$

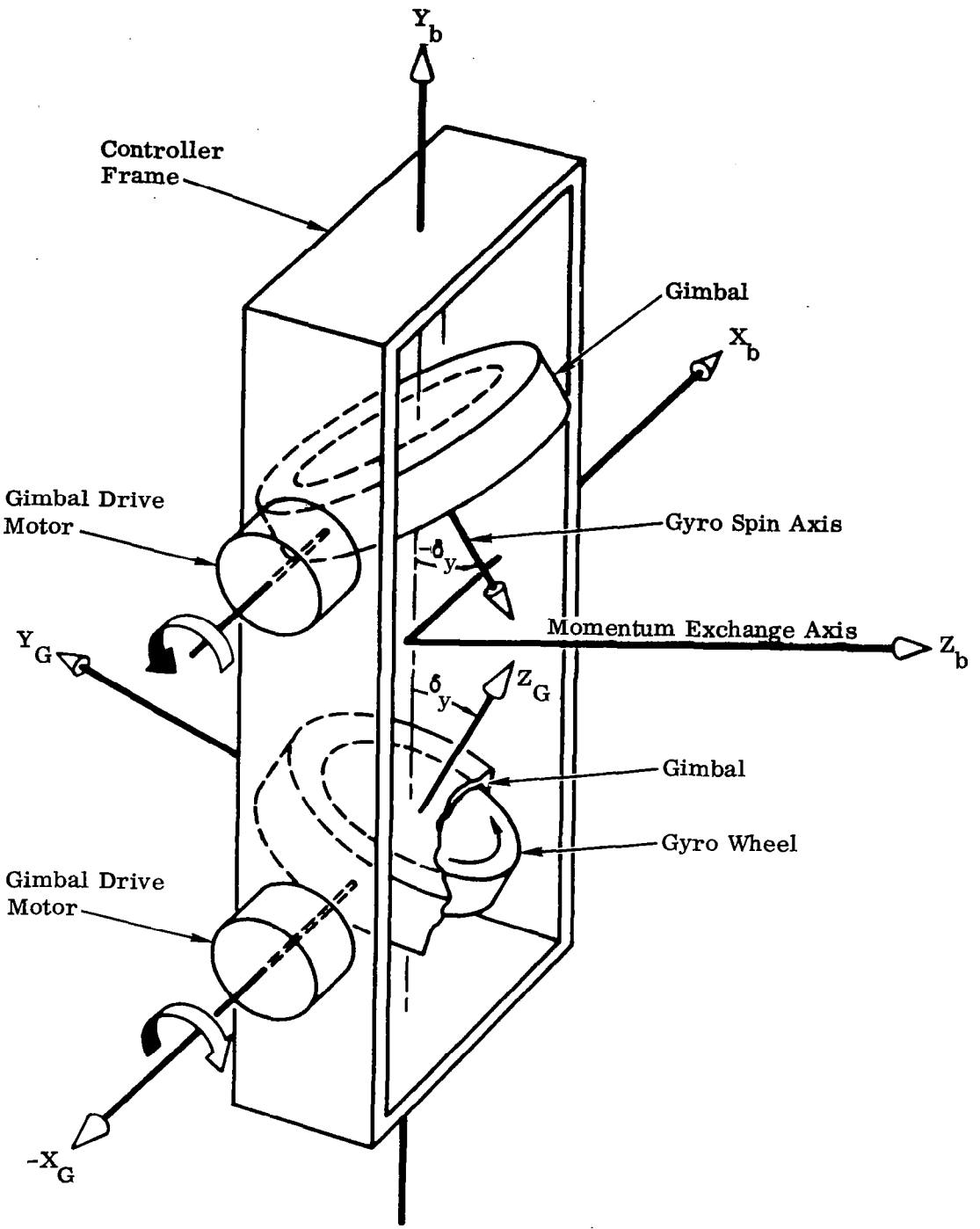

Figure 3. Diagram of a Twin-Gyro Controller

To specialize relations (31) - (34) to the two cases mentioned above, we simplify by noting that for twin gyrotorquer control,

$$\dot{\Omega}_x = \dot{\Omega}_y = \dot{\Omega}_z = 0$$

while for flywheel control

$$\delta_x = \dot{\delta}_x = \delta_y = \dot{\delta}_y = \delta_z = \dot{\delta}_z = 0$$

The equations of motion for each case then reduce to

1. Twin Gyrotorquer Unit on Each Body Axis

$$\begin{aligned}
I_x\dot{p} + (q - \omega_o)\,r\,(I_z - I_y) &= 2\,C_x\Omega_x r \sin\delta_x - 2\,C_y\Omega_y\,(q - \omega_o)\sin\delta_y \\
&\quad - 2\,C_z\Omega_z\,\dot{\delta}_z\cos\delta_z + L_x \\
I_y\dot{q} + pr\,(I_x - I_z) &= -2\,C_x\Omega_x\dot{\delta}_x\cos\delta_x + 2\,C_y\Omega_y p\sin\delta_y \\
&\quad - 2\,C_z\Omega_z\,(r - \omega_o)\sin\delta_z + L_y \\
I_z\dot{r} + (q - \omega_o)\,p\,(I_y - I_x) &= -2\,C_x\Omega_x\,(p - \omega_o)\sin\delta_x - 2\,C_y\Omega_y\dot{\delta}_y\cos\delta_y \\
&\quad + 2\,C_z\Omega_z q\sin\delta_z + L_z
\end{aligned} \tag{35}$$

2. One Flywheel Controller on Each Body Axis

$$\begin{aligned}
I_x\dot{p} + (q - \omega_o)\,r\,(I_z - I_y) &= -C_x\dot{\Omega}_x + C_y\Omega_y r - C_z\Omega_z q + L_x \\
I_y\dot{q} + pr\,(I_x - I_z) &= -C_x\Omega_x r - C_y\dot{\Omega}_y + C_z\Omega_z p + L_y \\
I_z\dot{r} + (q - \omega_o)\,p\,(I_y - I_x) &= C_x\Omega_x q - C_y\Omega_y p - C_z\dot{\Omega}_z + L_z
\end{aligned} \tag{36}$$

where

$$\bar{L} = L_x \bar{i}_b + L_y \bar{j}_b + L_z \bar{k}_b \tag{37}$$

The use of these equations in conjunction with particular control modes will be discussed in Subsection 3.3.

3.2.2 Effect of Moving Masses

We now suppose that there are N masses which move within (and with respect to) the vehicle in some arbitrary manner. The net effect of this motion is to introduce extraneous torques which cause the vehicle to deviate from a prescribed attitude — an effect which must be compensated for by the control system.

Formally, one may take account of this additional factor by including an extra term in the expression for the angular momentum as given by Eq. (17), viz.

$$\bar{H} = I \cdot (\bar{\omega}_b + \bar{\omega}_r) + J \cdot (\bar{\omega}_g + \bar{\omega}_G) + \sum_{i=1}^{N} \bar{r}_i \times m_i \bar{v}_i \tag{38}$$

where $\bar{r}_i$ is the radius vector from the origin of the body frame to the moving mass, m_i, and $\bar{v}_i$ is the velocity of m_i with respect to inertial space. Now

$$\begin{aligned} \bar{v}_i &= \frac{d}{dt}(\bar{r}_o + \bar{r}_i) \\ &= \bar{v}_o + \left(\frac{\delta \bar{r}_i}{\delta t}\right)_b + (\bar{\omega}_b + \bar{\omega}_r) \times \bar{r}_i \end{aligned} \tag{39}$$

where $\bar{v}_o$ is the velocity of the origin of the body frame with respect to inertial space. It follows that

$$\begin{aligned} \frac{d}{dt}\sum_{i=1}^{N} \bar{r}_i \times m_i \bar{v}_i = {} & \sum_{i=1}^{N} \bar{r}_i \times m_i \frac{d\bar{v}_o}{dt} + I^{(m)} \cdot \left[\frac{d\bar{\omega}_b}{dt} + \frac{d\bar{\omega}_r}{dt}\right] \\ & + (\bar{\omega}_b + \bar{\omega}_r) \times \left[I^{(m)} \cdot (\bar{\omega}_b + \bar{\omega}_r)\right] + \sum_{i=1}^{N} \bar{r}_i \times m_i \left(\frac{\delta^2 \bar{r}_i}{\delta t^2}\right)_b \\ & + 2\sum_{i=1}^{N} \bar{r}_i \times \left[(\bar{\omega}_b + \bar{\omega}_r) \times m_i \left(\frac{\delta \bar{r}_i}{\delta t}\right)_b\right] \end{aligned} \tag{40}$$

The x, y, and z components of this vector, expressed in body components, must be added to the first, second, and third equations, respectively, of the two sets of equations, (35) and (36). Here $I^{(m)}$ is the inertial dyadic associated with the moving masses. Its components with respect to the body frame are given by

$$I_x^{(m)} = \sum_{i=1}^{N} (y_i^2 + z_i^2)\, m_i \tag{41}$$

$$I_{xy}^{(m)} = \sum_{i=1}^{N} x_i\, y_i\, m_i \tag{42}$$

etc.

where

$$\bar{r}_i = x_i \bar{i}_b + y_i \bar{j}_b + z_i \bar{k}_b \tag{43}$$

Note that x_i, y_i, and z_i are functions of time; the dyadic $I^{(m)}$ is therefore time-varying.

It is apparent from the complexity of (40) that general conclusions regarding the effect of moving masses are hard to come by. However, in certain special cases, it is possible to obtain useful results with comparatively little effort. Suppose, for example, that there are two mass points (crew members) moving in a circumferential direction on diametrically opposite sides of a symmetrical space station. Assuming that $X_b\, Y_b$ is the plane of motion, the situation may be depicted as shown in Fig. 4. If we attach a crew coordinate system (X_c, Y_c, Z_c) with origin at O so that the X_c axis always passes through m_1 and m_2, then the inertial dyadic of the total system (vehicle plus two moving masses) is a constant (when referred to the crew frame), and there are no product-of-inertia terms (assuming that X_b and Y_b are principal inertial axes for the vehicle and Z_b is an axis of symmetry). In this case, Eq. (13) still holds, but now

$$\bar{H}_b = I \cdot (\bar{\omega}_c + \bar{\omega}_b + \bar{\omega}_r) \tag{44}$$

where

$$\bar{\omega}_c = \dot{\gamma}\, \bar{k}_c \tag{45}$$

and I is the constant inertial dyadic of the vehicle plus moving masses referred to the crew frame. Since I is constant, the system is then analyzed as an equivalent rigid body where the effect of the moving masses is contained in the additional terms

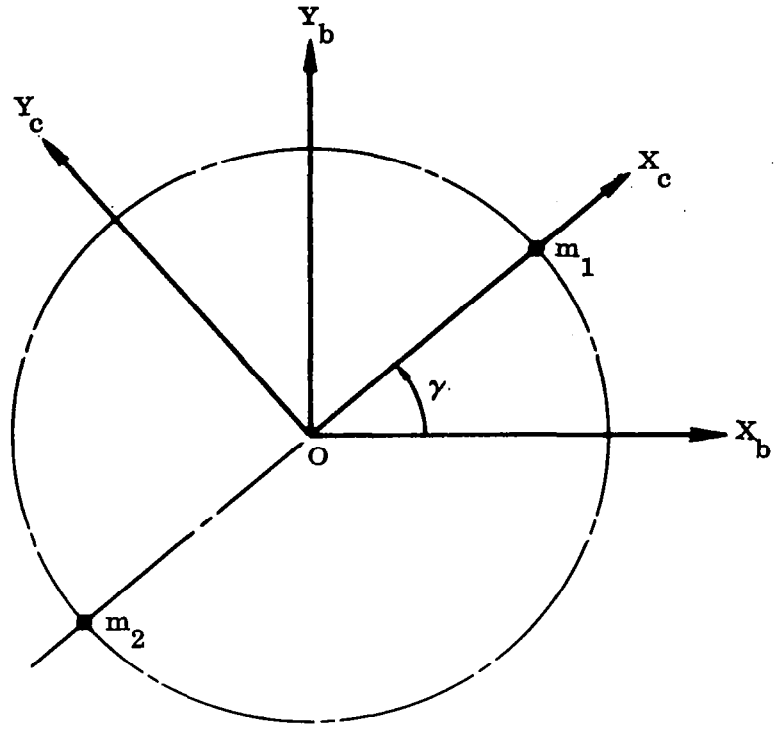

Figure 4. Coordinate Geometry for Circumferential Motion of Two Mass Points

involving $\bar{\omega}_c$. Thomson and Fung[7] use this approach to analyze the stability properties of a spinning space station when crew motions of the above type occur. A somewhat different approach is taken by Harding[26] who refers all motions to a composite center of mass, which yields crucial simplifications in the equations of motion.

3.2.3 Flexible Satellite

For certain types of space satellite missions, the structural compliance of the vehicle is a crucial factor in design and performance. The deleterious influence of elastic effects manifests itself in various ways. In an orbiting telescope, for example, elastic deformations in the mirror degrade the image received. Since payload weight is at a premium, the problem is essentially one of designing a minimum weight structure consistent with rigidity requirements. The problem is dynamic rather than static, since control devices in the attitude control system — and also extraneous disturbances — will tend to excite the elastic modes. One of the primary constraints on the control system is that these elastic displacements be small and reasonably well damped.

The effects of structural elasticity are perhaps more prominent in the way they influence the attitude-sensing instrumentation. For example, if rate gyros are used

for stability augmentation purposes, they will sense local elastic as well as rigid body motions. Unless this situation is carefully analyzed, the attitude control system will go unstable.

This is of course a basic problem in launch vehicle autopilots and has been studied extensively. Because of the fact that launch vehicles may be analyzed via slender beam theory, the basic structural dynamics are well understood, at least conceptually. Satellite vehicles, however, are more complicated structures, at least from the dynamic point of view. They may be spherical, parabolic, toroidal, or a multitude of other shapes. Of course, in theory at least, the vibration frequencies and mode shapes could be obtained for any structure by using a suitably refined lumped mass model. However, for purposes of preliminary analysis, this is an unwarranted effort, and one must seek simpler approaches.

One obvious solution is to approximate the actual structure by an equivalent geometric shape whose vibration frequencies and mode shapes can be obtained with relatively little effort. These would then be used to establish the general features of the attitude control system, especially as it relates to the influence of structural compliance. Two cases of this type are discussed in the following paragraphs.

3.2.3.1 Flat Plate Configuration

If the structure to be analyzed has the approximate shape of a thin circular plate, one may derive some basic features of the attitude control system in relatively simple fashion.[9] The vibration frequencies and mode shapes for this case are derived in Appendix B. The most general displacement normal to the plane of the plate is given by Eq. (B37), viz. (see also Fig. B1).

$$u(\rho,\alpha,t) = \sum_{n=0}^{\infty}\sum_{m=0}^{\infty}\left[q_{nm}^{(s)}(t)\varphi_{nm}^{(s)}(\rho,\alpha) + q_{nm}^{(c)}(t)\varphi_{nm}^{(c)}(\rho,\alpha)\right] \tag{46}$$

The terminology is defined in Appendix B. We are normally interested in the quantities sensed by a rate gyro, for example. In this case we neglect the mode ($n=0$, $m=0$) since this corresponds to rigid body translation. Furthermore, the mode ($n=1$, $m=0$) corresponds to rigid body rotation. If we now place a rate gyro so that its sensitive axis is coincident with the Y_b axis, then the gyro output will be

$$\frac{d}{dt}\left(\frac{1}{\rho}\frac{\partial u}{\partial \alpha}\right) = q + \sum_{n=2}^{\infty}\sum_{m=0}^{\infty}\left[\dot{q}_{nm}^{(s)}\psi_{nm}^{(s)} + \dot{q}_{nm}^{(c)}\psi_{nm}^{(c)}\right] \tag{47}$$

where q is the component of $\bar{\omega}_b$ about the Y_b axis; see Eq. (4). It is assumed in Eq. (47) that the angular velocity of the reference frame is negligible. In general, the gyro output gives values with respect to inertial space so that if the reference frame angular

velocity is not negligible, the rigid body output of the rate gyro will give the Y_b component of $(\bar{\omega}_b + \bar{\omega}_r)$. Normally, some gain value is associated with the gyro output (47) as well as gyro dynamics.

If now we place the rate gyro on Y_b so that its sensitive axis is normal to Y_b, the gyro output will be (we again refer to Fig. B1)

$$\frac{d}{dt}\left(\frac{\partial u}{\partial \rho}\right) = p + \sum_{n=2}^{\infty}\sum_{m=0}^{\infty}\left[\dot{q}_{nm}^{(s)}\sigma_{nm}^{(s)} + \dot{q}_{nm}^{(c)}\sigma_{nm}^{(c)}\right] \tag{48}$$

In short, the gyros may be located so that they pick up only circumferential modes, or only radial modes.

An examination of Eqs. (B45) and (B48) also indicates that the possibility exists for exciting only certain modes and not others. Thus, depending on the control system configuration, there exist preferred locations for the sensors and control actuators from the point of view of minimization of the deleterious influence of elastic distortions. This point will be discussed in detail in Subsection 3.3.

3.2.3.2 Toroidal Configuration

The toroidal shape is the one most commonly envisioned for manned space stations. Under various simplifying assumptions, the vibration frequencies and mode shapes for this case can be derived in a relatively simple manner. This is done in Appendix C. The main results are contained in Eqs. (C31) and (C32), viz. (see Fig. C1).

$$u(\alpha, t) = \sum_{n=0}^{\infty}\left[q_n^{(s)}(t)\varphi_n^{(s)}(\alpha) + q_n^{(c)}(t)\varphi_n^{(c)}(\alpha)\right] \tag{49}$$

$$\beta(\alpha, t) = \sum_{n=0}^{\infty}\lambda\left[q_n^{(s)}(t)\varphi_n^{(s)}(\alpha) + q_n^{(c)}(t)\varphi_n^{(c)}(\alpha)\right] \tag{50}$$

As in the previous subsection, we are interested in the signals sensed by a rate gyro. We may discard the mode due to n = 0 since this corresponds to rigid body translation. If we now locate a rate gyro with its sensitive axis coincident with the Y_b axis (again referring to Fig. C1), we note that its output is

$$\frac{d}{dt}\left(\frac{1}{a}\frac{\partial u}{\partial \alpha}\right) = q + \sum_{n=2}^{\infty}\left[\dot{q}_n^{(s)}\psi_n^{(s)} + \dot{q}_n^{(c)}\psi_n^{(c)}\right] \tag{51}$$

On the other hand, if the rate gyro is placed on Y_b so that its sensitive axis is normal to Y_b, the gyro output is given by

$$\frac{d\beta}{dt} = p + \sum_{n=2}^{\infty} \lambda \left[\dot{q}_n^{(s)} \varphi_n^{(s)} + \dot{q}_n^{(c)} \varphi_n^{(c)} \right] \tag{52}$$

Having the modes and frequencies of vibration, one may investigate the effect of locating the sensors and control devices at specified locations. Since this can be done only with reference to a specific control system configuration, a detailed discussion will be deferred until Subsection 3.3.

3.3 ACTIVE CONTROL

An active control system presupposes the availability of powered devices aboard the spacecraft to control the attitude in some prescribed fashion. The most common types are momentum-exchange devices (flywheels, gyrotorquers) and mass-expulsion elements (jets). In the following sections, typical applications are described for each of these, together with advantages and limitations for particular missions.

3.3.1 Flywheels

The equations which describe the motion of a flywheel-controlled satellite vehicle are given by Eqs. (36) which are repeated here.

$$I_x \dot{p} + (I_z - I_y)(q - \omega_o) r = -C_x \dot{\Omega}_x + C_y \Omega_y r - C_z \Omega_z q + L_x \tag{53}$$

$$I_y \dot{q} + (I_x - I_z) pr = -C_x \Omega_x r - C_y \dot{\Omega}_y + C_z \Omega_z p + L_y \tag{54}$$

$$I_z \dot{r} + (I_y - I_x)(q - \omega_o) p = C_x \Omega_x q - C_y \Omega_y p - C_z \dot{\Omega}_z + L_z \tag{55}$$

It is important to keep in mind the assumptions under which these equations were derived, namely,

a. There is one flywheel mounted on each body axis in such a way that the spin axis of the flywheel is parallel to the body axis.

b. The body axes are the principal axes of the satellite; there are no product-of-inertia terms.

c. The Euler angles (ψ, θ, φ) are with respect to a specified reference frame.

d. The satellite is in a circular orbit about the earth. In this case the $\bar{i}_r$ axis is tangent to the orbital path and in the direction of travel, with $\bar{k}_r$ directed toward the earth's center. The orbital rate is denoted by ω_o.

e. The quantities ψ, θ, φ, and ω_o are assumed small.

This particular situation characterizes the communication satellite problem; we now seek to determine the salient control features. For purposes of control analysis, it may be assumed further that p, q, and r are also small quantities; in which case, Eqs. (53) - (55) are further simplified to

$$I_x\ddot{\varphi} + H_z\dot{\theta} - H_y\dot{\psi} = L_{cx} + L_x \tag{56}$$

$$I_y\ddot{\theta} - H_z\dot{\varphi} + H_x\dot{\psi} = L_{cy} + L_y \tag{57}$$

$$I_z\ddot{\psi} + H_y\dot{\varphi} - H_x\dot{\theta} = L_{cz} + L_z \tag{58}$$

where

$$H_x = C_x\Omega_x \tag{59}$$

$$L_{cx} = -\dot{H}_x \tag{60}$$

etc.

We note that the various coefficients of $\dot{\varphi}$, $\dot{\theta}$, and $\dot{\psi}$ include H_x, H_y, and H_z, but these are in turn functions of φ, θ, and ψ (via the control loops to be specified). Therefore, even in the so-called linearized case, a set of nonlinear equations arise. It is apparent that the synthesis problem is thus enormously complicated. For purposes of preliminary design, it proves convenient to artificially uncouple the equations of motion and treat the problem as if there were three independent systems instead of one highly coupled one. Thus, one proceeds with the hope that a synthesis based on the separated set will be a satisfactory approximation to a synthesis based on the complete system. Needless to say, the final design must be carefully validated by computer simulation of the complete nonlinear system. Much of the published work on this problem proceeds on this basis, and there is extensive empirical evidence to suggest that this approach is useful.

A control loop for the pitch channel would then take the form shown in Fig. 5.* The transfer function for the motor flywheel unit is derived in Appendix D, and the other symbols have the following meanings:

C = moment of inertia of flywheel; slug ft^2

I_y = moment of inertia of vehicle; slug ft^2

K_A = servoamplifier gain; volts/rad

*For simplicity, the subscript on C has been dropped.

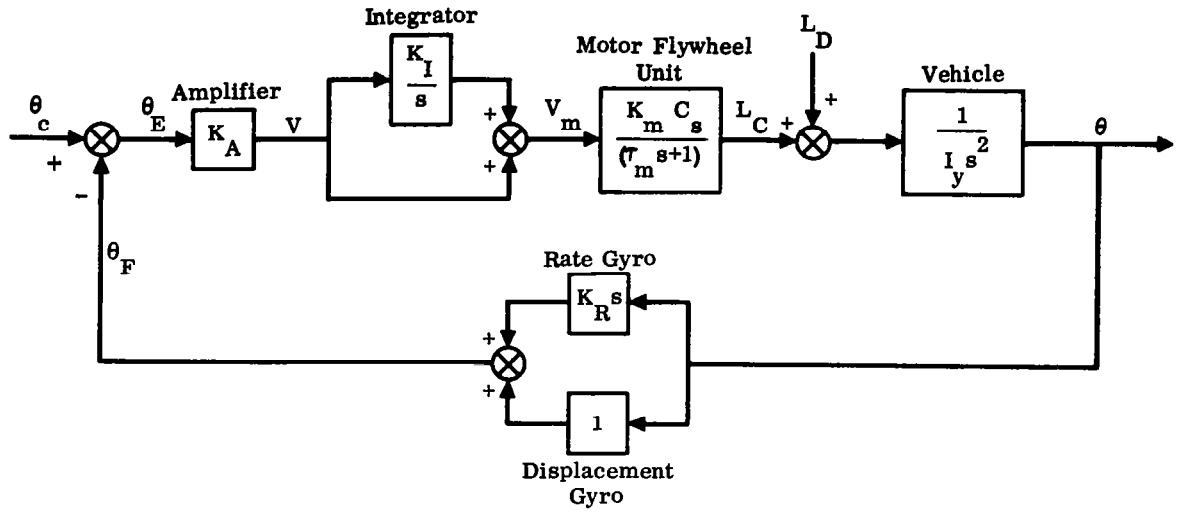

Figure 5. Pitch Control Channel for Flywheel Attitude Control

K_I = integrator gain; sec^{-1}

K_m = motor gain; (rad/sec)/volt

K_R = rate gyro gain; sec

L_c = control torque; lb ft

L_D = disturbance torque; lb ft

s = Laplace operator; sec^{-1}

V = output signal from amplifier; volts

V_m = input signal to motor flywheel unit; volts

θ = attitude angle; rad

θ_c = attitude command; rad

θ_E = error signal; rad

θ_F = feedback signal; rad

τ_m = motor time constant; sec

The open-loop transfer function is readily derived as follows,

$$\frac{\theta_F}{\theta_E} = \left[\frac{K_A K_m K_R C}{\tau_m I_y}\right] \frac{(s + K_I)\left(s + \frac{1}{K_R}\right)}{s^2\left(s + \frac{1}{\tau_m}\right)} \tag{61}$$

Depending on the relative values of τ_m and K_R, the root locus for the system would have the form shown in Fig. 6.

In order to determine system gains and parameters, one must generally take account of the following factors

a. Dynamic response of control loop.

b. Response to external disturbances.

c. Slewing rates.

Mission requirements, specifications, and accuracy constraints vary widely. Often there may be separate control loops for coarse and fine pointing (e.g., the orbiting astronomical observatory). Without confining ourselves to a specific case, however, we will indicate, in general, the means whereby the above factors are translated into constraints on the control system parameters.

The maximum flywheel speed and moment of inertia are determined primarily by the specification on slewing rate, $\dot{\theta}$. By conservation of momentum we have

$$I_y \dot{\theta} + C\Omega = 0 \tag{62}$$

Consequently, if I_y and $\dot{\theta}$ are given, this serves to define the required angular momentum, $C\Omega$, of the flywheel. To obtain some feel for the numerical orders of magnitude involved, suppose: 1) that $I_y = 1000$ slug ft^2 (which is typical of the OAO, for example) and 2) a slewing rate of $\dot{\theta} = 9$ deg/min is specified. We then find $C\Omega = 2.62$ lb-ft-sec. If the maximum speed of the motor flywheel unit is taken as 1500 rpm, then we find that $C = 0.0167$ slug ft^2. Typically, for a unit of this size, $\Omega = 1500$ rpm corresponds to an input voltage signal, $V_m = 30$ volts. From this, one may calculate the gain constant, K_m, of the motor flywheel unit, viz.

$$K_m = \frac{\Omega}{V_m} = \frac{1500}{60} \cdot \frac{2\pi}{30}$$

$$= 5.24 \text{ (rad/sec)/volt}$$

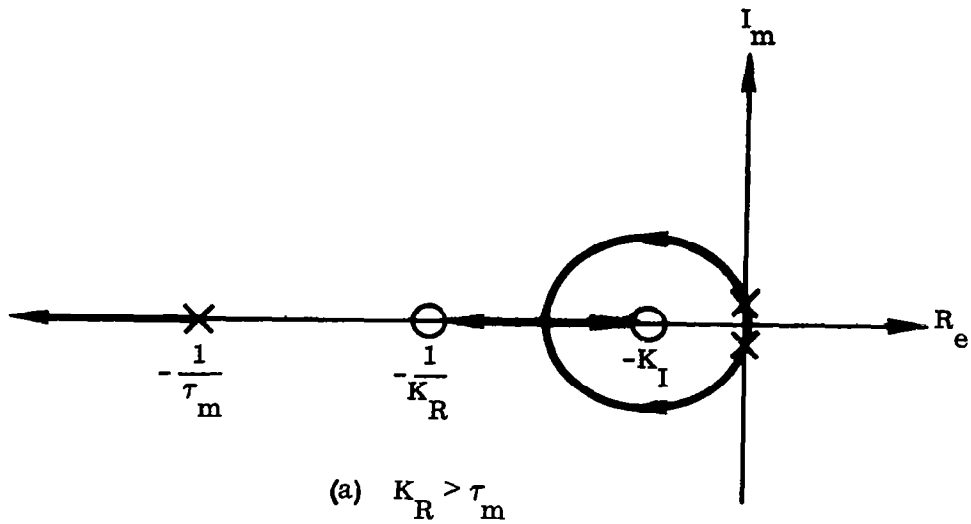

(a) $K_R > \tau_m$

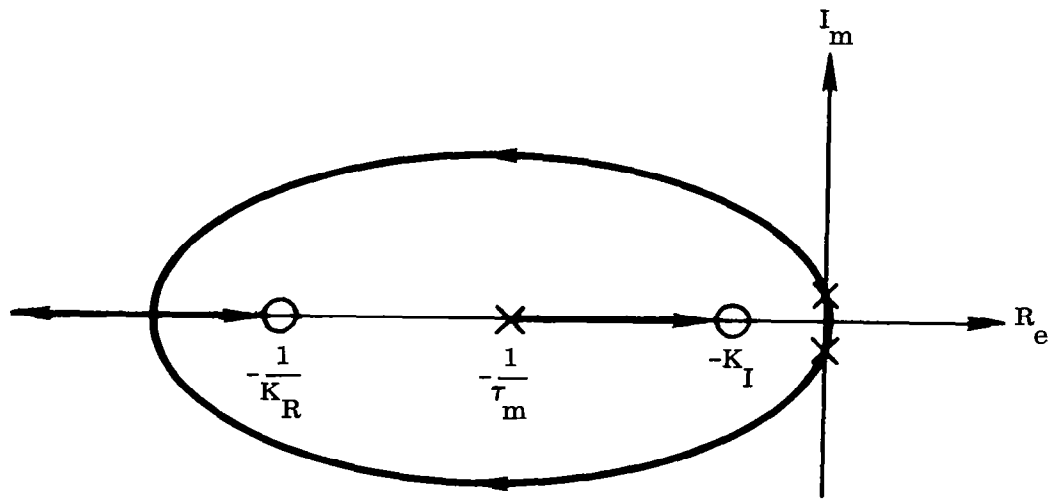

(b) $K_R < \tau_m$

Figure 6. Root Locus Plots for Attitude Control System

Having specified the size and type of motor flywheel unit, one may then determine the motor time constant from the physical characteristics of the unit (see Appendix D). A typical value of τ_m for the momentum specifications given above is 20 sec.

For a specified angular momentum requirement on the motor flywheel unit, there is some flexibility in the choice of C and Ω. Normally, for a fixed value of $C\Omega$, it is reasonable to specify C and Ω individually so that the total weight of the motor and flywheel is a minimum. A superficial examination would seem to indicate that the flywheel speed, Ω, should be made as large as practical, since a large C means a large wheel size and consequently more weight. Note, however, that the kinetic energy, $C\Omega^2$, will generally increase with increasing speed. For example, if we select particular values, C_1 and Ω_1, then

$$(K.E.)_1 = \frac{1}{2} C_1 \Omega_1^2$$

If we now double the speed and thereby halve the moment of inertia (to obtain the same angular momentum, i.e., $\Omega_2 = 2\Omega_1$ and $C_2 = \frac{1}{2} C_1$, then

$$(K.E.)_2 = C_1 \Omega_1^2$$

In other words, the kinetic energy is doubled. This means that the smaller flywheel has to be supplied with twice as much kinetic energy, which means a larger power supply. The optimal tradeoff point is usually determined by a parameter study.

Having made a preliminary determination of C, K_m, and τ_m, we must now investigate the response of the system to external disturbances. The disturbance response capability of the system may be specified in various ways — depending on the vehicle mission. One useful and important criterion is the value of the steady-state error in response to a disturbance step input. In Fig. 5 with $\theta_c = 0$, we find

$$\frac{\theta_E}{L_D} = \frac{-K_R}{I_y} \cdot \frac{\left(s + \frac{1}{K_R}\right)\left(s + \frac{1}{\tau_m}\right)}{\left[s^2\left(s + \frac{1}{\tau_m}\right) + \frac{K_A K_m K_R C}{I_y \tau_m}(s + K_I)\left(s + \frac{1}{K_R}\right)\right]} \tag{63}$$

For a step input disturbance

$$L_D(s) = \frac{L_o}{s}$$

$L_o \equiv$ constant

the steady state value of θ_E is found to be

$$\theta_E(t)\Big|_{ss} = -\frac{L_o}{K_A K_I K_m C} \tag{64}$$

If the values of L_o, K_m, C, and $\theta_E(t)|_{ss}$ are prescribed, this relationship determines the required value of $K_A K_I$. However, $K_A K_I$ may be limited by the fact that moderate step inputs in θ_c do not saturate the motor flywheel unit; i.e., there is a saturation limit for V_m. In this case, to meet the disturbance response constraint, it may be necessary to increase C and K_m — and thereby the size of the motor flywheel unit.

Note that with no integrator ($K_I = 0$), Eq. (63) shows that $\theta_E(t)$ diverges without bound with a step input in L_D. In certain cases, when the disturbance torque is known to be cyclic, an integrator may not be necessary. In any event, some reasonably good data on anticipated disturbances torques must be available in order to design the attitude control system effectively. Design guides for this problem are contained in Subsection 3.5.

As a final step in the synthesis procedure, the open-loop transfer function, Eq. (61), is used in conjunction with the root loci of Fig. 6 to establish open-loop gains and whatever filters may be required to yield acceptable dynamic response. Since this is a standard problem in conventional control theory, it will not be elaborated upon here.

A fundamental characteristic of attitude control systems employing flywheel controllers is the tendency of the flywheels to saturate.* For example, an inspection of the transfer function

$$\frac{\Omega}{L_D} = \left[\frac{K_A K_m K_R}{I_y \tau_m}\right] \frac{(s + K_I)\left(s + \frac{1}{K_R}\right)}{s\left[s^2\left(s + \frac{1}{\tau_m}\right) + \frac{K_A K_m K_R C}{I_y \tau_m}(s + K_I)\left(s + \frac{1}{K_R}\right)\right]} \tag{65}$$

indicates that a constant disturbance torque causes an unbounded increase in flywheel speed, Ω. This, of course, could also be inferred from (64) since a constant value of θ_E implies a constant flywheel acceleration. Provision must therefore be made to "dump" flywheel momentum (i.e., reduce the flywheel speed to near zero) when required. A means for doing this is indicated in Fig. 7. In the presence of a constant disturbing torque, L_D, the control torque, L_c, takes on a constant value (after transients have died out), which means that the flywheel experiences a constant acceleration.

*This characteristic is true in general for any momentum exchange controllers.

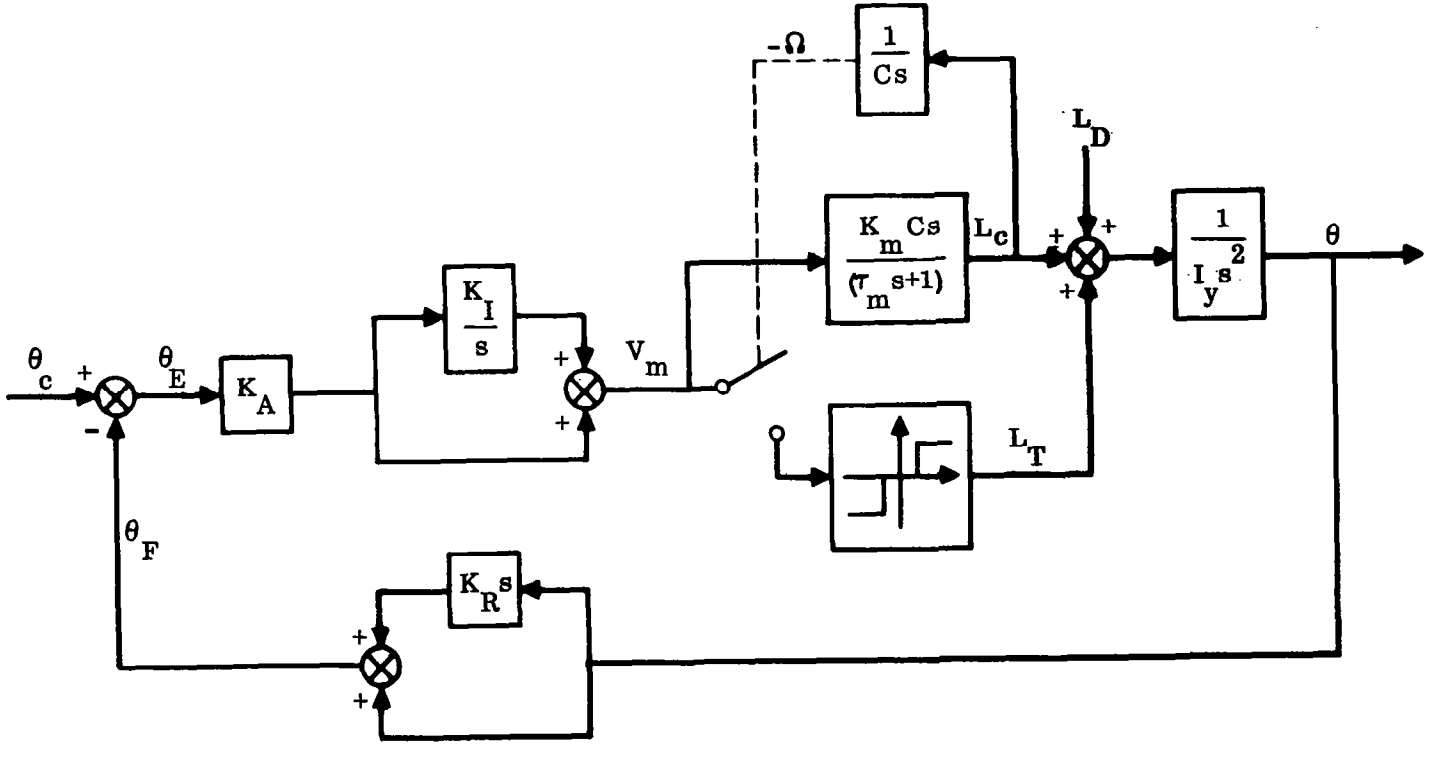

Figure 7. Flywheel Attitude Control System with Desaturation Capability

When the flywheel speed reaches a predetermined value, a pair of reaction jets is energized causing an external torque on the vehicle opposite to, and greater than, that of the disturbance torque. This then induces a signal which tends to reduce the flywheel speed, and the reaction jets are shut off when the flywheel speed is reduced to a predetermined value. The reaction jets also become active when large impulses are applied, either from the command signals or disturbances. The time consumed in "desaturating" the flywheel is obviously a function of the magnitude of the jet torque. Tradeoffs therefore exist between the size of the flywheel unit, the reaction jet system, and the time required to desaturate the flywheel.

It may be noted in passing that in the absence of external disturbance torques, the flywheel speed returns to zero (if its initial value was zero) after a step input in θ_c. This is apparent from the transfer function

$$\frac{\Omega}{\theta_c} = -\left[\frac{K_A K_m}{\tau_m}\right] \frac{s(s + K_I)}{\left[s^2\left(s + \frac{1}{\tau_m}\right) + \frac{K_A K_m K_R C}{I_y \tau_m}(s + K_I)\left(s + \frac{1}{K_R}\right)\right]} \tag{66}$$

On the other hand, the effect of external disturbance torques on the flywheel speed is cumulative. To see this, let the initial flywheel speed be zero and consider the external disturbance torque

$$L_D = L_o \qquad 0 \leq t \leq t_c$$

$$= 0 \qquad t \geq t_c$$

The Laplace transform of this function is

$$\mathcal{L}\left[L_D(t)\right] = \frac{L_o(1 - e^{-t_c s})}{s}$$

Substituting this in Eq. (65) and applying the final value theorem yields

$$\Omega(t)\Big|_{ss} = \frac{L_o t_c}{C} \tag{67}$$

3.3.1.1 Influence of Elastic Compliance

In order to exhibit the manner in which elastic compliance effects influence the control system design, we will consider the case of a satellite whose structural configuration may be closely approximated by a thin circular plate. Certain types of

orbiting astronomical telescopes fall in this category. If stability augmentation is to be provided by rate gyros, the problem arises of how to locate the gyros and control actuators (in the present case, flywheels) to minimize the deleterious influence of flexibility.

Using the results of Appendix B, we note that displacements normal to the plate may be represented as

$$u(\rho,\alpha,t) = \sum_{n=0}^{\infty}\sum_{m=0}^{\infty}\left[q_{nm}^{(s)}(t)\varphi_{nm}^{(s)}(\rho,\alpha) + q_{nm}^{(c)}(t)\varphi_{nm}^{(c)}(\rho,\alpha)\right] \tag{68}$$

This is merely Eq. (B37) of Appendix B, and the relevant geometry is depicted in Fig. B1.

The output from a rate gyro located so that its sensitive axis is parallel to a radial line is

$$K_R\sum_{n=0}^{\infty}\sum_{m=0}^{\infty}\left[\dot{q}_{nm}^{(s)}\psi_{nm}^{(s)} + \dot{q}_{nm}^{(c)}\psi_{nm}^{(c)}\right] \tag{69}$$

while if the sensitive axis is normal to a radial line the output is

$$K_R\sum_{n=0}^{\infty}\sum_{m=0}^{\infty}\left[\dot{q}_{nm}^{(s)}\sigma_{nm}^{(s)} + \dot{q}_{nm}^{(c)}\sigma_{nm}^{(c)}\right] \tag{70}$$

where K_R is the rate gyro gain. Only the gyros located in the plane of the plate will sense elastic distortions. In the derivation of the results of Appendix B, it has been assumed that torsional effects about an axis normal to the plane of the plate are negligible. Therefore, a gyro placed with its sensitive axis parallel to Z_b in Fig. B1 will sense only rigid body motions.

For purposes of attitude control, we must locate the gyros so that they sense angular rates about the X_b and Y_b axes respectively. For simplicity we shall refer to these as the x and y gyros.

Two possible locations for the x gyro are:

a. On the X_b axis ($\alpha_G = 0$) with its sensitive axis parallel to X_b.

b. On the Y_b axis ($\alpha_G = \frac{\pi}{2}$) with its sensitive axis normal to Y_b.

In the first case the gyro output is

$$K_R\left\{p + \sum_{n=2}^{\infty}\sum_{m=0}^{\infty}\left[\dot{q}_{nm}^{(s)}\psi_{nm}^{(s)}(0,\rho_G) + \dot{q}_{nm}^{(c)}\psi_{nm}^{(c)}(p,\rho_G)\right]\right\} \tag{71}$$

while in the second case

$$K_R\left\{p + \sum_{n=2}^{\infty}\sum_{m=0}^{\infty}\left[\dot{q}_{nm}^{(s)}\sigma_{nm}^{(s)}\left(\frac{\pi}{2},\rho_G\right) + \dot{q}_{nm}^{(c)}\sigma_{nm}^{(c)}\left(\frac{\pi}{2},\rho_G\right)\right]\right\} \tag{72}$$

Similarly, two possible locations for the y gyro are:

a. On the Y_b axis ($\alpha_G = \frac{\pi}{2}$) with its sensitive axis parallel to Y_b.

b. On the X_b axis ($\alpha_G = 0$) with its sensitive axis normal to X_b.

Here the y gyro output is

$$K_R\left\{q + \sum_{n=2}^{\infty}\sum_{m=0}^{\infty}\left[\dot{q}_{nm}^{(s)}\psi_{nm}^{(s)}\left(\frac{\pi}{2},\rho_G\right) + \dot{q}_{nm}^{(c)}\psi_{nm}^{(c)}\left(\frac{\pi}{2},\rho_G\right)\right]\right\} \tag{73}$$

for the first case and

$$K_R\left\{q + \sum_{n=2}^{\infty}\sum_{m=0}^{\infty}\left[\dot{q}_{nm}^{(s)}\sigma_{nm}^{(s)}(0,\rho_G) + \dot{q}_{nm}^{(c)}\sigma_{nm}^{(c)}(0,\rho_G)\right]\right\} \tag{74}$$

for the second case.

In (71) - (74) the quantities p and q are the components of $\bar{\omega}_b$ given by Eq. (4).

We need also the expressions for the generalized force due to a pure moment applied at some point on the plate. If the applied moment, L_c, (which we take to be the moment due to the flywheels) is such that its axis is parallel to a radial line, then*

$$Q_{nm}^{(s)} = L_c\psi_{nm}^{(s)}(\alpha_p,\rho_p) \tag{75}$$

$$Q_{nm}^{(c)} = L_c\psi_{nm}^{(c)}(\alpha_p,\rho_1) \tag{76}$$

*See Eq. (B56).

The usual procedure is to locate one flywheel with its spin axis along $X_b (\alpha_p = 0)$ and another with its spin axis along $Y_b (\alpha_G = \frac{\pi}{2})$. Denoting the moments due to the x and y flywheels by L_{cx} and L_{cy} respectively, the corresponding generalized moments are

$$Q_{nm}^{(s)}(L_{cx}) = L_{cx}\psi_{nm}^{(s)}(0,\rho_G)$$

$$= L_{cx}K_{nm} \tag{77}$$

$$Q_{nm}^{(c)}(L_{cx}) = L_{cx}\psi_{nm}^{(c)}(0,\rho_G)$$

$$= 0 \tag{78}$$

$$Q_{nm}^{(s)}(L_{cy}) = L_{cy}\psi_{nm}^{(s)}\left(\frac{\pi}{2},\rho_G\right)$$

$$= L_{cy}K_{nm}\cos\frac{n\pi}{2} \tag{79}$$

$$Q_{nm}^{(c)}(L_{cy}) = L_{cy}\psi_{nm}^{(c)}\left(\frac{\pi}{2},\rho_G\right)$$

$$= -L_{cy}K_{nm}\sin\frac{n\pi}{2} \tag{80}$$

where

$$K_{nm} = n\zeta_{nm}\left[J_n(k_{nm}\rho_G) + \Lambda_{nm}I_n(k_{nm}\rho_G)\right] \tag{81}$$

An examination of the above relationships shows that the x flywheel always excites the nm sine mode but never the nm cosine mode. On the other hand, the y flywheel excites the odd numbered nm cosine modes and the even numbered nm sine modes. Note also that Eq. (81) indicates the possibility of eliminating a mode excitation by an appropriate choice of ρ_G (i.e., setting $K_{nm} = 0$).

The above relationships also suggest the possibility of suppressing a mode excitation by using two flywheels per control axis (instead of one), each located 180 deg from the other. Other factors such as weight and added complexity must be considered in this regard.

According to Appendix B, the lowest elastic frequency occurs for n = 2 and m = 0. It is therefore desirable to investigate the possibility of locating the x and y gyros in such positions that this mode is not sensed by the control system.

We note first of all from Eqs. (77) - (80) that $Q_{nm}^{(c)}(L_{cx}) = Q_{nm}^{(c)}(L_{cy}) = 0$ for $n = 2$. Thus the flywheels excite only the sine mode in this case. Therefore, if we locate the x gyro at $\alpha_G = \frac{\pi}{2}$ and the y gyro at $\alpha_G = 0$, in each case with the sensitive axis normal to a radial line, the gyro outputs are given by Eqs. (72) and (74) respectively. The parameters of interest are therefore

$$\sigma_{20}^{(s)}\left(\frac{\pi}{2}, \rho_G\right) \qquad \sigma_{20}^{(c)}\left(\frac{\pi}{2}, \rho_G\right)$$

$$\sigma_{20}^{(s)}(0, \rho_G) \qquad \sigma_{20}^{(c)}(0, \rho_G)$$

Using Eqs. (B53), (B32), and (B33), we find that

$$\sigma_{20}^{(s)}\left(\frac{\pi}{2}, \rho_G\right) = \sigma_{20}^{(s)}(0, \rho_G) = 0$$

while $\sigma_{20}^{(c)}\left(\frac{\pi}{2}, \rho_G\right)$ and $\sigma_{20}^{(c)}(0, \rho_G)$ are, in general, finite.

It follows that, since only the sine modes are excited by the flywheels and only the cosine modes are sensed by the gyros, the $n = 2$, $m = 0$ mode does not affect the control system for this particular configuration.

Of course, these results must be interpreted with due regard for the approximations which characterized the analysis. The general approach, however, is valid and is useful in ascertaining the overall features of the control system insofar as the influence of elastic distortions is concerned. Fig. 8 illustrates the attitude control loop for one channel with one elastic mode taken into account. A stability-and-control analysis proceeds along the same lines as for a launch vehicle autopilot. In the present case, however, a realistic analysis must include the cross-coupling between pitch, roll, and yaw modes. In this sense the satellite attitude control problem is substantially more complicated than the launch vehicle control problem. However, for satellites the mass, inertial, and elastic properties of the vehicle are essentially constant, so that in this respect the problem is simpler than for launch vehicle autopilots.

3.3.2 Gyrotorquers

The flywheel controller generates a torque on the vehicle by accelerating the flywheel. It is also possible to generate a control torque by keeping the flywheel speed constant and rotating the spin axis with respect to the vehicle. The latter method, because of the fact that it exploits the gyroscopic properties of a spinning rotor, is called gyrotorquer control.

Both the flywheel and gyrotorquer (also called "control moment gyro") are essentially momentum-exchange devices. Attitude control via flywheels was studied

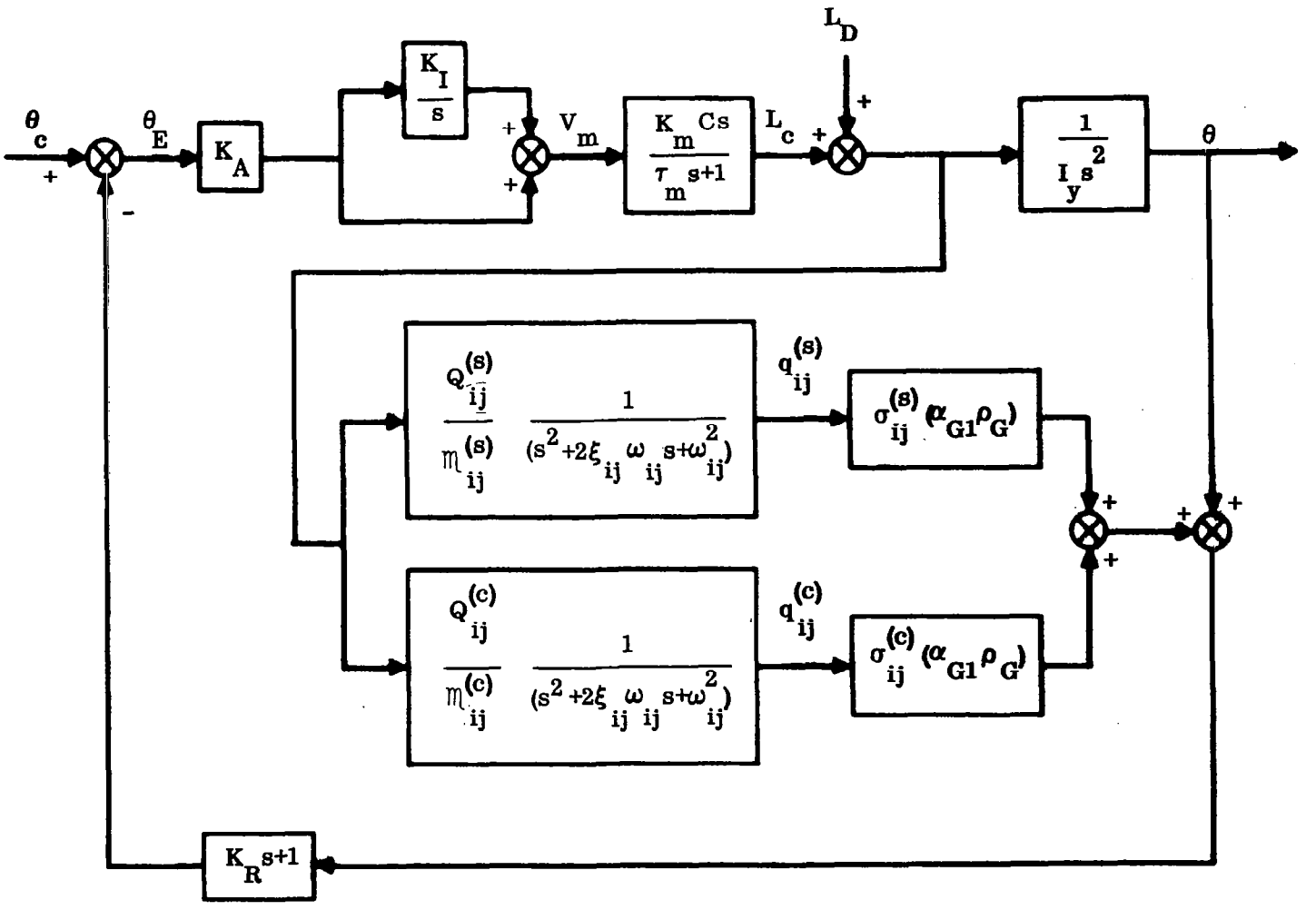

Figure 8. Attitude Control Loop with One Elastic Mode

extensively in the early stages of the problem, while the use of gyrotorquers has received close attention in recent years. This is due to the fact that in many respects gyrotorquers, properly employed, exhibit marked advantages over flywheels. By using two gyrotorquers per axis in the manner shown in Fig. 3, one may eliminate the first-order cross-coupling moments and thus permit independent control of each vehicle axis. The control synthesis problem is thereby immeasurably enhanced. Ease of analysis, by itself, is, however, not the most convincing argument for choosing one type of control over another. A more important point is that the twin gyro controller is more efficient in the sense that it requires less power and weight for a given momentum capability as compared with the flywheel.[6]

In order to develop the basic control system properties employing gyrotorquers, we will take as our point of departure the set of equations (35). We will assume that the reference coordinate frame and the inertial frame are coincident, which means that $\omega_o = 0$. Furthermore, it will be supposed that p, q, r, δ_x, δ_y, and δ_z are small quantities. Equations (35) then take the form

$$I_x \dot{p} = -2 C_z \Omega_z \dot{\delta}_z + L_x \tag{82}$$

$$I_y \dot{q} = -2 C_x \Omega_x \dot{\delta}_x + L_y \tag{83}$$

$$I_z \dot{r} = -2 C_y \Omega_y \dot{\delta}_y + L_z \tag{84}$$

and

$$\begin{aligned} p &= \dot{\varphi} \\ q &= \dot{\theta} \\ r &= \dot{\psi} \end{aligned} \tag{85}$$

It is apparent that the small perturbation assumption has enabled us to decouple the three control channels. In the ensuing discussion we will consider only one of these, the yaw mode, Eq. (84).

To derive an expression for the motor-gimbal dynamics, we must calculate the gimbal load torque referred to the gimbal axes. From Eq. (30), we find that the load torque on the lower gimbal in Fig. 3 is

$$A_y \ddot{\delta}_y + C_y \Omega_y (q \sin\delta_y - r \cos\delta_y)$$

and

$$-\left[-A_y \ddot{\delta}_y - C_y \Omega_y (-q \sin\delta_y - r \cos\delta_y\right]$$

for the upper gimbal.

Adding the above two expressions and dropping the subscripts, for simplicity, we find for the total load torque on the gimbal axes.*

$$2A\ddot{\delta} - 2C\Omega r \tag{86}$$

To precess the gimbals we may use two a-c servomotors, one on each gimbal axis, as shown in Fig. 3. An alternate configuration is shown in Fig. 9, wherein one motor and appropriate gearing are used to precess the gimbals. Restricting our attention to the latter case, we write the expression for the motor output torque as

$$L_m = K_c V_m - K_f \dot{\delta} \tag{87}$$

where

K_c = torque - voltage constant; lb ft/volt

V_m = input signal to motor; volts

K_f = torque - speed constant; lb ft/(rad/sec)

*and writing $\cos \delta_y \approx 1$.

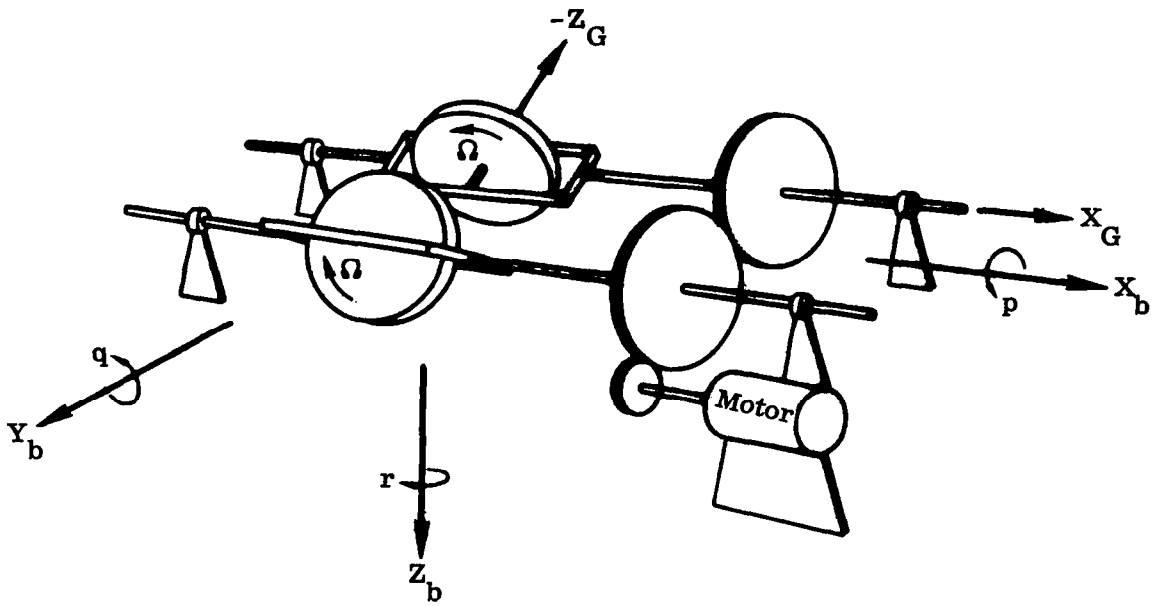

Figure 9. Twin-Gyro Controller with One Drive Motor

The torque delivered by the motor is equated to the sum of the gimbal, gearing, and rotor inertia referred to the gimbal shaft plus the total load torque of Eq. (86), viz.

$$K_c V_m - K_f \dot{\delta} = 2 I_a \ddot{\delta} + 2 A \ddot{\delta} - 2 C \Omega r \tag{88}$$

where I_a is the sum of gimbal, rotor, and gearing inertia for one gimbal.

Using an input signal to the motor of the form

$$V_m = - K_B \frac{r_E}{s} - K_g \delta \tag{89}$$

a simple yaw rate control system would then appear as shown in Fig. 10. After some elementary manipulations, this configuration may be simplified to the form shown in Fig. 11.

It is instructive to estimate the order-of-magnitude response characteristics of a typical system. For this purpose we take

$I_z = 150,000$ slug ft^2

$K_c = 2$ lb ft/volt

$K_f = 60$ lb ft/(rad/sec)

$I_a = 4$ slug ft^2

$A = 0.5$ slug ft^2

$C = 1$ slug ft^2

$\Omega = 400$ rad/sec

$K_g = 100$ volts/rad

$K_B = 40,000$ volts/rad

From Fig. 11, we find for the open-loop transfer function

$$\frac{r}{r_E} = \frac{K_o \omega_c^2}{s (s^2 + 2 \xi_c \omega_c s + \omega_c^2)} \tag{90}$$

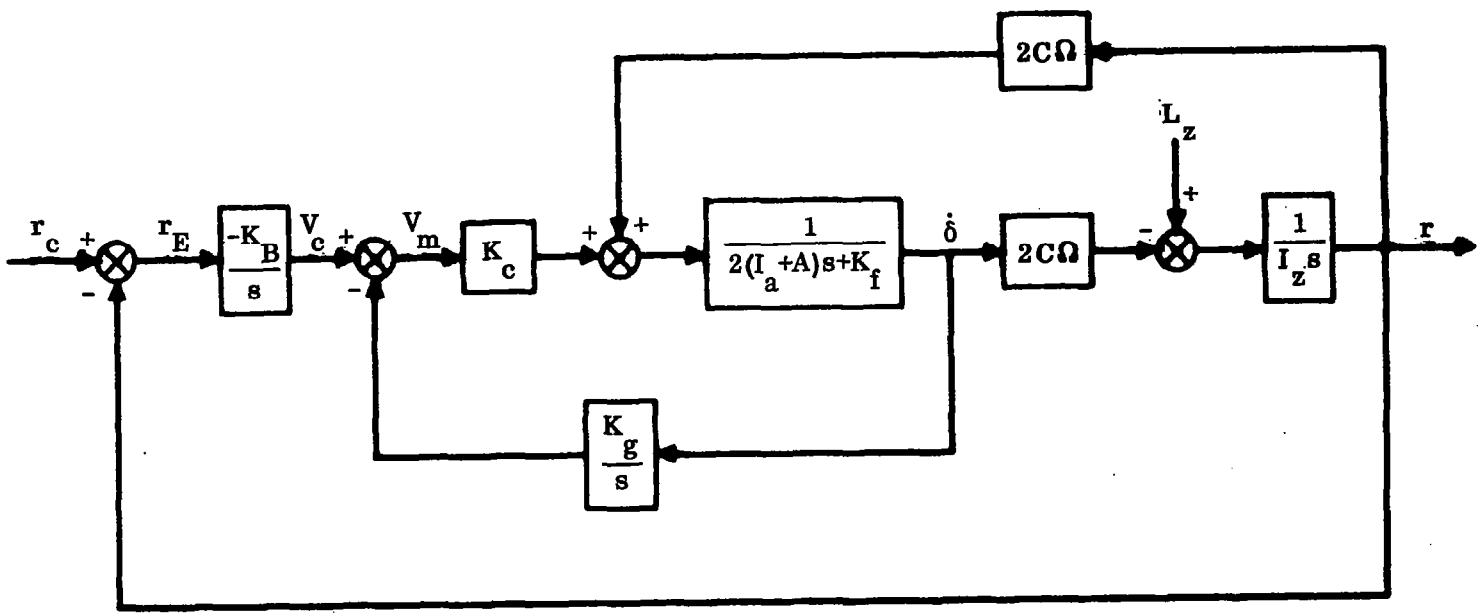

Figure 10. Yaw Rate Control System

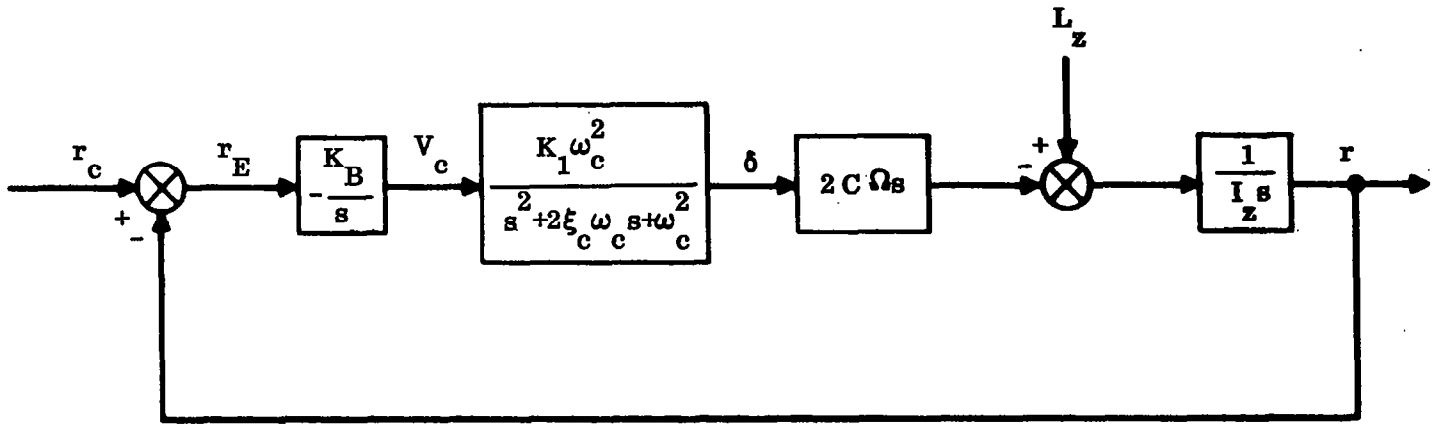

$$K_1 = \frac{K_c I_z}{4C^2\Omega^2 + I_z K_c K_g}$$

$$\omega_c^2 = \frac{4C^2\Omega^2 + I_z K_c K_g}{2I_z(I_a + A)}$$

$$\xi_c = \frac{K_f}{4\omega_c(I_a + A)}$$

Figure 11. Simplified Form of Yaw Rate Control System

where

$$K_o = \frac{2C\Omega K_B K_c}{4C^2\Omega^2 + I_z K_c K_g}$$

$$\omega_c^2 = \frac{4C^2\Omega^2 + I_z K_c K_g}{2I_z(I_a + A)}$$

$$\xi_c = \frac{K_f}{4\omega_c(I_a + A)}$$

Using the given values, these become

$$K_o = 2.09$$

$$\omega_c = 4.76$$

$$\xi_c = 0.70$$

The root locus plot for the system is shown in Fig. 12. A simple calculation shows that for a step input of 0.002 rad/sec, the response time (time to reach 95% of steady-state value) is approximately 5 seconds.

Within the range of the small angle, linearized approximations, the rate control system analysis thus reduces to a simple elementary type for each control axis.

A more complicated situation arises when attempting to control a spinning vehicle. In the case of a manned space station, for example, it is desirable to maintain a constant spin about one body axis (say the X_b axis) for purposes of providing an "artificial gravity" environment. It is also desired to maintain this spin axis fixed relative to inertial space so that solar panels, say, would always be pointed toward the sun. An active control system, using gyrotorquers, may be employed to achieve this while driving all other body angular rates to zero. In order to examine the scope of the problem, we refer again to Eqs. (35) and make the following assumptions:

r, q, θ, ψ, δ_x, and δ_y, are small

$$p = \dot{\varphi} \equiv p_o = \text{constant}$$

Then, from Eqs. (8) - (10), we have

$$\dot{\theta} = q\cos\varphi - r\sin\varphi \qquad (91)$$

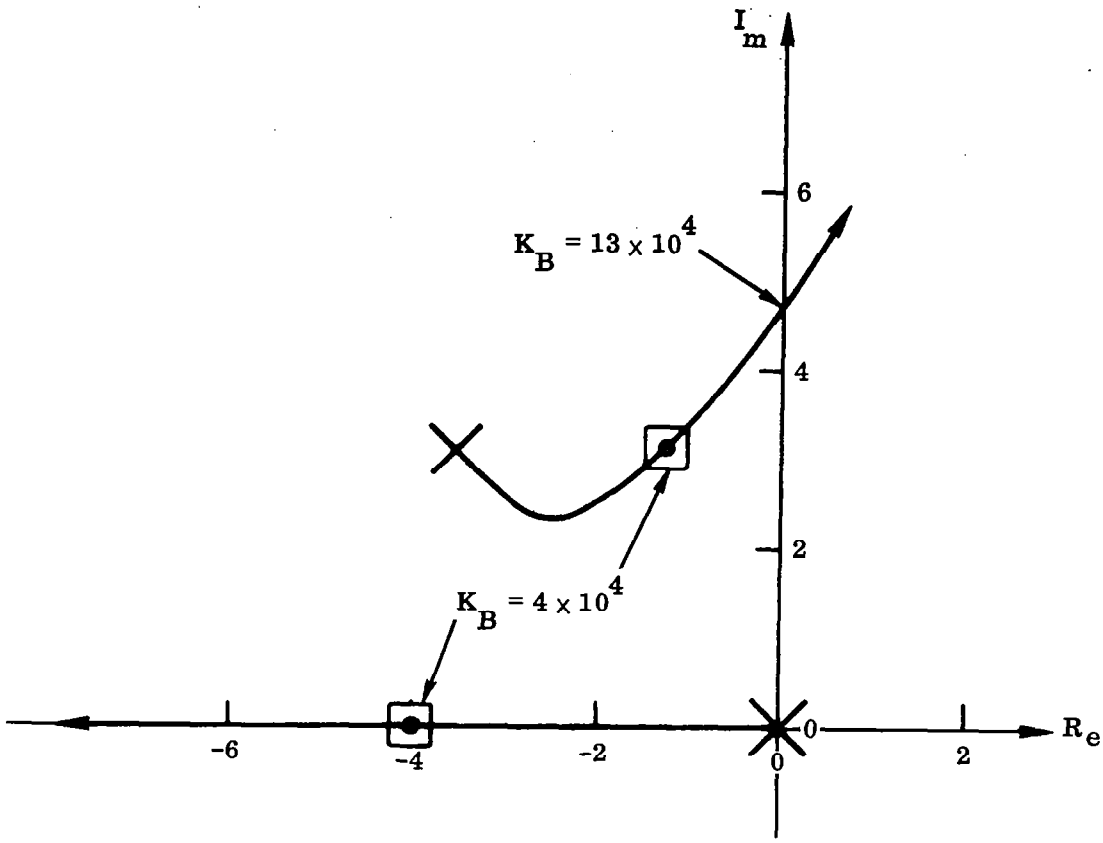

Figure 12. Root Locus Plot for Yaw Rate Control System

$$\dot{\psi} = q \sin\varphi + r \cos\varphi \tag{92}$$

or, equivalently,

$$q = \dot{\theta} \cos\varphi + \dot{\psi} \sin\varphi \tag{93}$$

$$r = \dot{\psi} \cos\varphi - \dot{\theta} \sin\varphi \tag{94}$$

For simplicity, we put

$$C_x = C_y = C$$

$$\Omega_x = \Omega_y = \Omega \tag{95}$$

Notice that there is no gyrotorquer on the Z_b axis since we will not attempt to control spin rates about X_b.

Eqs. (35) then take the form

$$p \equiv p_o = \dot{\varphi} = \text{constant} \tag{96}$$

$$I_y \dot{q} + p_o r (I_x - I_z) = -2 C_x \Omega_x \dot{\delta}_x + 2 C_y \Omega_y p_o \delta_y + L_y \tag{97}$$

$$I_z \dot{r} + p_o q (I_y - I_x) = -2 C_y \Omega_y \dot{\delta}_y - 2 C_x \Omega_x p_o \delta_x + L_z \tag{98}$$

If we we let

$$a = p_o \frac{(I_y - I_x)}{I_y} \tag{99}$$

the preceding equations may be written as

$$\dot{q} - ar = \frac{1}{I}\left[L_y - 2C\Omega(\dot{\delta}_x - p_o \delta_y)\right] \tag{100}$$

$$\dot{r} + aq = \frac{1}{I}\left[L_z - 2C\Omega(\dot{\delta}_y + p_o \delta_x)\right] \tag{101}$$

where, for simplicity, we have assumed that $I_y = I_z$.

In the absence of applied torques, these reduce to

$$\dot{q} - ar = 0 \tag{102}$$

$$\dot{r} + aq = 0 \tag{103}$$

and we have the classical problem of the force-free motion of a spinning body, which is treated extensively in standard texts.[4] The characteristic equation for the system (102), (103) is

$$s^2 + a^2 = 0 \tag{104}$$

where the quantity "a" is termed the wobble frequency. This wobbling motion may be damped out in various ways. A passive control scheme for doing this is considered in Subsection 3.4.2. The problem to be treated here is one of active control whereby gyrotorquers are used to give a "tight" control. A choice between the two depends on the specific mission, which involves a tradeoff between the power required for active devices versus the simplicity and reliability of passive techniques.

The choice of a suitable control law for the coupled system (100), (101) is not as simple as for the uncoupled case. Assuming that $L_y = L_z = 0$, we may write Eqs. (100) and (101) in matrix form as follows

$$\begin{bmatrix} s & -a \\ a & s \end{bmatrix} \begin{bmatrix} q \\ r \end{bmatrix} = -\frac{2C\Omega}{I_y} \begin{bmatrix} s & -p_o \\ p_o & s \end{bmatrix} \begin{bmatrix} \delta_x \\ \delta_y \end{bmatrix} \tag{105}$$

Therefore, if we define

$$U = \begin{bmatrix} s & -a \\ a & s \end{bmatrix}$$

$$W = \frac{2C\Omega}{I_y} \begin{bmatrix} s & -p_o \\ p_o & s \end{bmatrix}$$

$$y = \begin{bmatrix} q \\ r \end{bmatrix} \qquad u = \begin{bmatrix} \delta_x \\ \delta_y \end{bmatrix}$$

a vector matrix feedback control loop of the type shown in Fig. 13 could be formulated. The problem is in the proper selection of the elements of the compensation matrix V, which are, in general, a function of the Laplace operator, s. Although some theoretical studies for systems of this type are available,[31, 32] there is little that can be called routine in the way of synthesis. At present, the most workable techniques are mostly

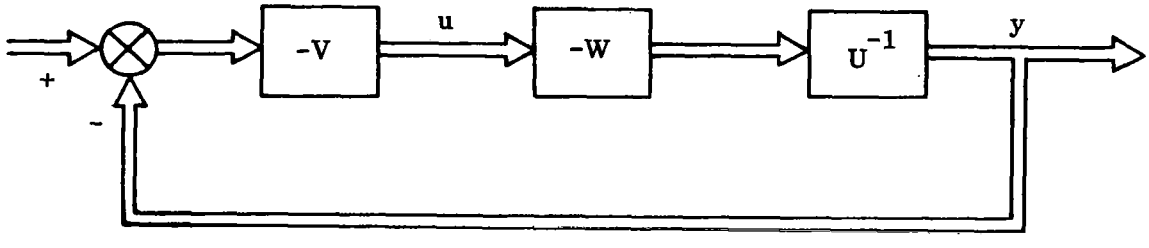

Figure 13. Matrix Feedback Control Loop

intuitive and based on extrapolation from single-input/single-output systems. To simplify the problem for purposes of preliminary analysis, we assume that gyrotorquer dynamics may be neglected. Thus we assume that in Fig. 11

$$\frac{\delta}{V_c} = K_1$$

We now postulate a control law of the form

$$\delta_x = \frac{K_1 K_B}{s} q + K_2 r \tag{106}$$

$$\delta_y = \frac{K_1 K_B}{s} r - K_2 q \tag{107}$$

Substituting these in Eqs. (100) and (101),* we obtain for the characteristic equation of the system

$$(1+\gamma^2)s^4 + 2\left[\lambda + \gamma p_o(1-\sigma)\right]s^3 + \left[\lambda^2 + p_o^2(\sigma^2+\gamma^2)\right]s^2$$

$$+ 2p_o^2\lambda\sigma s + p_o^2\lambda^2 = 0 \tag{108}$$

where

$$\sigma = 1 - \frac{I_x}{I_y} \tag{109}$$

$$\lambda = \frac{2C\Omega K_1 K_B}{I_y} \tag{110}$$

$$\gamma = \frac{2C\Omega K_2}{I_y} \tag{111}$$

The usual configuration for a spinning manned space station is such that $I_x > I_y$, which means that σ is negative. Noting that necessary (but not sufficient) conditions for stability are that

*with $L_y = L_z = 0$

$$b_0 = \lambda\sigma > 0 \tag{112}$$

$$b_1 = \lambda + \gamma p_o(1 - \sigma) > 0 \tag{113}$$

we see that if σ is negative then we must take $\lambda < 0$ and $\gamma > 0$. The sufficient conditions for stability are found from the Routh criterion, viz.

$$b_2 = \lambda^2 + p_o^2\left[\sigma^2 + \gamma^2 - \frac{\lambda\sigma}{b_1}(1 + \gamma^2)\right] > 0 \tag{114}$$

$$b_3 = \lambda\sigma - \frac{\lambda^2 b_1}{b_2} > 0 \tag{115}$$

The gain parameters, λ and γ, remain to be determined. It will facilitate the discussion if we consider a specific case, namely, the Manned Orbital Space Station (MOSS) for which the basic data is[33]

$$I_y = I_z = 9.1 \times 10^6 \quad \text{slug ft}^2$$

$$I_x = 16.7 \times 10^6 \quad \text{slug ft}^2$$

$$p_o = 1/3 \text{ rad/sec}$$

$$2C\Omega = 5 \times 10^4 \quad \text{slug ft}^2/\text{sec}$$

$$\sigma = -0.835$$

If we take $\lambda = -2$ and $\gamma = 6$, we find

$$b_1 = 1.67$$

$$b_2 = 3.97$$

$$b_3 = -0.01$$

which indicates instability. However, with $\lambda = -2$ and $\gamma = 9$, we obtain

$$b_1 = 3.505$$

$$b_2 = 8.74$$

$$b_3 = 0.07$$

Thus, with these parameters we have a stable system. While the Routh scheme permits one to determine whether or not we have a stable condition, it provides no insight into the degree of stability or the characteristics of the time response. For this purpose, a root locus study is desirable. However, an inspection of the characteristic equation (108) does not reveal any feasible way to isolate γ so that the equation may be put in a form suitable for root locus study.

We may, however, proceed as follows. When $\gamma \to 0$, Eq. (108) reduces to

$$s^4 + 2\lambda s^3 + (\lambda^2 + p_o^2\sigma^2)s^2 + 2p_o^2\lambda\sigma s + p_o^2\lambda^2 = 0 \tag{116}$$

while for $\gamma \to \infty$, it becomes

$$s^2(s^2 + p_o^2) = 0 \tag{117}$$

The roots of Eq. (116) are the poles, and the roots of Eq. (117) are the zeros of the root locus of (108) as a function of the gain, γ. Typically, (116) has a pair of complex roots in the left half plane and a pair in the right half plane. The root locus would then appear as shown in Fig. 14.

It is apparent that as long as γ exceeds some minimum value, the system is stable for all values of γ no matter how large.* Actually this could also be inferred from the Routh conditions (112) - (115). Note that for very large γ,

$$b_1 \approx \lambda p_o(1-\sigma)$$

$$b_2 \approx p_o^2\gamma^2$$

$$b_3 \approx \gamma\sigma$$

Therefore, the Routh coefficients are always positive as long as $\lambda < 0$ and $\sigma < 0$. A basic feel for the required gains, λ and γ, could be obtained by running a check similar to the above for a set of values of λ. This would serve to establish a preliminary set of control system parameters which could be further refined as the simulation is expanded to include other dynamic effects.

It should be noted also when going to the complete system that gyrotorquer saturation will occur when δ_x or δ_y approaches 90 deg. Reaction (mass-expulsion) devices may then be employed to desaturate the system in the manner shown in Fig. 7, except that now a rotor angle (rather than flywheel speed) is used as the desaturation signal.

*It must be remembered that we are dealing with an approximation to the real system. Actually, the inclusion of sensor and actuator dynamics would place an upper limit on allowable γ.

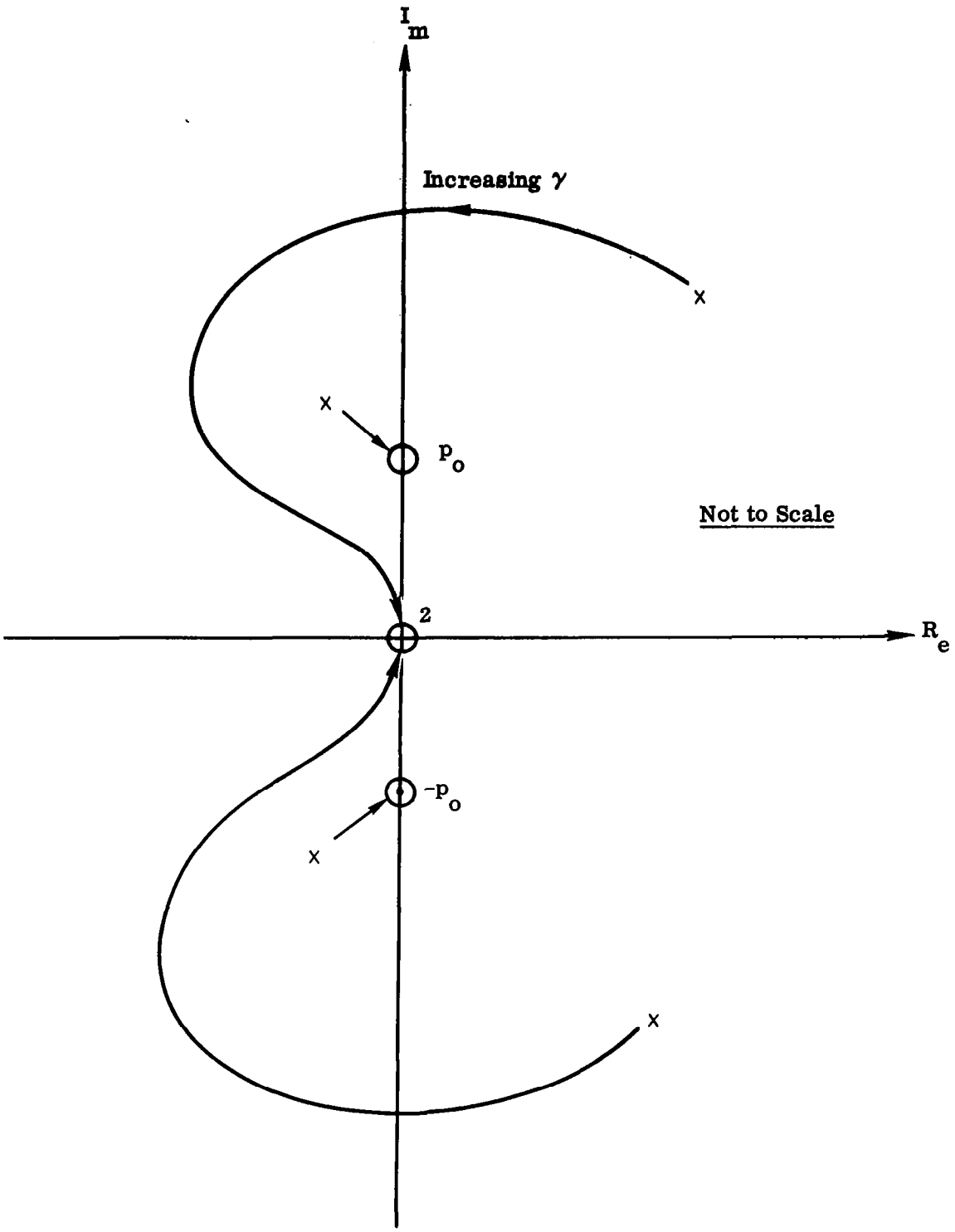

Figure 14. Root Locus as a Function of γ

The discussion thus far has centered mainly on the rate-stabilization problem. The synthesis of the attitude control loop will generally depend on the specific mission. Thus a particular design will vary in implementation, if not in concept, depending on whether coarse or fine pointing accuracy is required. This will also be influenced by the sensing and actuation methods employed. In any event, momentum-exchange devices (flywheels, gyrotorquers) may not be used to change the orientation of the satellite spin vector. This is of course due to the fact that the vector sum of the control and vehicle angular momenta remain constant in the absence of external torque (principle of angular momentum).

For a nonspinning satellite, a simple additional loop for attitude control may be added to the schematic of Fig. 11 to give the form shown in Fig. 15. Conventional linear design techniques may be used to determine appropriate gains and filters to achieve satisfactory performances.

Some information on the properties of attitude sensors is given in Appendix E.

3.3.3 Mass Expulsion

Conceptually, the simplest means of orienting the satellite is by placing pairs of mass-expulsion devices (reaction jets) about each of the control axes. However, since fuel storage is limited, this procedure is not used for conventional attitude control. The momentum-exchange devices are more efficient for this purposes.

Primarily, reaction jets are used for

a. Detumbling.

b. Desaturation of momentum-exchange devices.

c. Orienting the spin vector of the satellite.

It has already been noted in Subsection 3.3.2 that momentum-exchange devices are incapable of reorienting the spin vector of a spinning satellite. When such a mode of operation is required, the use of an externally applied torque, such as reaction jets, is mandatory. This is then incorporated as the basic power element in an attitude control loop.

The use of reaction jets for desaturating control flywheels has been mentioned in Subsection 3.3.1. A typical configuration is shown in Fig. 7, and a similar scheme may be used for gyrotorquers.

The tumbling situation arises when the satellite is first placed in orbit and is rotating with respect to inertial space at some arbitrary angular velocity. The first problem, prior to implementing any type of attitude control, is to remove by some means this angular velocity.

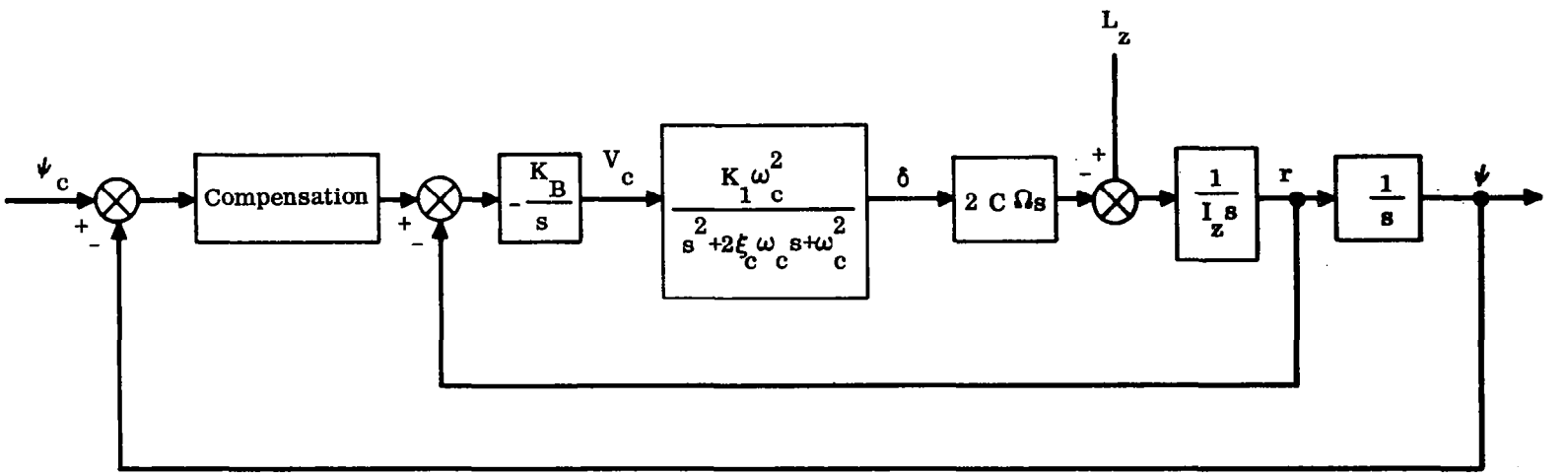

Figure 15. Yaw Attitude Control System

Assuming that the orbital angular velocity is small compared with the tumbling angular velocity, the motion of the satellite, in the absence of control or disturbance torques, is obtained from Eqs. (36) as

$$I_x \dot{p} + q r (I_z - I_y) = 0 \tag{118}$$

$$I_y \dot{q} - p r (I_z - I_x) = 0 \tag{119}$$

$$I_z \dot{r} + p q (I_y - I_x) = 0 \tag{120}$$

If we represent the control torques due to the reaction jets about each of the body axes by L_{cx}, L_{cy}, L_{cz}, then, if rate gyros are available to measure the rates (p, q, and r), we may take for a control law

$$\begin{aligned} L_{cx} &= -k_x p \\ L_{cy} &= -k_y q \\ L_{cz} &= -k_z r \end{aligned} \tag{121}$$

where k_x, k_y, and k_z are positive constants.

Combining (121) with Eqs. (118) - (120), the result may be expressed in vector notation as

$$\frac{d}{dt}\left[I \cdot \bar{\omega}_b \right] + k \cdot \bar{\omega}_b = 0 \tag{122}$$

where I is the inertial dyadic, and

$$k = k_x \bar{i}_b \bar{i}_b + k_y \bar{j}_b \bar{j}_b + k_z \bar{k}_b \bar{k}_b$$

From this, it is easy to show that[47]

$$\lim_{t \to \infty} \left[\bar{\omega}_b (t) \right] = 0 \tag{123}$$

Thus, the control law (121) reduces the spin to zero. In practice, the reaction jets may be de-energized when the spin is reduced to a predetermined level.

A control of the type (121) implies throttleable jets. In practice, this is difficult to implement, and indeed it is an unessential requirement. It is sufficient to formulate the control law as*

$$L_{cx} = -k_x \operatorname{sgn} p$$

$$L_{cy} = -k_y \operatorname{sgn} q \tag{124}$$

$$L_{cz} = -k_z \operatorname{sgn} r$$

The asymptotic stability of the resulting system may be established by the Lyapunov method.[48]

Actually, a control law of the form (124) usually results when one seeks to determine the control function which optimizes the system in some fashion (e.g., minimum fuel required to reduce $\bar{\omega}_b$ to zero).[49]

The calculation of the fuel weight necessary to accomplish certain objectives is an important part of the attitude control study. If, for any mode of operation, the thrust history as a function of time is known, then from the relation

$$T = \frac{\dot{w}}{g_o} V_e = \dot{w} I_{sp} \tag{125}$$

T = thrust

$\dot{w}$ = fuel rate

g_o = gravity acceleration at earth's surface

V_e = exhaust velocity of propellant

I_{sp} = specific impulse of propellant (fuel)

we may calculate the required fuel weight by

$$w = \int \frac{T}{I_{sp}} dt \tag{126}$$

*$\operatorname{sgn} A = +1$ if $A > 0$
$= -1$ if $A < 0$

Consider, for example, the problem of calculating the weight of fuel required for a reorientation maneuver. Assuming that initial spin rates are zero, and that two jets a distance ℓ apart are available to torque the vehicle, say about the Y_b axis, the motion is described by

$$2T\ell = I_y\ddot{\theta} \tag{127}$$

To bring the angular rate to zero at the completion of the maneuver, a thrust application in the opposite direction will be necessary at some intermediate point, after which the equation of motion is

$$-2T\ell = I_y\ddot{\theta} \tag{128}$$

The initial conditions for (127) are

$$\theta(0) = 0, \qquad \dot{\theta}(0) = 0$$

which means that (127) has the solution

$$\theta = \frac{T\ell t^2}{I_y} \tag{129}$$

$$\dot{\theta} = \frac{2T\ell t}{I_y} \tag{130}$$

If thrust is reversed at time t_1, then the initial conditions for (128) are

$$\theta(t_1) = \theta_1 = \frac{T\ell t_1^2}{I_y}$$

$$\dot{\theta}(t_1) = \dot{\theta}_1 = \frac{2T\ell t_1}{I_y}$$

and (128) has the solution

$$\theta = -\frac{T\ell}{I_y}(t^2 - 4t_1 t + 2t_1^2) \tag{131}$$

$$\dot{\theta} = -\frac{2T\ell}{I_y}(t - 2t_1) \tag{132}$$

It follows from these relationships that when $t = 2t_1 \equiv t_T$,

$$\theta(t_T) \equiv \theta_T = 2\theta_1$$

$$\dot{\theta}(t_T) \equiv \dot{\theta}_T = 0$$

Thus, in order to rotate the vehicle by an amount θ_T, a positive torque is applied by the reaction jets until $\theta = \frac{\theta_T}{2}$, at which point thrust is reversed and then shut off at $\theta = \theta_T$. In this way the angular velocity is zero when the vehicle reaches the desired position.

The thrust magnitude required for the maneuver is

$$T = \frac{I_y \theta_T}{2\ell t_1^2} = \frac{2 I_y \theta_T}{\ell t_T^2} \tag{133}$$

Using (126), the fuel weight for one reaction jet is found to be

$$w = \int_o^{t_T} \frac{2 I_y \theta_T}{I_{sp} \ell t_T^2} dt$$

$$= \frac{2 I_y \theta_T}{I_{sp} \ell t_T}$$

Therefore, the total fuel weight required (two reaction jets) is

$$w_{tot} = \frac{4 I_y \theta_T}{I_{sp} \ell t_T} \tag{134}$$

This result is sometimes expressed in terms of the "required momentum for vehicle positioning" as follows

$$H_T \equiv w_{tot} I_{sp} \ell = \frac{4 I_y \theta_T}{t_T} \tag{135}$$

This equation is plotted in Fig. 16 for selected values of t_T.

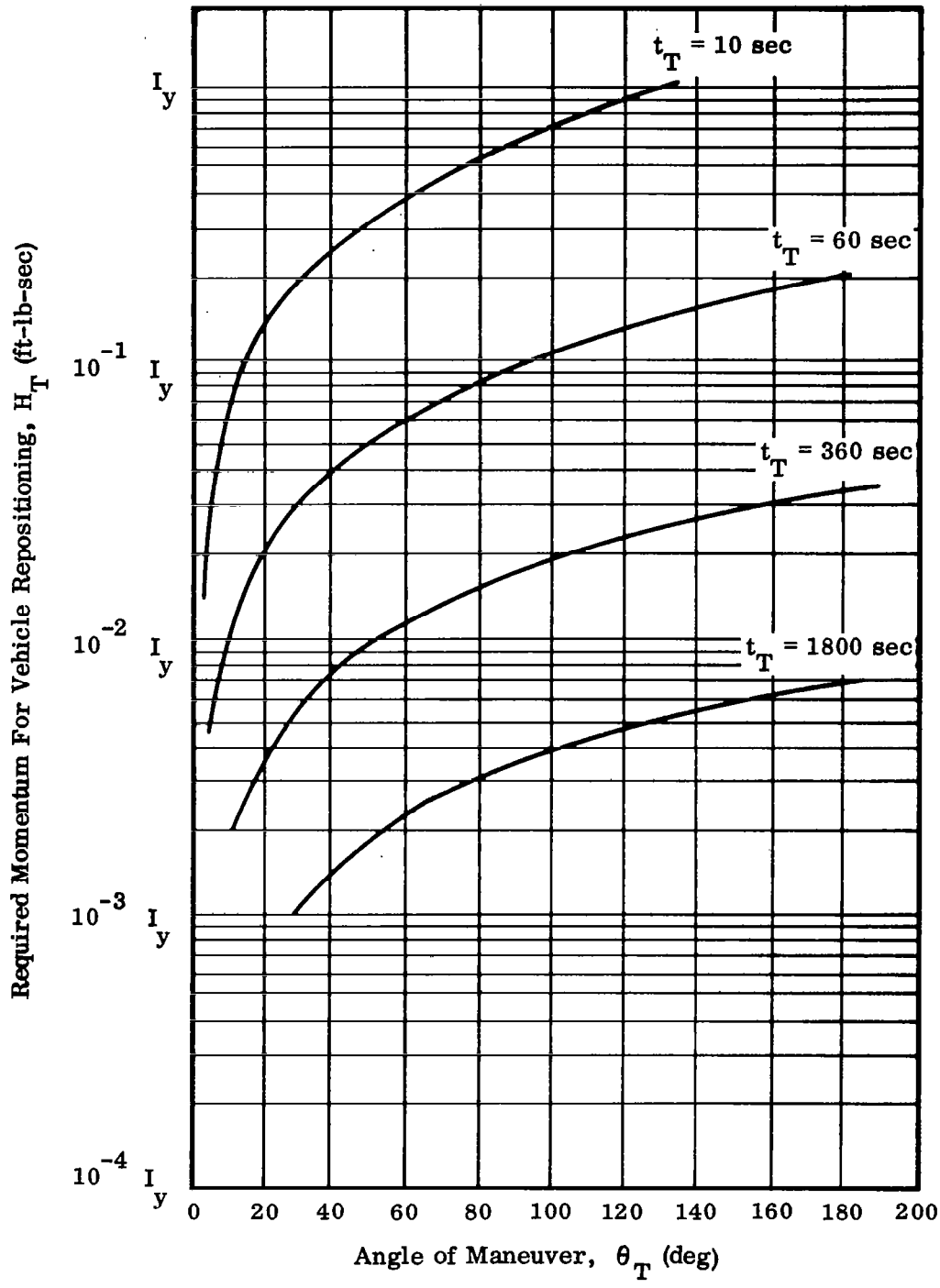

Figure 16. Momentum Required for Vehicle Maneuvering

In certain situations it is expedient to employ reaction jets in an on-off type of attitude control system. The resulting attitude motion is then characterized by a limit cycle of the type shown in Fig. 17. This means that fuel is being continually expended and it is necessary to estimate the fuel required for a specified time of operation.

Proceeding in a manner similar to the above, we find that the fuel expended per cycle is

$$w_{cycle} = \frac{4 I_y (\Delta \dot{\theta})}{I_{sp} \ell} \tag{136}$$

Over any long period of operation, t_c, the weight of fuel consumed in limit-cycle operation is

$$W = \frac{t_c}{p} w_{cycle}$$

$$= \frac{4 I_y t_c (\Delta \dot{\theta})}{I_{sp} \ell P} \tag{137}$$

where P is the period of the limit cycle.

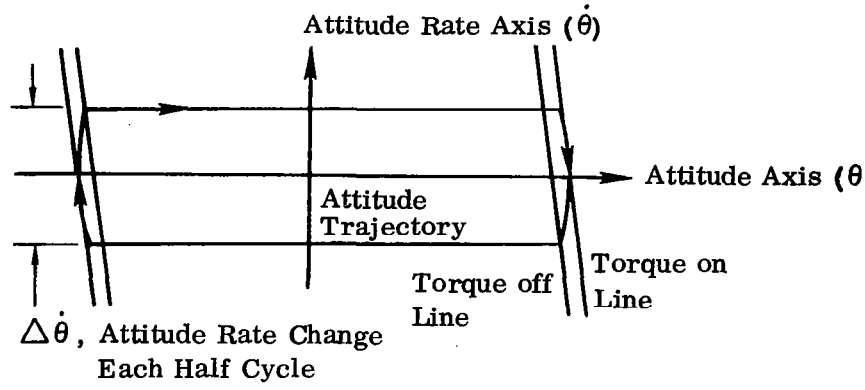

Figure 17. Phase Plane Showing Attitude Limit Cycle

Now, during one of the limit cycle coast trajectories the motion is described by

$$I_y \ddot{\theta} = 0$$

$$\theta(0) = \theta_o, \qquad \dot{\theta}(0) = -\dot{\theta}_o$$

Hence, during this time θ is given by

$$\theta - \theta_o = -\dot{\theta}_o t$$

which means that when $\theta = -\theta_o$, the corresponding time is

$$t = \frac{2\theta_o}{\dot{\theta}_o} = \frac{2\theta_o}{\left(\frac{\Delta\dot{\theta}}{2}\right)} = \frac{4\theta_o}{\Delta\dot{\theta}}$$

Consequently, if the "torque on" time is small compared with the period, P, then

$$P = \frac{8\theta_o}{\Delta\dot{\theta}} \tag{138}$$

where $\pm\theta_o$ denotes the deadband limits.

The total weight consumed in limit-cycle operation over a time period, t_c, is therefore

$$W = k_T t_c (\Delta\dot{\theta})^2 \tag{139}$$

where

$$k_T = \frac{I_y}{2 I_{sp} \ell \theta_o}$$

3.4 PASSIVE CONTROL

For long lifetime satellite missions, the use of active devices for attitude control is not desirable, for obvious reasons. In this respect, the use of passive techniques appears attractive especially when pointing accuracy requirements are not stringent. One simple means of maintaining attitude in space is to provide a spin about the axis which is to be controlled. Other techniques involve some sort of interaction with the satellite environment. Among these are gravitational gradient, magnetic, and

radiation pressure control. In all these systems, an undamped oscillation about the control axis results from the action of external torque disturbances. A necessary part of the design is therefore a means of damping out these oscillations. Two typical passive control systems are described in the following subsections.

3.4.1 Gravity Gradient

The basic principle of orientation by gravity gradient is that a body in a gravitational field, having one moment of inertia less than the other two, will experience a torque tending to align the axis of least inertia with the field direction.

This action may be easily established as follows. With reference to Fig. 18, suppose that a body is in a circular orbit of radius, R_o, about the earth. We define a reference coordinate system ($\bar{i}_r$, $\bar{j}_r$, $\bar{k}_r$) such that $\bar{k}_r$ is always directed radially toward the earth, and whose origin coincides with the mass center of the body. Then the vector radius $\bar{R}$ has components in the reference coordinate frames as follows

$$\bar{R} = -R_o \bar{k}_r$$

$$= R_x \bar{i}_b + R_y \bar{j}_b + R_z \bar{k}_b \qquad (140)$$

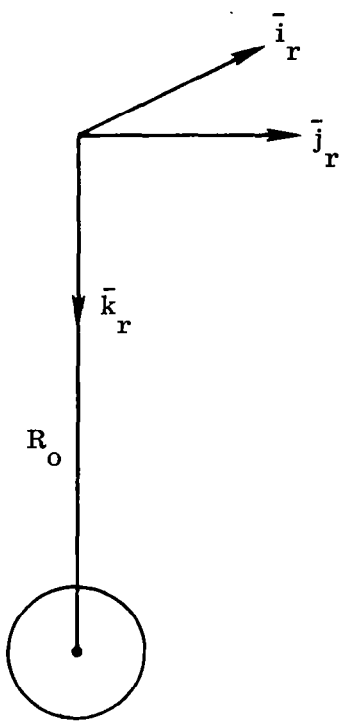

Figure 18. Orbit Reference Frame

These components are related by the rotation matrix of Eq. (1), viz.

$$\begin{bmatrix} R_x \\ R_y \\ R_z \end{bmatrix} = C_b^r \begin{bmatrix} 0 \\ 0 \\ -R_o \end{bmatrix} \qquad (141)$$

In expanded form

$$R_x = R_o \sin\theta$$

$$R_y = -R_o \sin\varphi\cos\theta \qquad (142)$$

$$R_z = -R_o \cos\varphi\cos\theta$$

Now let $\bar{\rho}$ denote the radius vector from the body's center of mass to a generic mass element, dm.

$$\bar{\rho} = x\bar{i}_b + y\bar{j}_b + z\bar{k}_b \tag{143}$$

Then the radius vector from the earth's center to this mass element is

$$\bar{r} = \bar{R} + \bar{\rho} \tag{144}$$

The force due to gravity on a mass element is

$$d\bar{F} = -\frac{\mu\, dm}{r^3}\bar{r} \tag{145}$$

where

$$\mu = G M_e$$

$$= g_e R_e^2$$

$$= 1.407 \times 10^{16} \text{ ft}^3/\text{sec}^2$$

G = universal constant of gravity

M_e = mass of earth

g_e = gravity acceleration at earth's surface

R_e = radius of earth

This causes a torque about the mass center of the vehicle, given by

$$d\bar{L} = \bar{\rho} \times d\bar{F} = -\frac{\mu\, dm}{r^3}\bar{\rho} \times \bar{r}$$

$$= -\frac{\mu\, dm}{r^3}\bar{\rho} \times (\bar{R} + \bar{\rho})$$

$$= -\frac{\mu\, dm}{r^3}\bar{\rho} \times \bar{R} \tag{146}$$

Now since

$$r^2 = (\bar{R} + \bar{\rho}) \cdot (\bar{R} + \bar{\rho})$$

$$= R_o^2 + \rho^2 + 2\bar{R} \cdot \bar{\rho}$$

$$= R_o^2 \left[1 + \left(\frac{\rho}{R_o} \right)^2 + \frac{2\bar{R} \cdot \bar{\rho}}{R_o^2} \right]$$

we may write

$$\frac{1}{r^3} = \frac{1}{R_o^3} \left[1 + \left(\frac{\rho}{R_o} \right)^2 + \frac{2\bar{R} \cdot \bar{\rho}}{R_o^2} \right]^{-3/2}$$

The second term inside the brackets may be discarded since it is usually negligible compared to unity. Expanding the resulting expression and dropping higher order terms, we obtain

$$\frac{1}{r^3} = \frac{1}{R_o^3} \left(1 - \frac{3\bar{R} \cdot \bar{\rho}}{R_o^2} \right)$$

After this is substituted in (146), the latter becomes

$$d\bar{L} = -\frac{\mu\, dm}{R_o^3} \left(1 - \frac{3\bar{R} \cdot \bar{\rho}}{R_o^2} \right) \bar{\rho} \times \bar{R} \tag{147}$$

Integrating:

$$\bar{L} = -\frac{\mu}{R_o^3} \int (\bar{\rho}\, dm) \times \bar{R} + \frac{3\mu}{R_o^2} \int \frac{(\bar{R} \cdot \bar{\rho})(\bar{\rho} \times \bar{R})}{R_o^2}\, dm$$

The first term on the right-hand side of this expression is zero since, by assumption, the origin of the body frame is at the mass center. Therefore, the above reduces to

$$\bar{L} = \frac{3\mu}{R_o^5} \int (\bar{R} \cdot \bar{\rho})(\bar{\rho} \times \bar{R})\, dm \tag{148}$$

Using (140), (142), and (143), and performing the indicated vector operations, the final result in scalar form is

$$L_x = \frac{3\mu}{2R_o^3}(I_z - I_y)\sin 2\varphi \cos^2\theta \tag{149}$$

$$L_y = \frac{3\mu}{2R_o^3}(I_z - I_x)\sin 2\theta \cos\varphi \tag{150}$$

$$L_z = \frac{3\mu}{2R_o^3}(I_x - I_y)\sin 2\theta \sin\varphi \tag{151}$$

Here

$$I_x = \int (y^2 + z^2)\, dm, \text{ etc.}$$

and the product-of-inertia terms,

$$I_{xy} = \int xy\, dm$$

are zero since the principal moments of inertia are on the body axes. Eqs. (149) - (151) are the gravitational torques acting on the body.

The angular momentum of a body in a circular orbit satisfies the relationship[4]

$$\sqrt{\mu R_o} = R_o^2 \omega_s$$

where ω_s is the angular orbital velocity of the body. Consequently

$$\omega_s = \sqrt{\frac{\mu}{R_o^3}} \tag{152}$$

Substituting this in Eqs. (149) - (151) and making the small-angle approximation for φ and θ, we find

$$L_x = 3\omega_s^2 (I_z - I_y)\varphi \tag{153}$$

$$L_y = 3\omega_s^2 (I_z - I_x)\theta \tag{154}$$

$$L_z = 0 \tag{155}$$

If the orbit is in the x-z plane, then $\varphi = 0$ and $L_x = 0$. In this case the rotational motion of the body about its mass center is given by

$$I_y \ddot{\theta} = 3\omega_s^2 (I_z - I_x)\theta$$

or (assuming $I_x = I_y$)

$$\ddot{\theta} + 3\omega_s^2 \left[1 - \frac{I_z}{I_y}\right]\theta = 0 \tag{156}$$

Thus, as long as $I_z < I_y$, the body will execute simple harmonic motion about the local vertical (this motion is often called "libration").

However, in order to be useful as reference for local vertical, some means must be found to damp the oscillations. An active system could, of course, be used but this is contrary to the spirit of passive control. There are many schemes described in the literature for doing this.* Two of these will be described here.

The first one, due to Newton,[58] is based on the fact that an oscillatory motion difficult to damp directly can still be damped by coupling it strongly to another oscillation that can be damped.

Consider the configuration of Fig. 19. In it, a satellite of mass M is considered to be in counter-clockwise orbital motion, at a distance R_o from the center of the earth; let the line from the center of the earth to the satellite make the angle Φ with an inertial reference x axis. The long axis of the satellite makes the angle θ, positive in the sense shown in the figure, with the direction of R_o.

Suppose that a helical spring of length ℓ has one end attached to the outer end of the satellite, at a distance ℓ_M from its center of mass, and has its other end attached to a mass m. Assuming that the spring is always extended along a straight line, let δ be the angle between it and the satellite axis, which is positive as drawn in the figure. As the satellite librates, the outer end of the satellite tends to move relative to m, thus exciting longitudinal oscillations in the spring. Since it is possible to make the spring have high losses, and since it is impossible for the satellite to librate without making the spring oscillate, this system should provide damping of the libration.

The equations of motion for the system are readily obtained as follows. Assume that the origin of the inertial reference frame is at the center of the earth, and let (X_1, Z_1) denote the inertial coordinates of M, and (X_2, Z_2) the inertial coordinates of m.

---

*Cf. Refs. (58) - (64)

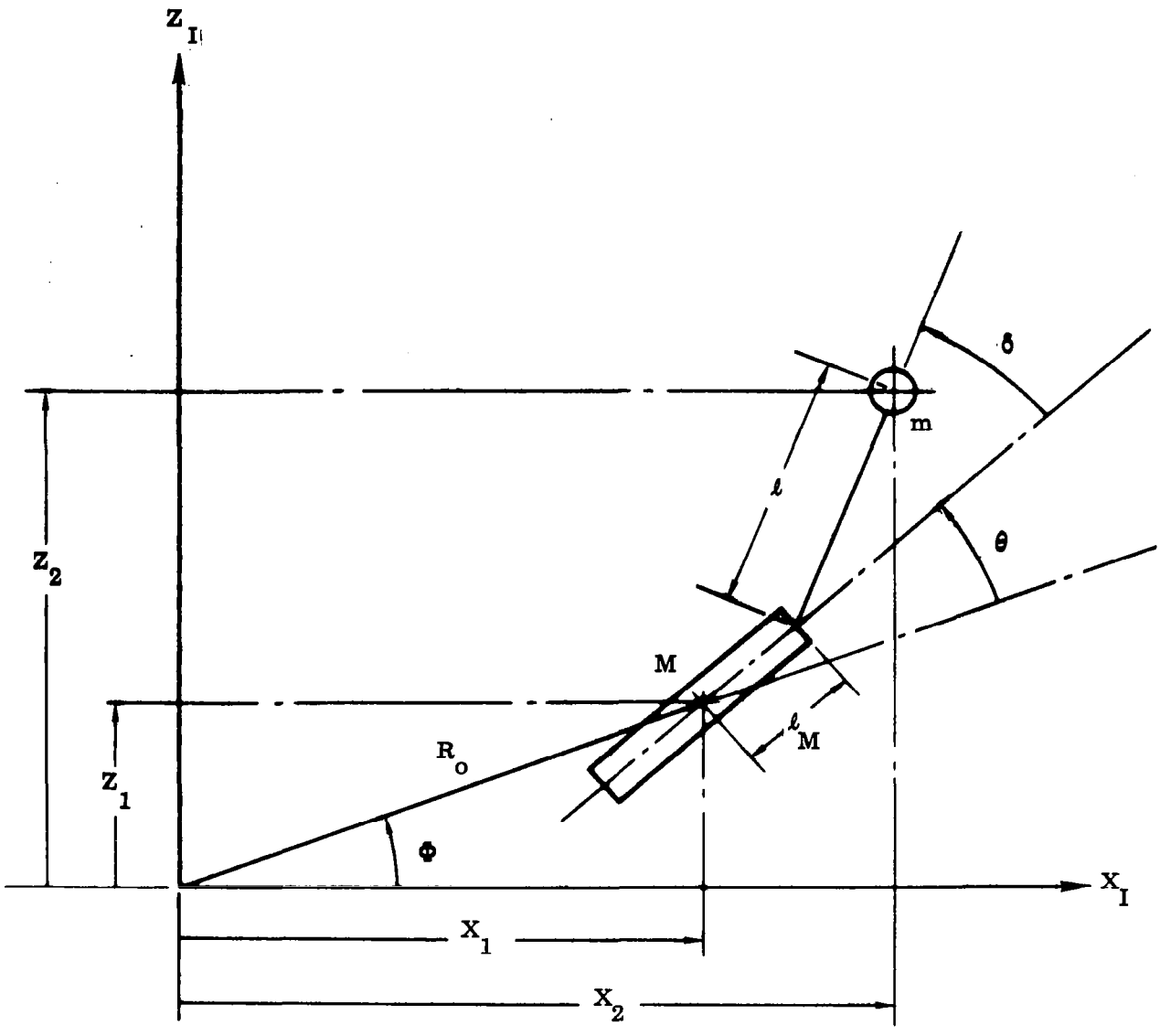

Figure 19. Configuration for Libration Damping

We then have

$$M\ddot{X}_1 = -\frac{M\mu}{R_o^3} X_1 + T\cos(\Phi + \theta + \delta) \tag{157}$$

$$M\ddot{Z}_1 = -\frac{M\mu}{R_o^3} Z_1 + T\sin(\Phi + \theta + \delta) \tag{158}$$

$$m\ddot{X}_2 = -\frac{m\mu}{r_2^3} X_2 - T\cos(\Phi + \theta + \delta) \tag{159}$$

$$m\ddot{Z}_2 = \frac{m\mu}{r_2^3} Z_2 - T\sin(\Phi + \theta + \delta) \tag{160}$$

where r_2 is the distance from m to the earth's center and T is the tension in the spring.

The satellite is subject to two torques; one is the libration (gravity-gradient) torque

$$-\frac{3\mu}{2R_o^3}(I_X - I_Z)\sin 2\theta$$

where I_X is the transverse moment of inertia, and I_Z is the axial (about the long axis) moment of inertia.

The other torque is due to the spring and is given by

$$T\ell_M \sin\delta$$

Consequently, the remaining equation of motion is

$$I_X(\ddot{\Phi} + \ddot{\theta}) = T\ell_M \sin\delta - \frac{3\mu}{2R_o^3}(I_X - I_Z)\sin 2\theta \tag{161}$$

Equations (157) - (161) completely describe the motion. They are, however, too cumbersome for purposes of preliminary analysis. Certain reasonable simplifying assumptions can be introduced. First of all, we assume that m and T are negligible compared with M. This has the effect of uncoupling Eqs. (157) - (158) from the set (159) - (161). In other words, the orbital motion is essentially unaffected by the libration of M and the oscillations in the spring.

We shall also assume that the orbit is circular. Thus R_o and $\dot{\Phi}$ are constant and we have immediately

$$X_1 = R_o \cos\Phi, \qquad \Phi = \omega_s t$$
$$Z_1 = R_o \sin\Phi, \qquad \omega_s = \left(\frac{\mu}{R_o^3}\right)^{1/2} \tag{162}$$

Now since $[R_o + \ell_M \cos\theta + \ell \cos(\theta + \delta)]$ is the coordinate of m along the direction of R_o (the local vertical), and $[\ell_M \sin\theta + \ell \sin(\theta + \delta)]$ is the perpendicular coordinate, we may eliminate the coordinates (X_2, Z_2) in favor of (ℓ, δ). At the same time, we approximate r_2 by the vertical coordinate $[R_o + \ell_M \cos\theta + \ell \cos(\theta + \delta)]$, thus neglecting quantities of order greater than one in ℓ_M/R_o and ℓ/R_o. Finally, assuming that θ and δ as well as their derivatives are small and that I_z/I_x is negligible compared to unity, Eqs. (159) - (161) take the form

$$\ddot{\ell} - 2\omega_s\left[\ell_M\dot{\theta} + \dot{\ell}(\theta + \delta) + \ell(\dot{\theta} + \dot{\delta})\right] - 3\omega_s^2(\ell_M + \ell) + \frac{T}{m} = 0 \tag{163}$$

$$\ell\ddot{\delta} + (\ell_M + \ell)\ddot{\theta} + \ddot{\ell}(\theta + \delta) + 2\dot{\ell}(\dot{\theta} + \dot{\delta}) + 2\omega_s\dot{\ell} + \frac{T}{m}(\theta + \delta) = 0 \tag{164}$$

$$\ddot{\theta} - \frac{\ell_M T}{I_x}\delta + 3\omega_s^2\theta = 0 \tag{165}$$

The tension in the spring is a function of $\dot{\ell}$ and ℓ. Assuming a linear spring and viscous damping, we take

$$T = k\ell + 2B\dot{\ell} \tag{166}$$

It should be noted that in the equilibrium position (that is, when all libration motion has ceased), the spring will not revert to its unstressed length. To see this, we calculate the equilibrium length of the spring by setting θ and δ, together with their derivatives equal to zero in Eqs. (163) - (165), and replacing T by its value from Eq. 166. The resulting value of ℓ is then found to be

$$\ell_o = \frac{\ell_M}{\left(\frac{k}{3\omega_s^2 m} - 1\right)} \tag{167}$$

The explanation of this is that, at equilibrium, when M and m are separated by the radial distance $\ell_M + \ell_o$, a tension must be supplied between them in order to keep them in circular orbits of different radii with the same period. One can easily

calculate that this needed tension is $3\,m\,\omega_s^2(\ell_M + \ell_o)$. Since the only source of tension is the spring, the spring tension $k\,\ell_o$ must equal the required tension. This result has the immediate corollary that $k > 3\,\omega_s\,m$ in order to have a stable system.

It is convenient to introduce a dimensionless time, defined by

$$\tau = \omega_s t \tag{168}$$

Then with

$$\alpha = \frac{k}{m\,\omega_s^2} \qquad \beta = \frac{B}{m\,\omega_s}$$

$$\lambda = \frac{\ell}{\ell_M} \qquad \lambda_o = \frac{\ell_o}{\ell_M} \tag{169}$$

$$\sigma = \frac{m\,\ell_M^2}{I_x}$$

Eqs. (163) - (166) become

$$\lambda'' = 2\theta' + 2\lambda(\theta' + \delta') - \alpha\lambda - 2\beta\lambda' + 3(1 + \lambda) \tag{170}$$

$$\lambda\delta'' = -\theta''(\lambda + 1) - 2\lambda'(\theta' + \delta') - 2\lambda' - 3(\theta + \delta) \tag{171}$$

$$\theta'' = \sigma(\alpha\lambda + 2\beta\lambda')\delta - 3\theta \tag{172}$$

where the primes denote derivatives with respect to τ.

In order to linearize these equations, we write

$$\lambda = \Lambda + \lambda_o \tag{173}$$

where λ_o is the reference (equilibrium) value of λ and Λ is a perturbation - assumed small.

Substituting (173) in Eqs. (170) - (172) and discarding higher order terms in Λ, δ, θ and their derivatives, we find

$$\Lambda'' + 2\beta\Lambda' + (\alpha - 3)\Lambda = 2(1 + \lambda_o)\theta' + 2\lambda_o\delta' - (\alpha - 3)\lambda_o + 3 \tag{174}$$

$$\lambda_o \delta'' + 2\lambda_o \delta' + 3\delta = -(\lambda_o + 1)\theta'' - 2\lambda_o \theta' - 3\theta - 2\Lambda' \tag{175}$$

$$\theta'' + 3\theta = \alpha\sigma(\Lambda + \lambda_o) \tag{176}$$

The problem now reduces to that of choosing α, β, and λ_o (or equivalently, m, B, and k) in such a way that the satellite librations are damped in the most effective manner. This is most conveniently investigated by examining the characteristic equation for the system (170) - (172), viz.

$$\nu^6 + \frac{1}{\lambda_o}\left[6(1+\lambda_o) + 4\lambda_o + 3\sigma(1+\lambda_o)^2\right]\nu^4$$

$$+\frac{3}{\lambda_o}\left[\lambda_o + 3\left(2+\frac{1}{\lambda_o}\right)(1+\lambda_o) + \left(7+\frac{3}{\lambda_o}\right)\sigma(1+\lambda_o^2)\right]\nu^2$$

$$+\frac{27(1+\lambda_o)}{\lambda_o^2}\left[1+\sigma(1+\lambda_o)\right] + \frac{\beta\nu}{\lambda_o}\Big\{2\lambda_o\nu^4 + 6\left[1+2\lambda_o+\sigma(1+\lambda_o)^2\right]\nu^2$$

$$+ 18(1+\lambda_o)\left[1+\sigma(1+\lambda_o)\right]\Big\} = 0 \tag{177}$$

For given values of α, and λ_o, an optimum β can be obtained from (177) by root locus methods. However, since there is latitude in the choice of both α and λ_o, an extensive numerical effort is required. It turns out, incidentally, that for practical values of α, λ_o, and β, the time required to damp out the librations is on the order of days. Thus, such a scheme is feasible only when the pointing accuracy requirements are not stringent.

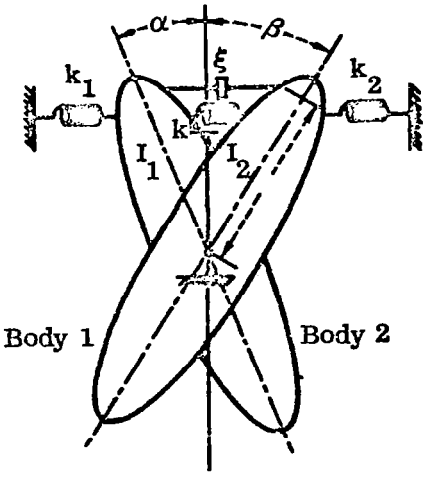

Figure 20. Lumped Parameter Model

Many other stabilization schemes can be devised which utilize the same principle. Zajac[59] considers a two-body satellite wherein the bodies are assumed joined at their mass center. It is assumed that the orbit is circular, and that the bodies are subject to gravitational torques as well as spring and viscous torques.

A lumped model of the resulting system is shown in Fig. 20. The inertias of bodies 1 and 2 are given by A_1 and A_2, ground is the rotating frame, the restoring

forces of the gravitational gradient are given by the springs k_1 and k_2, the coupling spring is k, and the damping coefficient is ζ. Body 2 is distinguished as the body with the higher natural "frequency," i.e., $(k_2/A_2) > (k_1/A_1)$, which includes the possibility that k_1 is negative. The damping rate clearly attains a maximum as the damping coefficient ζ is varied. For, as $\zeta \to 0$, an undamped system is approached. On the other hand, as $\zeta \to \infty$, the force required to pull A_1 and A_2 apart at any nonzero velocity approaches infinity. The bodies tend to stick together, and again the damping rate approaches zero.

It is also assumed that when the bodies are at rest in the rotating reference frame, their principal axes are along the local vertical, the tangent to the orbital path, and the normal to the orbital plane. Referring to Fig. 20, one easily derives the pertinent equations (for small motions) as follows.

$$A_1 \frac{d^2\alpha}{dt^2} + 3\omega_s^2 (B_1 - C_1)\alpha + k(\alpha - \beta) + \zeta\left(\frac{d\alpha}{dt} - \frac{d\beta}{dt}\right) = 0 \tag{178}$$

$$A_2 \frac{d^2\beta}{dt^2} + 3\omega_s^2 (B_2 - C_2)\beta - k(\alpha - \beta) - \zeta\left(\frac{d\alpha}{dt} - \frac{d\beta}{dt}\right) = 0 \tag{179}$$

where α and β are deviations from the local vertical, A_1, A_2, B_1, B_2, C_1, C_2 are the principal moments of inertia of the two bodies, ω_s is the orbital frequency, k is the spring constant of the coupling spring, and ζ is the damping coefficient. The gravitational "spring constants" (k_1 and k_2 in the model, Fig. 20) are given by $k_1 = 3\omega_s^2 (B_1 - C_1)$ and $k_2 = 3\omega_s^2 (B_2 - C_2)$.

If $(B_1 - C_1)/A_1 = (B_2 - C_2)/A_2$ (the bodies have the same natural frequencies when uncoupled), then the fundamental mode of Eqs. (178), (179) is undamped. Hence, in a damped case, these inertia ratios cannot be equal. The body with the greater inertia ratio is designated by the subscript 2, i.e., $(B_1 - C_1)/A_1 < (B_2 - C_2)/A_2$. Then, making the following change of variables

$$\sigma_1 = \frac{B_1 - C_1}{A_1} \qquad \tau = \omega_s (3\sigma_2 t)^{1/2}$$

$$\sigma_2 = \frac{B_2 - C_2}{A_2} \qquad \frac{\sigma_1}{\sigma_2} = U$$

$$F = \frac{k}{3\sigma_2 A_1 \omega_s^2} \qquad G = \frac{\zeta}{A_1 \omega_s (3\sigma_2)^{1/2}} \tag{180}$$

$$\gamma = A_1/A_2$$

Equations (178), (179) become

$$\alpha'' + G\alpha' + (U + F)\alpha = F\beta + G\beta' \tag{181}$$

$$\beta'' + \gamma G\beta + (1 + \gamma F)\beta = \gamma(F\alpha + G\alpha') \tag{182}$$

where

$$(\ )' \equiv \frac{d}{d\tau}(\ )$$

The characteristic equation for this system is

$$\nu^4 + \left[1 + U + (1+\gamma)F\right]\nu^2 + \left[U + (1+\gamma U)F\right] + G\nu\left[(1+\gamma)\nu^2 + (1+\gamma U)\right] = 0 \tag{183}$$

Here again, the damping parameter, G, occurs linearly so that root locus methods suggest themselves as the appropriate means for obtaining an optimum relative damping factor. Zajac shows that an upper bound on the damping rate is given by

$$t_o \lesssim \frac{0.86}{\omega_s} \tag{184}$$

where t_o is the time required for the oscillation amplitude to be reduced by a factor of 1/e.

3.4.2 Spin Stabilization

Spin stabilization is an accepted means of maintaining vehicle attitude, since a spinning body has a natural resistance to torques about axes other than the spin axis. However, a spin-stabilized body will generally exhibit conical wobble or free precession of its spin axis because of imperfections in the spacecraft ejection process and because of various internal and external disturbances such as crew motions, equipment deployment, docking transients, etc.

Most spin-stabilized vehicles will require that the spin axis be aligned with one of the principal axes within a minimum degree of tolerance. This is particularly true of photographic satellites, where any slight misalignment between spin and optical axes would impair the quality and interpretability of the photographs being taken. In the absence of an active system, a passive damper performs the function of dissipating the energy associated with wobble of the spin axis, eventually causing the spin axis to align itself in a desired attitude within preset limits.

The passive damper can be mechanized in various ways.[8, 61] The scheme to be considered here is due to Wadleigh [60] and utilizes a relatively small mass-spring arrangement, wherein the mass can be excited into large-amplitude motion on a confined shaft or guide.

The main idea is based on the fact that for a spinning body with the spin moment of inertia larger than the lateral moments of inertia, the removal of energy from the system is dynamically stabilizing and will cause a decrease in the amplitude of nutation. The reverse is true when the spin moment of inertia is less than the lateral moments of inertia. This may be readily established as follows. Let the X_b body axis be the spin axis and assume that $I_y = I_z$. In the absence of applied torques, the motion is described by*

$$\dot{q} - ar = 0 \tag{185}$$

$$\dot{r} + aq = 0 \tag{186}$$

where

$$a = p_o \frac{(I_y - I_x)}{I_y} \tag{187}$$

and $p_o \equiv$ const.

A solution of (102, (103) is given by

$$q = N \sin at \tag{188}$$

$$r = N \cos at \tag{189}$$

where N is the amplitude of nutation

The angular momentum of the system is then

$$\bar{H} = I \cdot \bar{\omega}_b$$

or

$$H^2 = I_x^2 p_o^2 + I_y^2 q^2 + I_z r^2$$

*See Eqs. (102) and (103) in Subsection 3.3.2.

$$= I_x^2 p_o^2 + I_y^2 (q^2 + r^2)$$

$$= I_x^2 p_o^2 + I_y^2 N^2 \tag{190}$$

The kinetic energy is

$$\text{K.E.} = \frac{1}{2}\left[I_x p_o^2 + I_y q^2 + I_z r^2\right]$$

$$= \frac{1}{2}\left[I_x p_o^2 + I_y N^2\right] \tag{191}$$

Using (190) to eliminate p_o from this expression, we obtain

$$\text{K.E.} = \frac{1}{2 I_x}\left[H^2 + (I_x - I_y) I_y N^2\right] \tag{192}$$

Now the motion of passive parts within the satellite will not change the angular momentum of the system, but it may decrease the kinetic energy because of frictional losses. From (192) we see that if $I_x > I_y$ a decrease in the kinetic energy is accompanied by a decrease in N, the amplitude of nutation. On the other hand, when $I_x < I_y$, a decrease in kinetic energy means an increase in N.

Therefore, in cases where the spin moment of inertia is less than the lateral moments, an active control system must be used to damp the wobble motion.

Consider now the wobble damper configuration shown in Fig. 21. The satellite equations of motion take the form

$$\dot{p} = \frac{L_x}{I_x} \tag{193}$$

$$\dot{q} - a r = \frac{L_y}{I_y} \tag{194}$$

$$\dot{r} + a q = \frac{L_z}{I_z} \tag{195}$$

The housing of the sliding mass-spring is rigidly fixed in the body and oriented parallel to the Y_b axis. The only applied moments to the body are those resulting from the motion of the sliding mass. Thus, there is a spring force of magnitude ky

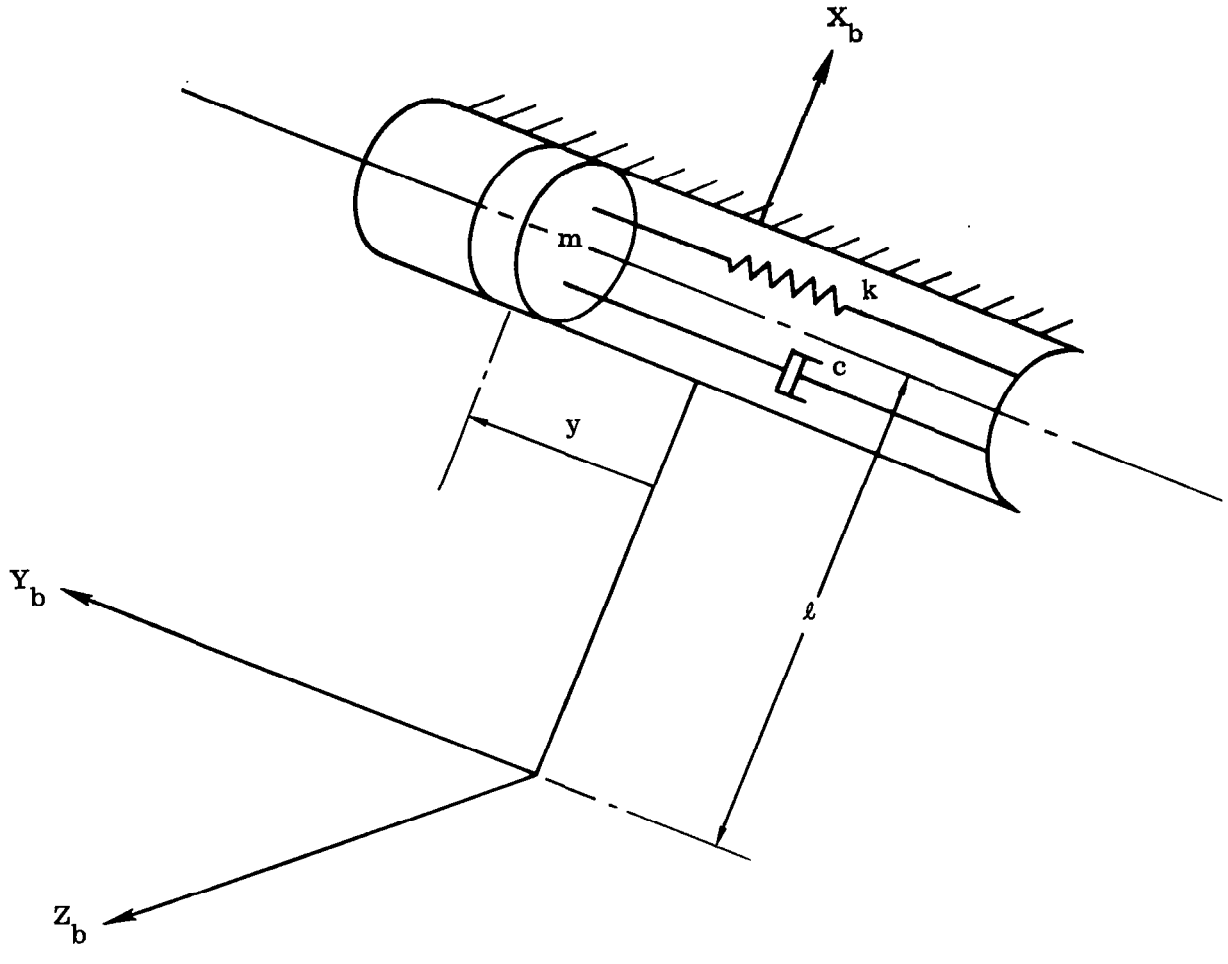

Figure 21. Damper Configuration

and a viscous frictional force of magnitude $c\dot{y}$. Consequently, the torques applied to the body are

$$\begin{aligned} L_x &= 0 \\ L_y &= 0 \\ L_z &= c\ell\dot{y} + k\ell y \end{aligned} \tag{196}$$

In order to derive the equation of motion for the spring mass, it is necessary to write the expression for the acceleration of this mass with respect to inertial space.

Denoting by $\bar{v}$ the vector velocity of m with respect to inertial space, we have*

$$\frac{d\bar{v}}{dt} = \dot{\bar{\omega}}_b \times \bar{\rho} + \bar{\omega}_b \times (\bar{\omega}_b \times \bar{\rho}) + \ddot{\bar{\rho}} + 2\bar{\omega}_b \times \dot{\bar{\rho}}$$

where

$$\bar{\omega}_b = p_o \bar{i}_b + q \bar{j}_b + r \bar{k}_b$$

and

$$\bar{\rho} = \ell \bar{i}_b + y \bar{j}_b$$

Expanding this expression we obtain

$$\frac{d\bar{v}}{dt} = \bar{i}_b \left[-\dot{r}y + q(p_o y - q\ell) - r^2 \ell - 2r\dot{y} \right]$$

$$+ \bar{j}_b \left[\ell \dot{r} - r^2 y - p_o (p_o y - q\ell) + \ddot{y} \right]$$

$$+ \bar{k}_b \left[-\ell \dot{q} + p_o r \ell + qry + 2p_o \dot{y} \right]$$

Equating the product of m and the $\bar{j}_b$ component of the above acceleration to the resisting spring and viscous forces, we obtain

$$m\left[\ell \dot{r} - r^2 y - p_o (p_o y - q\ell) + \ddot{y} \right] = -c\dot{y} - ky$$

or

$$\ddot{y} + 2\xi_n \omega_n \dot{y} + (\omega_n^2 - p_o^2) y + \ell p_o q + \ell \dot{r} = 0 \qquad (197)$$

where

$$\omega_n = \sqrt{\frac{k}{m}}$$

---

*We use the conventional notation:

$\dot{(\ )}$ ≡ time derivative with respect to inertial space

$\bar{(\dot{\ })}$ ≡ time derivative with respect to body axis system

$$\xi_n = \frac{c}{2}\sqrt{\frac{m}{k}}$$

and the term containing r^2 has been dropped since it is negligible compared with p_o^2. From (194) - (196) we have also

$$\dot{q} - ar = 0 \tag{198}$$

$$\dot{r} + aq = \frac{m\ell}{I_y}\left[2\xi_n\omega_n\dot{y} + \omega_n^2 y\right] \tag{199}$$

The damping and stabilization properties of the system may now be inferred by studying the solution to the linearized set of equations (197) - (199).

The characteristic equation is

$$s^4 + 2\xi_n\omega_n\left(1 + \frac{m\ell^2}{I_y}\right)s^3 + \left[\omega_n^2\left(1 + \frac{m\ell^2}{I_y}\right) + a^2 - p_o^2\right]s^2$$

$$+ 2\xi_n\omega_n a^2\left(1 + \frac{m\ell^2 p_o}{aI_y}\right)s + a^2\left[\omega_n^2\left(1 + \frac{m\ell^2 p_o}{aI_y}\right) - p_o^2\right] = 0 \tag{200}$$

The analysis now proceeds in a manner identical to that for Eq. (108) and will therefore not be repeated.

Note that the case

$$\omega_n^2\left(1 + \frac{m\ell^2 p_o}{aI_y}\right) < p_o^2$$

represents an unstable condition wherein the slider moves to one of the end stops and stays there.

3.5 DISTURBANCE TORQUES

A basic prerequisite for the rational design of an attitude control system for a satellite vehicle is a knowledge of the disturbance torques due to the space environment. The major sources of disturbance torque are gravity gradient, solar radiation pressure, earth's magnetic field, aerodynamic pressure, meteoritic impact, electromagnetic emission, and internal mass shifts. Each of these is discussed below.

Gravity Gradient

For a body of revolution in a circular orbit around a spherical earth, the gravity-gradient torque is*

$$L_{gg} = \frac{3\mu}{2R_o^2}(I_z - I_x)\sin 2\theta \tag{201}$$

where the symbols have the meaning defined in Subsection 3.4.1. In Fig. 22 is shown a plot of the gravity constant, $2\mu/R_o$, as a function of altitude.

A more precise evaluation of the gravity-gradient torque, which takes into account the oblateness effects of the earth, is given by[66]

$$L_{ggx} = \frac{3\mu}{R_o^3}(I_z - I_y)\left[\varphi + 2.185 \times 10^{-3}\left(\frac{R_E}{R_o}\right)^2 \sin 2\nu \sin\eta\right] \tag{202}$$

$$L_{ggy} = \frac{3\mu}{R_o^3}(I_z - I_x)\left[\theta - 2.185 \times 10^{-3}\left(\frac{R_E}{R_o^2}\right)^2 \sin^2\nu \sin 2\eta\right] \tag{203}$$

$$L_{ggz} = \frac{3\mu}{R_o^3}(I_x - I_y)\left[\theta\varphi + 0.545 \times 10^{-3}\left(\frac{R_E}{R}\right)^2 \sin 2\nu \cos\eta\right] \tag{204}$$

where

R_E = earth radius at the poles

ν = orbit plane inclination

η = angular advance from ascending node

and other symbols are as defined in Subsection 3.4.1.

The gravity-gradient torque in the pitch plane for a 500-statute-mile circular orbit at a 45-deg inclination is shown in Fig. 23.

*See Eq. (150)

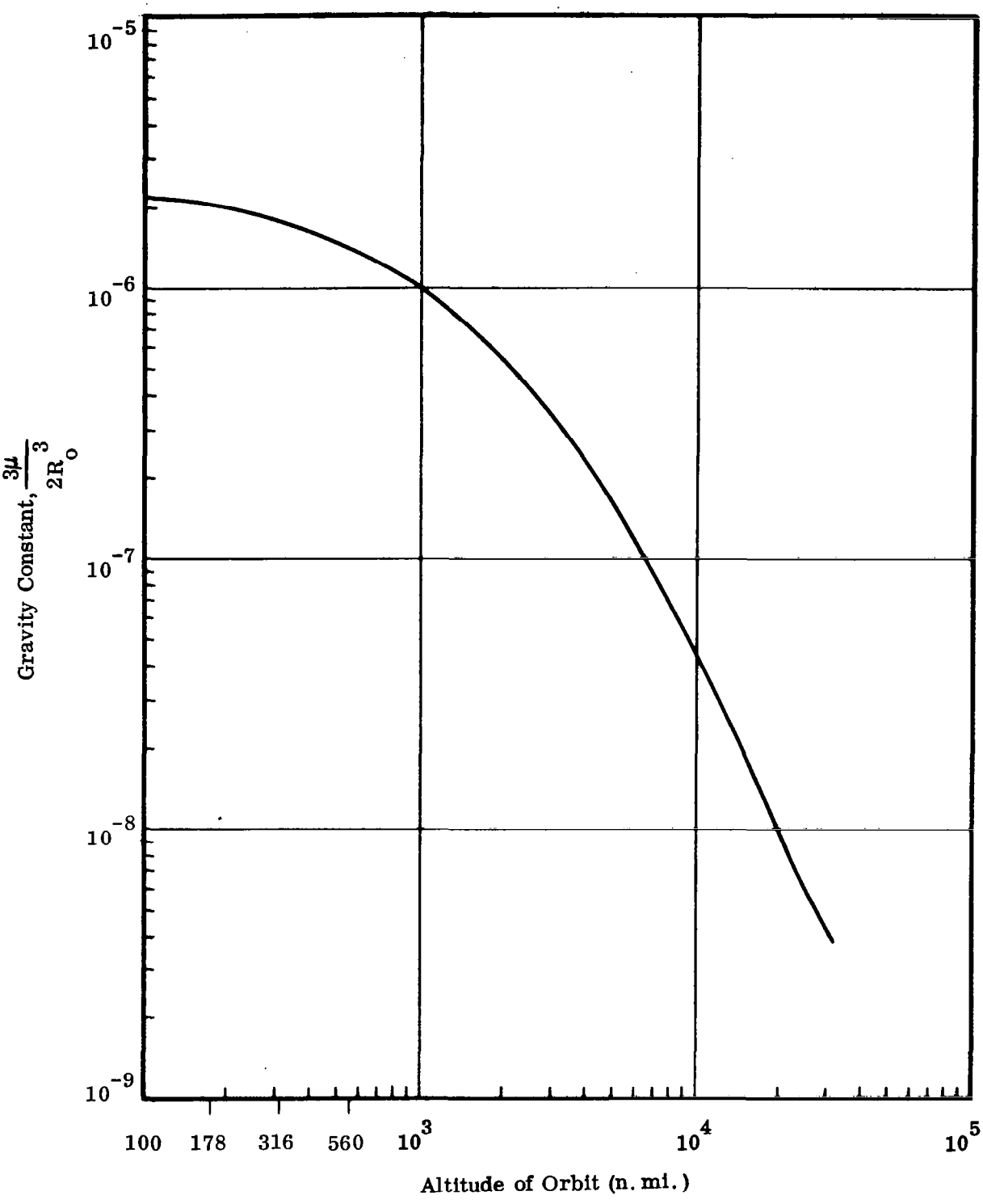

Figure 22. Evaluation of the Gravity Constant $\frac{3\mu}{2R_o^3}$ as a Function of Altitude

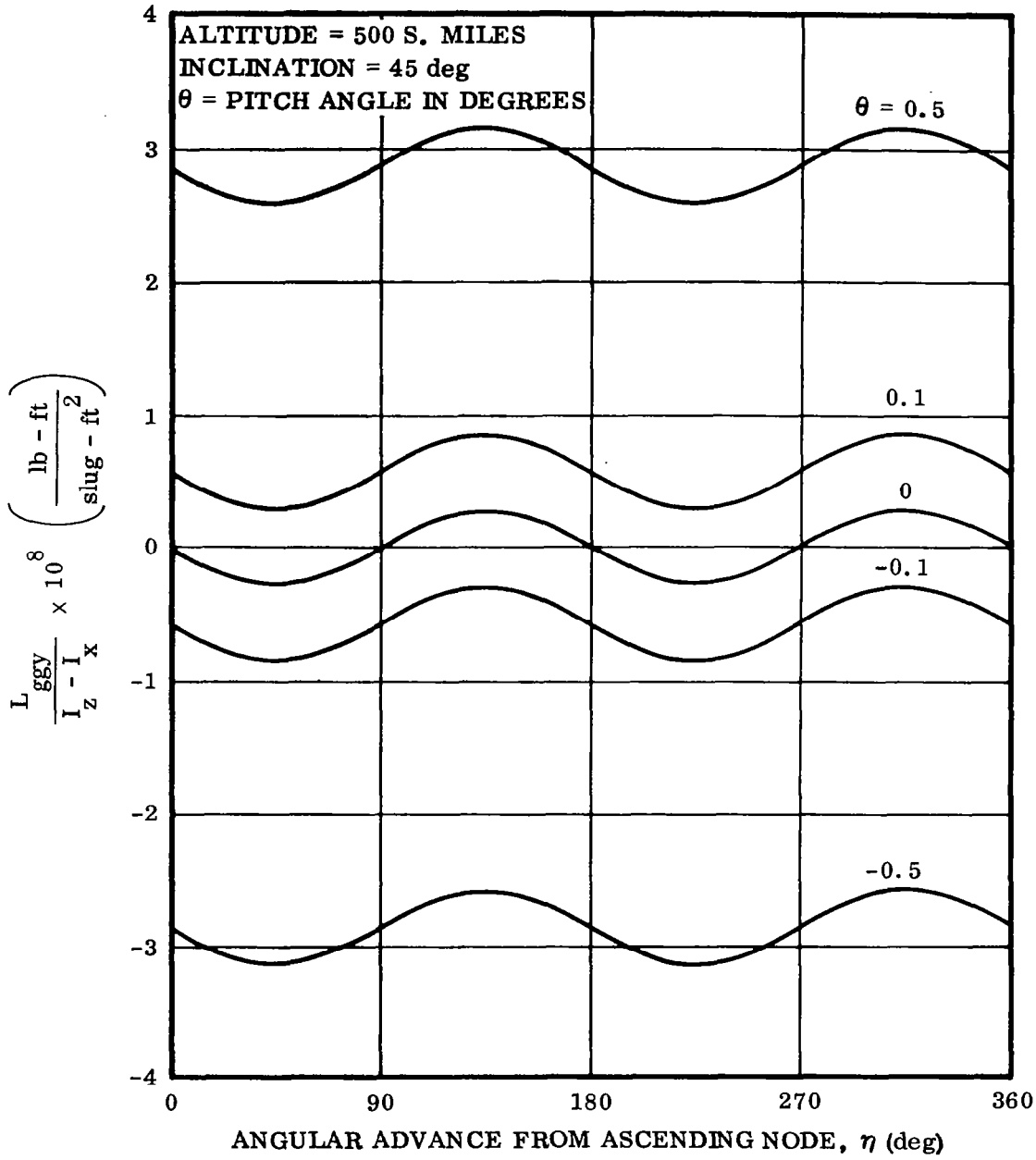

Figure 23. Gravitational Torque on a Satellite in Circular Orbit

For a maximum amplitude of (φ, θ) of approximately 0.1 degree, all terms in (202) - (204) are of the same order of magnitude. For larger amplitudes, the terms involving ν and η become negligible.

In any event, a conservative estimate of the maximum torque due to gravitational gradient is obtained from (201) as

$$L_{gg}\Big|_{max} = \frac{3\mu}{R_o^2}(I_z - I_x) \tag{205}$$

Note that when $I_x = I_y$ and $I_z \ll I_x$, this torque is cyclic with frequency $(3\mu/R_o^2)^{1/2}$

Solar Radiation Pressure

The torque on a space vehicle due to solar radiation pressure can be expressed as:

$$L_s = P_s \ell_s A_s \cos\epsilon \quad \text{(absorbent body)} \tag{206}$$

$$L_s = 2 P_s \ell_s A_s \cos^2\epsilon \quad \text{(reflective body)} \tag{207}$$

where:

L_s = torque due to solar radiation; foot pounds

P_s = radiation pressure; lb/ft^2

= 9.65×10^{-8} lb/ft^2 for earth orbiting vehicles

ℓ_s = distance between vehicle center of mass and center of radiation pressure; feet

A_s = projected area of the satellite normal to the sun; $feet^2$

ϵ = angle of incidence; degrees

Earth's Magnetic Field

The torques due to coupling of currents within the satellite with the earth's magnetic field are extremely difficult to calculate without knowing the actual generator currents, satellite circuit currents, and eddy currents within the satellite. As a crude order-of-magnitude estimate, a satellite in a low earth orbit containing about 20 pounds of iron would, under the most unfavorable circumstances, experience a torque of approximately[66]

$$L_m = 20 \times 10^{-8} \text{ lb ft} \tag{208}$$

Proper shielding can reduce these effects considerably

Aerodynamic Pressure

A simplified expression used in computing the aerodynamic torque is:

$$L_a = P_a \ell_a A_a \sin \alpha \tag{209}$$

where:

L_a = torque due to aerodynamic pressure; foot-pounds

P_a = aerodynamic pressure; pounds/ft^2

ℓ_a = distance between center of mass and center of aerodynamic pressure; feet

A_a = surface area exposed to aerodynamic pressure; feet^2

α = vehicle angle of attack; radians

Aerodynamic pressure as a function of orbit altitude is given in Fig. 24.

The aerodynamic torque as a function of altitude, exposed area, and lever arm is plotted in Fig. 25.

Meteoritic Impact

Table 1, constructed from information obtained in Ref. 67, indicates the meteoritic effects on the attitude control of space vehicles. The probability of various magnitude meteorites hitting a three-meter-diameter satellite is given. The angular

Table 1. Meteoritic Data (Three-Meter Diameter Satellite)

METEORITE VISUAL MAGNITUDE	MASS (grams)	HIT PROBABILITY	VELOCITY (ft/second)
20	2.5×10^{-7}	6.45/day	4.92×10^4
18	1.58×10^{-6}	1.02/day	5.52×10^4
15	2.5×10^{-5}	23.5/year	6.65×10^4
13	1.58×10^{-4}	3.72/year	7.47×10^4
10	2.5×10^{-3}	0.24/year	8.2×10^4

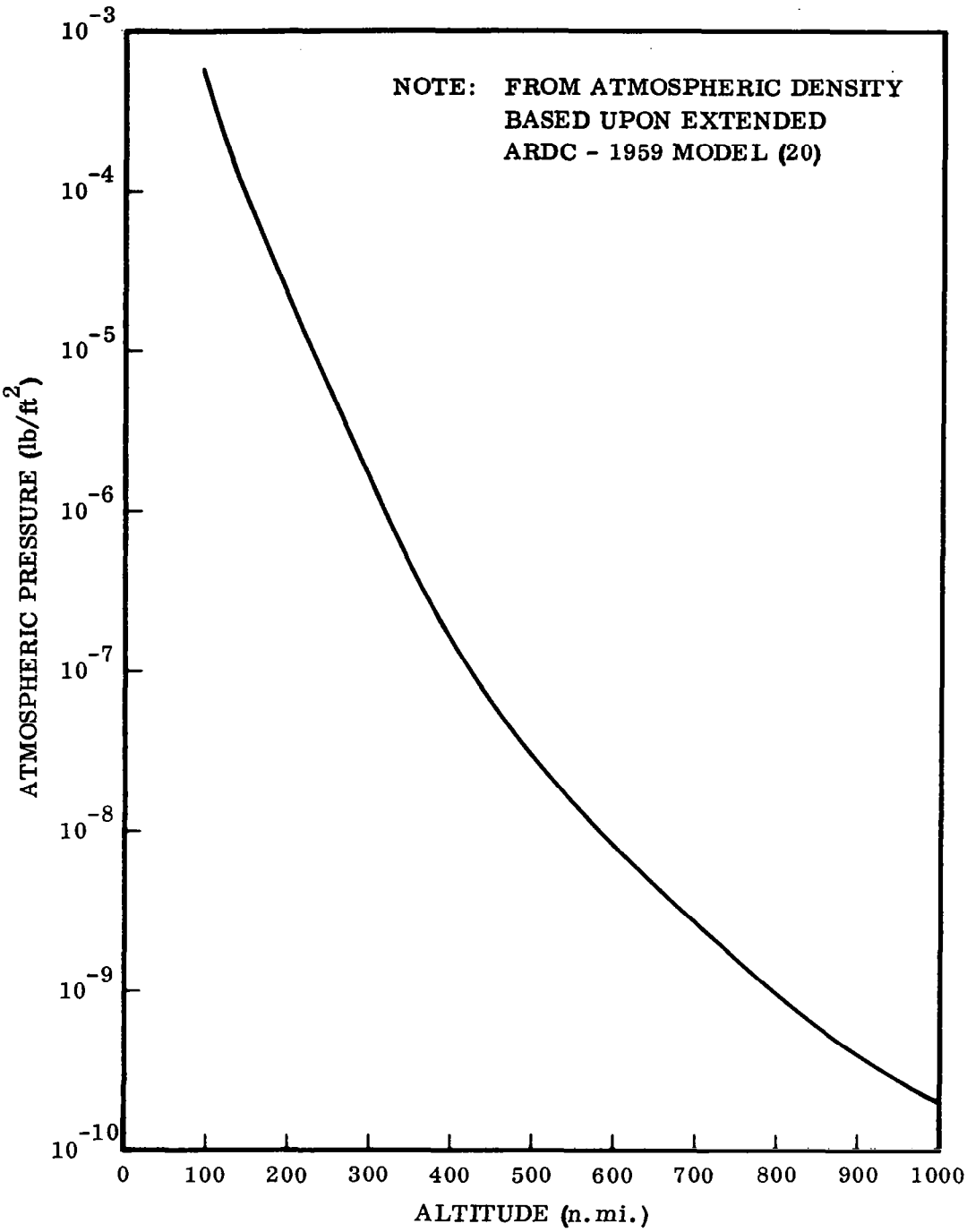

Figure 24. Atmospheric Pressure as a Function of Orbit Altitude (Assuming Circular Orbits)

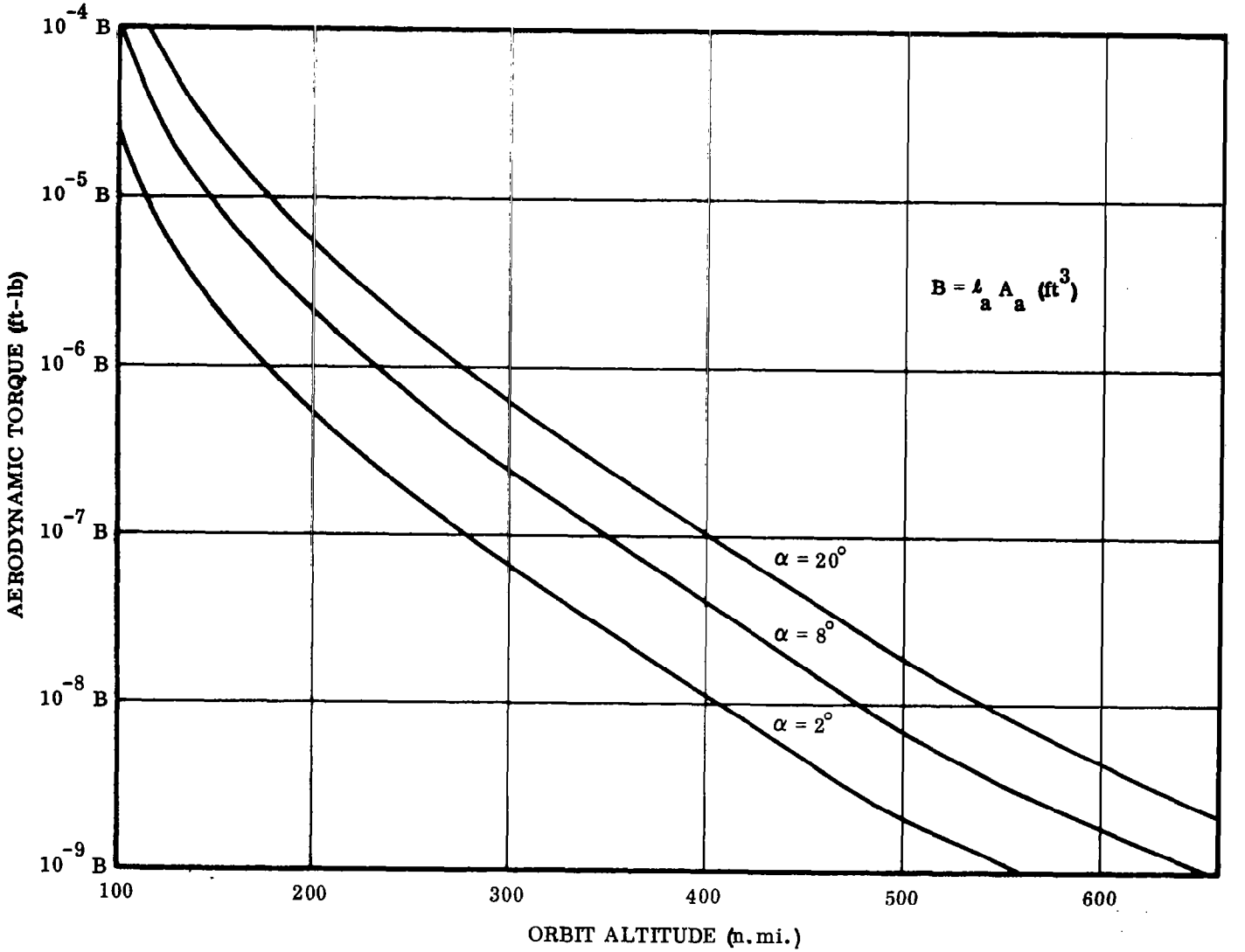

Figure 25. Aerodynamic Torque as a Function of Orbit Altitude

momentum imparted to the vehicle also is presented. The range of meteorites presented covers those whose hit probability and mass were sufficient to warrant investigation as to their effects on satellite attitude control.

The angular momentum imparted to the vehicle due to a meteoritic particle of mass m having velocity $\bar{v}$ is (in vector notation)

$$\Delta[I \cdot \bar{\omega}] = \bar{\ell}_m \times [\Delta(m\bar{v})] \tag{210}$$

Here, $\bar{\ell}_m$ is the radius vector from the vehicle mass center to the point of impact.

It is easily verified that in most cases the effect of meteoritic impact is negligible.

Electromagnetic Emission

Radiating energy in the form of electromagnetic waves which are emitted by radio and radar antennas and thermal radiators results in a pressure force on the emitting surfaces. These forces, multiplied by the effective moment arms, result in disturbing moments.

According to Ref. 1, one kilowatt of electromagnetic radiation results in about 7.5×10^{-7} pounds force.

One Btu/hr of thermal radiation results in about 1.6×10^{-10} pounds force.

Internal Mass Shifts

The more sophisticated space vehicles will contain or support bodies which are moved relative to the main body. These may be cameras, solar paddles, antennas, or — in the larger vehicles — animate passengers. The torques caused by these motions are largely cyclic in nature because these sub-bodies must first be accelerated and then decelerated to attain a new position. It is not possible to list typical disturbance torques in this case because of too wide a range in the parameters involved. Calculations with varying degrees of sophistication may be obtained using the equations of 3.2.2.

3.6 SUMMARY OF CONTROL REQUIREMENTS

The design of an attitude control system for an orbiting vehicle must take into account three primary requirements. These are: reliability, performance (accuracy, momentum, dynamic response, etc.), and the weight of the control system and power source. Additional consideration must be given to cost, maintainability, and producibility; however, it is seldom that a major compromise is made in the primary requirements in favor of the secondary considerations. For the particular mission, the

primary control requirements must be met. That is, the attitude control system must meet the particular reliability and performance requirements within the acceptable weight and power limits set by the mission.

Given the mission parameters, the control and power requirements are then derived — from which the basic design data for the control system is established. The necessary procedure may be displayed graphically as shown in Fig. 26, which is abstracted from Ref. 23. The notation for item 4 — Dynamic Response, f(A, F, G) — means that the dynamic response is a function of the type of mission, accuracy, and maneuvering anticipated. A similar interpretation applies to the other symbols f( ).

In order to evaluate the tradeoffs between control capability, weight, power, and mission requirements, an extensive survey of available design data was conducted by Nichol.[23] The basic control requirements for a total of 3 missions were presented. These were characterized by mission objective as follows:

Military Missions

This area generally covers a wide range of missions. However, since the smaller satellites in this category are similar to other mission types, only the larger manned Apollo-type vehicles were of concern here. These vehicles, which range in weight from 10, 000 to 200, 000 pounds, will be used primarily as reconnaissance and weapon systems. The control of these vehicles is critical as it is difficult to point them accurately at a specific ground target or enemy satellite. For example, an attitude error of one one-hundredth degree will cause an error of approximately one mile in scanning the earth's surface at an altitude of 5, 000 miles.

The number of maneuvers will be high since the vehicle will be repositioned continually to scan a larger area. The mission life will be relatively short, between two weeks and an upper limit of two years for an unmanned bombing satellite. Reliability is critical as human lives are involved either directly or indirectly.

Space Stations

Space stations can serve two purposes: as a flying laboratory and as a launching platform. The station will most likely be spin-stabilized as this will also serve to simulate gravity aboard the satellite. Symmetry around at least one axis will also be an advantage. The station would probably be designed in the shape of a sphere, cylinder, or torus.

Used as a laboratory, the station can carry out experiments in geophysics, meteorology, astronomy, etc., where the experiments aboard the platform will be enhanced by its location above most of the earth's atmosphere. In cases where the station serves as an astronomical laboratory and long-exposure photographs of stars and galaxies are taken, a high degree of accuracy, in the order of seconds of arc, will

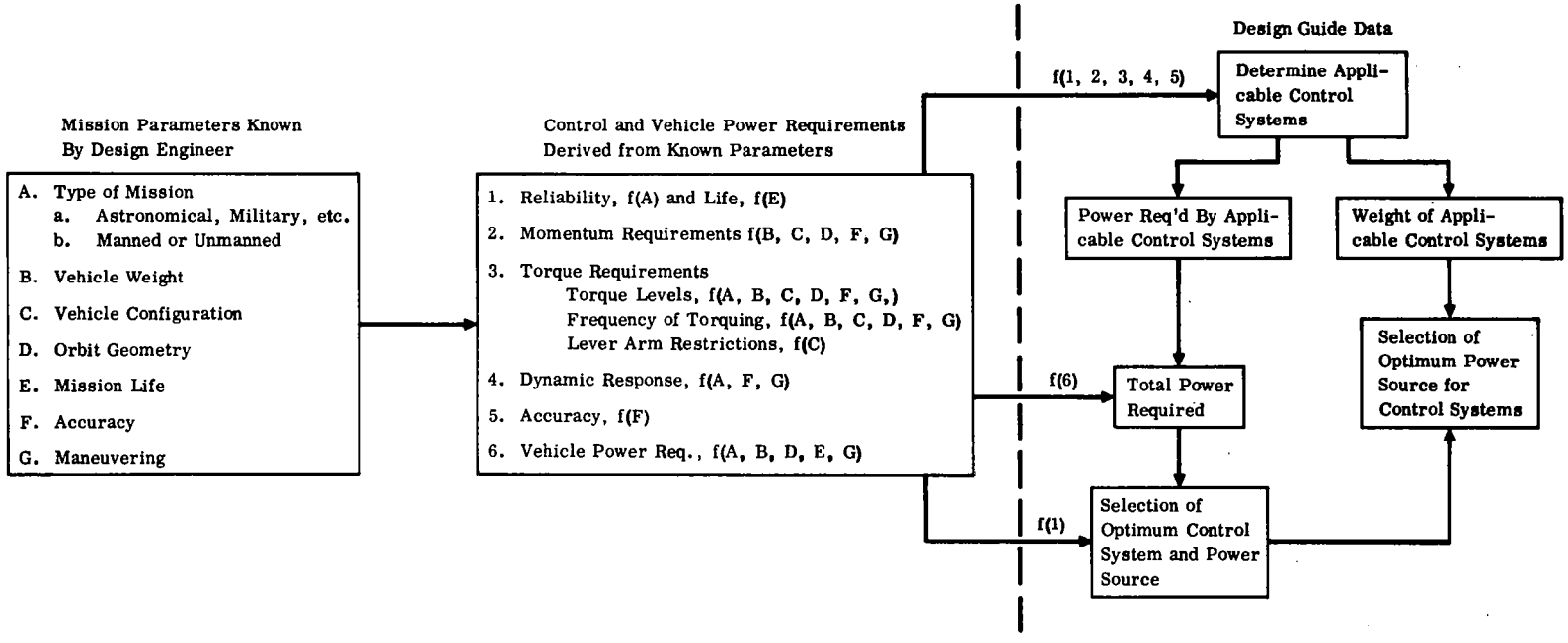

Figure 26. Flow Chart Showing the Selection Method of Optimum Control System and Power Sources

be required. Except for this case, accuracy requirements should be moderate, in the order of ± one degree. Reliability of a space station does not appear to be a primary problem as maintenance can be performed as trouble occurs.

Astronomical Missions

Astronomical missions consist of observations of the solar systems and beyond. The telescopic equipment on board will require extremely accurate attitude control. These vehicles will be in the moderate weight class, from 600 to 6,000 pounds, with a mission life ranging from four months to two years. The vehicle will be referenced inertially and the number of maneuvers generally will be fairly high to enable the system to acquire information on more than one "target."

Meteorological Mission

This mission is used for gathering information on cloud cover and other weather data. The vehicle generally will be earth-referenced with an approximate accuracy requirement of ± one degree. There will be few, if any, short maneuvers, which fact indicates a low momentum requirement of the attitude control system. The required life of the system should be approximately one year.

Communications Mission

This satellite, to be competitive with other means of global communications, must have a long life, in the order of 5 to 20 years. This, plus the fact that the maneuver requirements are low, necessitates that a reliable, low-powered attitude control system be employed. The altitude of the orbit will vary from 500 miles to synchronous, and the accuracy requirement will call for control within one degree.

Space Environment Missions

Space environment missions, such as those epitomized by the Orbiting Geophysical Observatory series, have the objectives of measuring the structure of the atmosphere and ionosphere as well as the study of high-energy particles in space. The missions generally will require rather coarse attitude control, in the order of ± one to ± five degrees. The vehicle could be either inertially- or earth-referenced, and the orbit may be highly elliptical.

The control requirements for these missions are summarized in Table 2, while Table 3 lists the corresponding disturbance torque requirements.

For purposes of sizing the control actuators, the satellite vehicles were divided into four classes as follows:

Class A: Vehicles with little or no control requirements. The Tiros (spin-stabilized) vehicle is an example of this class. These vehicles were given little attention during the study as most of the effort was directed toward the active control techniques.

Class B: This class consists of vehicles in the 400- to 2,000-pound range. These vehicles require active control in all three axes. An example of this class is the Nimbus meteorological satellite.

Class C: This class consists of vehicles with the same requirements as Class B vehicles but weigh 2,000 to 10,000 pounds. The Orbiting Astronomical Observatory is in this class.

Class D: This class represents the larger future vehicles and space stations (10,000 to 200,000 pounds).

Three modes of control are considered

a. Inertia wheel.

b. Gyrotorquer.

c. Reaction jet.

Weight and power requirements are given in each case for class B, C, and D vehicles. These are summarized as follows.

Inertia Wheel Control

The weight of an inertia wheel system for three-axis control consists of the weight of three momentum packages (motor plus wheel) plus the weight of wiring and miscellaneous hardware and the weight of the control electronics. The power required by the system is the motor power plus the power dissipated by the electronics.

The weight of the wheel is dependent upon the amount of momentum capability required of the system, while the motor weight varies with the stall torque. The weight of the wiring and miscellaneous hardware was set at 20 percent of the calculated momentum package weight for Class B and C vehicles and 10 percent for Class D vehicles. The weight of the control electronics was set at seven pounds. The single-axis inertia wheel system weights for the Class A, B and C vehicles are given in Figures 27, 28 and 29.

Table 2. Control Requirements of Satellite Missions

MISSION		MISSION LIFE (months) (See Note a)	ALTITUDE (n. mi.)	WEIGHT (pounds)	MAX. PRINCIPAL MOMENT OF INERTIA – I (slug-ft^2)	MEAN DIAMETER OF SATELLITE (feet)	TORQUE AND MOMENTUM REQUIRED TO OVERCOME DIST. TORQUES		MAXIMUM MANEUVER REQUIREMENTS						RELIABILITY REQUIREMENTS	ACCURACY REQUIREMENTS (See Note d)	
									LOW MANEUVERS		NOMINAL MANEUVERS		HIGH MANEUVERS				
							L_{max} (ft-lb)	MOM (ft-lb-sec)	L_{max} (ft-lb)	MOM (ft-lb-sec)	L_{max} (ft-lb)	MOM (ft-lb-sec)	L_{max} (ft-lb)	MOM (ft-lb-sec)			
I.	Military	1. 0.2 (L) 12 (U)	100	10,000	10K	10	10	30	2.5	60	15	350	15	350	High	10% Fine	90% Coarse
		2. 0.2 (L) 0.5 (N)	100	200,000	500K	25	50	670	125	3×10^3	750	1.75×10^4	750	1.75×10^4	High	10% Fine	90% Coarse
		3. 4 (L) 24 (U)	5,000	10,000	10K	10	10^{-2}	1.5[b]	No Maneuvers		0.65	30	0.65	30	High	20% Fine	80% Medium
II.	Space Station	4. 6 (L) 60 (U)	100	10^5	10^6	60	100	1700	No Maneuvers		No Maneuvers		4	10^3	Medium	Medium except astronomical	
		5.	1,000	10^5	10^6	60	100	580	No Maneuvers		No Maneuvers		4	10^3	Medium	mission which is very fine	
III.	Astronomical	6.	3,000	600	150	4	0.02	0.04	0.022	0.38	0.038	0.9	0.076	0.38	Low-Med	Very Fine	
		7. 4 (L)	3,000	3,000	1,000	7	0.1	0.1	0.15	2.5	0.25	6	0.5	2.5	Low-Med	Very Fine	
		8.	3,000	6,000	3,000	9	0.1	0.1	0.45	7.5	0.75	18	1.5	7.5	Low-Med	Very Fine	
		9. 24 (U)	1,000	600	150	4	0.02	0.04	0.022	0.38	0.038	0.9	0.076	0.38	Low-Med	Very Fine	
		10.	1,000	3,000	1,000	7	0.1	0.1	0.15	2.5	0.25	6	0.5	2.5	Low-Med	Very Fine	
		11.	1,000	6,000	3,000	9	0.1	0.1	0.45	7.5	0.75	18	1.5	7.5	Low-Med	Very Fine	
IV.	Meteorological	12.	200	400	100	3	10^{-3}	0.4[b]	No Maneuvers		No Maneuvers		6.5×10^{-3}	0.3	Low-Med	Medium or Low	
		13. 4 (L)	200	1,000	250	5	10^{-2}	0.9[b]	No Maneuvers		No Maneuvers		1.6×10^{-2}	0.75	Low-Med	Medium or Low	
		14.	200	5,000	1,000	8	0.1	4.8[b]	No Maneuvers		No Maneuvers		6.5×10^{-2}	3	Low-Med	Medium or Low	
		15. 12 (N)	5,000	400	100	3	10^{-3}	0.03	No Maneuvers		No Maneuvers		6.5×10^{-3}	0.3	Low-Med	Medium or Low	
		16.	5,000	1,000	250	5	10^{-2}	0.06	No Maneuvers		No Maneuvers		1.6×10^{-2}	0.75	Low-Med	Medium or Low	
		17. 36 (U)	5,000	5,000	1,000	8	0.1	0.24	No Maneuvers		No Maneuvers		6.5×10^{-2}	3	Low-Med	Medium or Low	
V.	Communications	18.	500	400	100	3	10^{-4}	0.016[c]	No Maneuvers		6.5×10^{-3}	0.3	6.5×10^{-3}	0.3	Medium	Medium	
		19. 6 (L)	500	1,000	250	5	10^{-3}	0.04[c]	No Maneuvers		1.6×10^{-2}	0.75	1.6×10^{-2}	0.75	Medium	Medium	
		20.	500	5,000	1,000	8	10^{-2}	0.16[c]	No Maneuvers		6.5×10^{-2}	3	6.5×10^{-2}	3	Medium	Medium	
		21. 60 (N)	4,000	400	100	3	10^{-4}	0.026	No Maneuvers		No Maneuvers		No Maneuvers		Medium	Medium	
		22.	4,000	1,000	250	5	10^{-3}	0.052	No Maneuvers		No Maneuvers		No Maneuvers		Medium	Medium	
		23. 240 (U)	4,000	5,000	1,000	8	10^{-2}	0.1	No Maneuvers		No Maneuvers		No Maneuvers		Medium	Medium	
		24.	19,400	400	100	3	10^{-4}	0.014	No Maneuvers		No Maneuvers		4×10^{-4}	0.06	Medium	Fine	
		25.	19,400	1,000	250	5	10^{-3}	0.022	No Maneuvers		No Maneuvers		10^{-3}	0.15	Medium	Fine	
		26.	19,400	5,000	1,000	8	10^{-2}	0.16	No Maneuvers		No Maneuvers		4×10^{-3}	0.06	Medium	Fine	
VI.	Space Environment	27.	100-50,000	1,000	250	5	0.02	1.0	No Maneuvers		10^{-3}	1.5×10^{-2}	1.6×10^{-2}	0.75	Low	2% Med	98% Coarse
		28. 4 (L)	100-50,000	3,000	1,000	7	0.1	4.0	No Maneuvers		4×10^{-3}	0.06	6.5×10^{-2}	3.0	Low	2% Med	98% Coarse
		29.	300	1,000	250	5	0.02	0.08	No Maneuvers		No Maneuvers		10^{-3}	1.5×10^{-2}	Low	Medium	
		30. 24 (U)	300	3,000	1,000	7	0.1	0.25	No Maneuvers		No Maneuvers		4×10^{-3}	1.5×10^{-2}	Low	Medium	

NOTES:
a. The symbol L, N and U represent lower, nominal and upper respectively.
b. Represents the momentum requirement for 1/2 orbital revolution.
c. Represents the momentum requirement for one orbital revolution.
d. Coarse control is defined as attitude error greater than ±2 deg, medium as a error from ±2 to ±0.1 deg, fine from ±0.1 to ±0.001 deg, and very fine an error less than ±0.001 deg.
e. The mean diameter of the satellite was determined by assuming a spherical vehicle with a density of 15 lb/ft^3. This information is used in determining the lever arms for mass-expulsion systems.

Table 3. Disturbance Torque Requirements for the Various Missions

	MISSION		ALTITUDE (n. mi.)	ORBITAL PERIOD (10^3 sec)	LARGEST PRINCIPAL MOMENT OF INERTIA (slug-ft^2)	DISTURBANCE TORQUES								SUMMED TORQUE AND MOMENTUM REQUIRED TO OVERCOME DISTURBANCE TORQUES	
						GRAVITY GRADIENT		SOLAR PRESSURE		AERODYNAMIC PRESS.		EARTH'S MAGNETIC FIELD		MOVEMENT OF PERSONNEL AND EQUIPMENT			
						MAX. TORQUE (ft-lb)	MOMENTUM (ft-lb-sec)	MAX. TORQUE (ft-lb)	MOMENTUM (ft-lb-sec)	MAX. TORQUE (ft-lb)	MOMENTUM (ft-lb-sec)	MAX. TORQUE (ft-lb)	MOMENTUM (ft-lb-sec)	L_{max} (ft-lb)	MOM (ft-lb-sec)	L_{max} (ft-lb)	MOM (ft-lb-sec)
I.	Military	1.	100	5.08	10K	2.4×10^{-3}	6.1[a]	4×10^{-5}	6.2×10^{-2}	0.12	30	10^{-4}	0.16	10(for 1 sec)	5	10	30
		2.	100	5.08	500K	0.12	300[a]	6×10^{-4}	0.97	2.62	670	2×10^{-3}	3.2	300(for 5 sec)	150	50	670
		3.	5,000	19.2	10K	1.6×10^{-4}	1.5[a]	4×10^{-5}	0.24	Negligible		4×10^{-5}	0.24	10^{-2}	10^{-2}	10^{-2}	1.5[a]
II.	Space Stations	4.	100	5.08	10^6	1.05	890	5×10^{-4}	2.4[b]	1.05	1700	10^{-4}	0.16	600(for 5 sec)	300	100	1700
		5.	1,000	7.36	10^6	0.5	580	5×10^{-4}	3.7[b]	3×10^{-7}	7×10^{-4}	4×10^{-5}	9.5×10^{-2}	600(for 5 sec)	300	100	580
III.	Astronomical	6.	300	5.72	150	4.2×10^{-6}	3.7×10^{-3}	1.2×10^{-7}	3.4×10^{-3} [a]	1.1×10^{-6}	2×10^{-3}	10^{-5}	1.8×10^{-2}	0.02	0.04	0.02	0.04
		7.	300	5.72	1,000	2.8×10^{-5}	0.025	6.5×10^{-7}	1.9×10^{-3}	6×10^{-6}	1.1×10^{-2}	2×10^{-5}	3.6×10^{-2}	0.1	0.1	0.1	0.1
		8.	300	5.72	3,000	8.4×10^{-5}	0.075	1.3×10^{-6}	3.7×10^{-3}	1.2×10^{-5}	2.2×10^{-2}	5×10^{-5}	9×10^{-2}	0.1	0.1	0.1	0.1
		9.	1,000	7.36	150	1.5×10^{-6}	1.75×10^{-3}	1.2×10^{-7}	4.4×10^{-4}	3×10^{-10}	7×10^{-6}	5×10^{-6}	1.2×10^{-2}	0.02	0.04	0.02	0.04
		10.	1,000	7.36	1,000	9.8×10^{-6}	0.011	6.5×10^{-7}	2.4×10^{-3}	1.6×10^{-9}	3.7×10^{-5}	10^{-5}	2.4×10^{-2}	0.1	0.1	0.1	0.1
		11.	1,000	7.36	3,000	2.9×10^{-5}	0.034	1.3×10^{-6}	4.8×10^{-3}	3.3×10^{-9}	7.8×10^{-5}	3×10^{-5}	7×10^{-2}	0.1	0.1	0.1	0.1
IV.	Meteorological	12.	200	5.5	100			10^{-6}	1.75×10^{-3}	3.6×10^{-4}	0.4[a]	2×10^{-5}	3.5×10^{-2}	10^{-3}	2×10^{-3}	10^{-3}	0.4[a]
		13.	200	5.5	250			2.2×10^{-6}	3.9×10^{-3}	7.8×10^{-4}	0.9[a]	4×10^{-5}	7×10^{-2}	10^{-2}	10^{-2}	10^{-2}	0.9[a]
		14.	200	5.5	1,000	Stabilizing		1.2×10^{-5}	2.1×10^{-2}	4.3×10^{-3}	4.8[a]	10^{-4}	0.175	0.1	0.1	0.1	4.8[a]
		15.	5,000	19.2	100	Torque		10^{-6}	6.1×10^{-3}	Negligible		5×10^{-6}	3×10^{-2}	10^{-3}	2×10^{-3}	10^{-3}	0.03
		16.	5,000	19.2	250			2.2×10^{-6}	1.3×10^{-2}	Negligible		10^{-5}	6×10^{-2}	10^{-2}	10^{-2}	10^{-2}	0.06
		17.	5,000	19.2	1,000			1.2×10^{-5}	2.3×10^{-2}	Negligible		4×10^{-5}	0.24	0.1	0.1	0.1	0.24
V.	Communications	18.	500	6.2	100	2.6×10^{-6}	1.6×10^{-2}	5×10^{-7}	9.6×10^{-4}	2.5×10^{-7}	6.2×10^{-4} [b]	10^{-5}	2×10^{-2}	10^{-4}	10^{-3}	10^{-4}	0.016[a]
		19.	500	6.2	250	6.5×10^{-6}	4×10^{-2}	8×10^{-7}	1.6×10^{-3}	4.1×10^{-7}	10^{-3} [b]	2×10^{-5}	4×10^{-2}	10^{-3}	2×10^{-3}	10^{-3}	0.04[a]
		20.	500	6.2	1,000	2.6×10^{-5}	0.16	6×10^{-6}	1.2×10^{-2}	3×10^{-5}	7.5×10^{-2} [b]	5×10^{-5}	0.1	10^{-2}	2×10^{-2}	10^{-2}	0.16[a]
		21.	4,000	16.2	100	1.6×10^{-7}	2.6×10^{-3}	5×10^{-7}	2.6×10^{-3}	Negligible		5×10^{-6}	2.6×10^{-2}	10^{-4}	10^{-3}	10^{-4}	0.026
		22.	4,000	16.2	250	4.1×10^{-7}	6.6×10^{-3}	8×10^{-7}	4.1×10^{-3}	Negligible		10^{-5}	5.2×10^{-2}	10^{-3}	2×10^{-3}	10^{-3}	0.052
		23.	4,000	16.2	1,000	1.6×10^{-6}	2.6×10^{-2}	6×10^{-6}	3.1×10^{-2}	Negligible		2×10^{-5}	0.1	10^{-2}	2×10^{-2}	10^{-2}	0.1
		24.	19,400	86.4	100	4.9×10^{-9}	4.2×10^{-4}	5×10^{-7}	1.4×10^{-2}	Negligible		Negligible		10^{-4}	10^{-3}	10^{-4}	0.014
		25.	19,400	86.4	250	1.2×10^{-8}	10^{-3}	8×10^{-7}	2.2×10^{-2}	Negligible		Negligible		10^{-3}	2×10^{-3}	10^{-3}	0.022
		26.	19,400	86.4	1,000	4.9×10^{-8}	4.2×10^{-3} [b]	6×10^{-6}	0.16	Negligible		Negligible		10^{-2}	2×10^{-2}	10^{-2}	0.16
VI.	Space Environment	27.	100-50,000	80.5	250	3.9×10^{-6}	5×10^{-3}	4×10^{-6}	8.5×10^{-2}	8×10^{-4}	1.0	2×10^{-5}	1.6×10^{-2}	0.02	0.04	0.02	1.0
		28.	100-50,000	80.5	1,000	1.6×10^{-6}	2×10^{-3}	1.7×10^{-5}	0.44	3.2×10^{-3}	4.0	5×10^{-5}	4×10^{-2}	0.1	0.1	0.1	4.0
		29.	300	5.67	250	3.2×10^{-6}	1.8×10^{-6}	4×10^{-6}	7.2×10^{-3}	3.2×10^{-6}	1.9×10^{-2}	1.6×10^{-5}	1.4×10^{-2}	0.02	0.04	0.02	0.08
		30.	300	5.67	1,000	1.3×10^{-5}	6.2×10^{-2}	1.7×10^{-5}	3×10^{-2}	1.3×10^{-5}	7.4×10^{-2}	4×10^{-5}	3.6×10^{-2}	0.1	0.1	0.1	0.25

NOTES: a. Represents the momentum requirements for 1/2 orbital revolution.
b. Represents the momentum requirements for one orbital revolution.

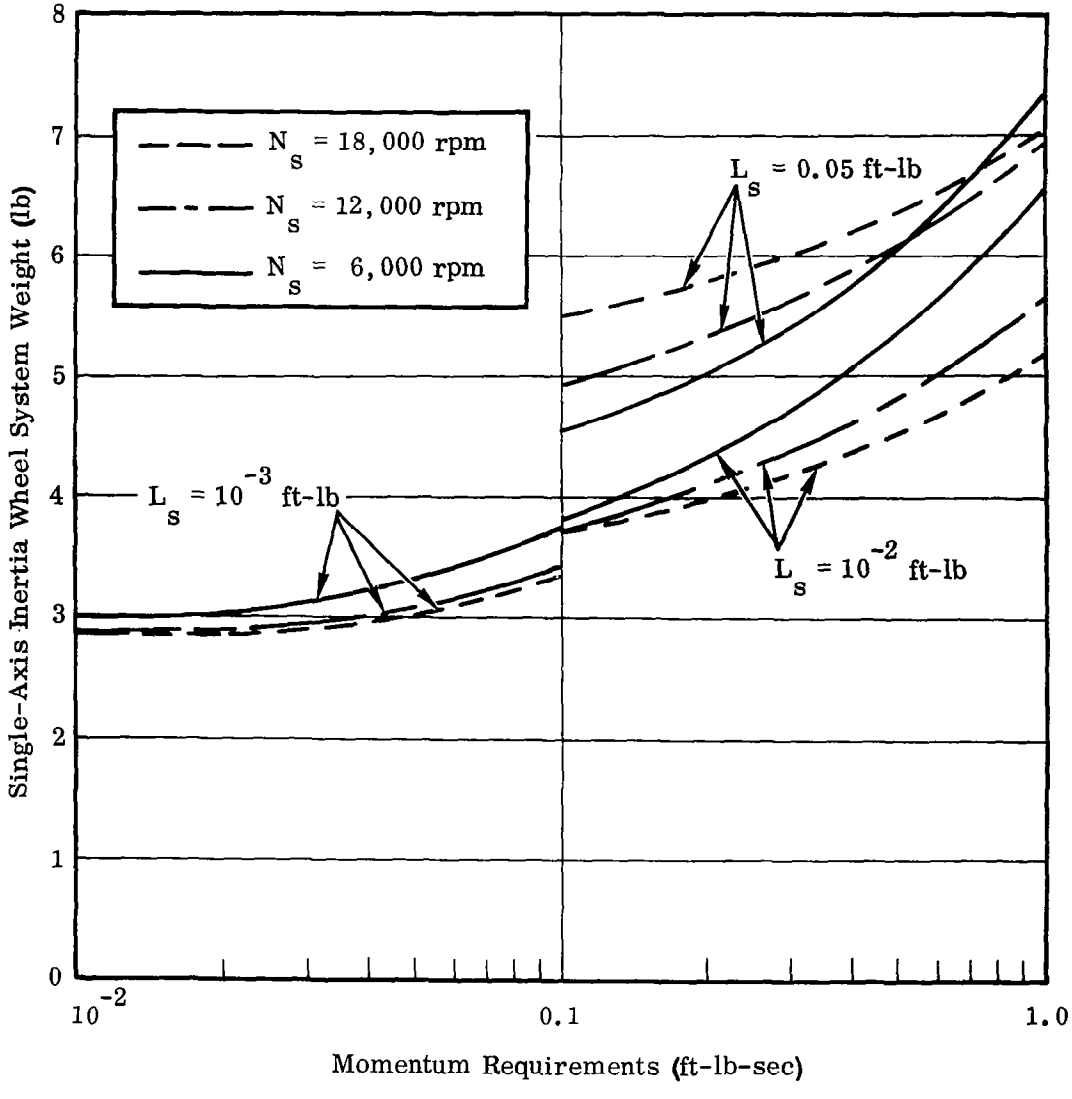

Figure 27. Inertia Wheel System Weight (Single Axis) as a Function of Momentum Capability — Class B Vehicles

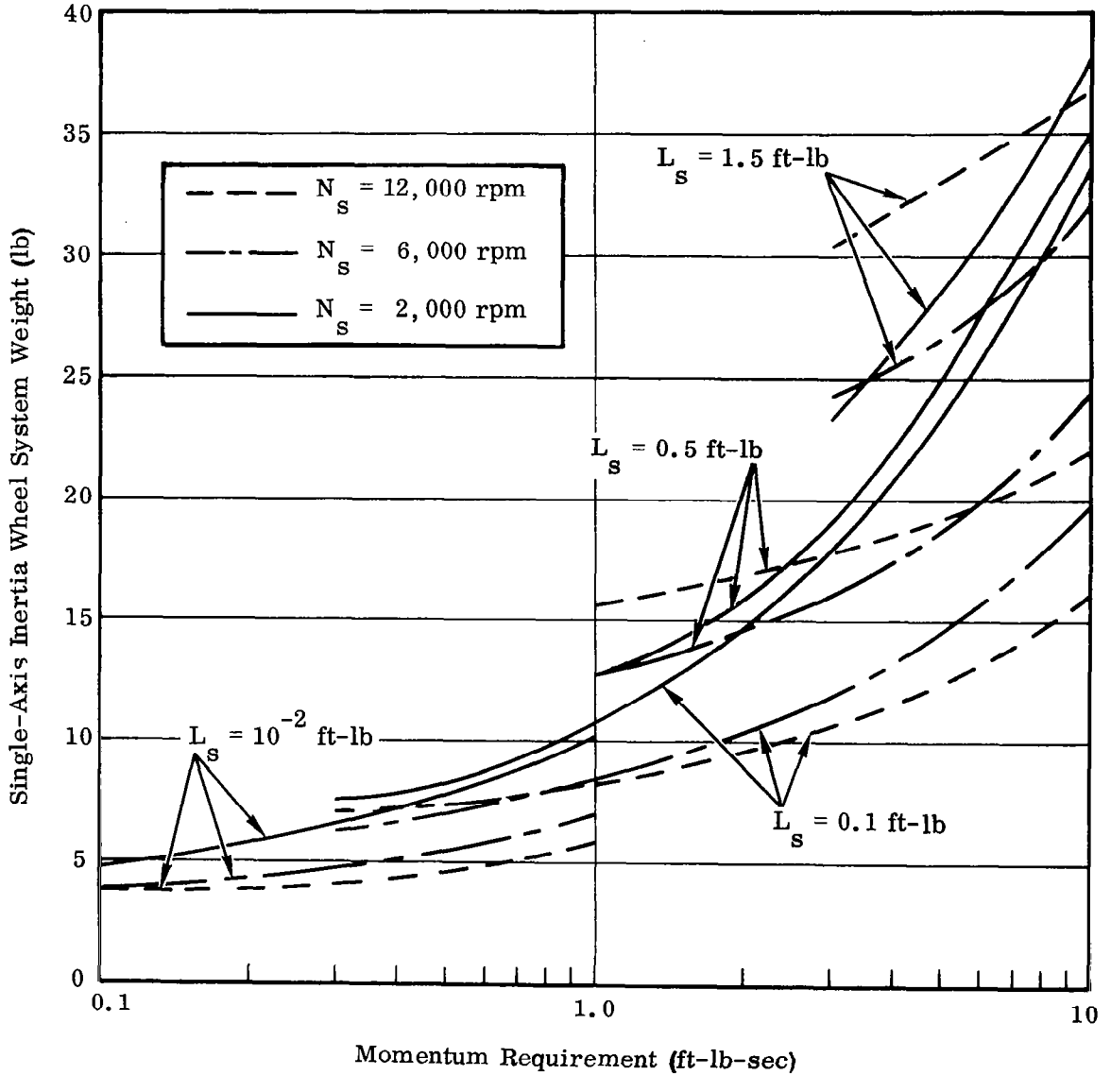

Figure 28. Inertia Wheel System Weight (Single Axis) as a Function of Momentum Capability — Class C Vehicles

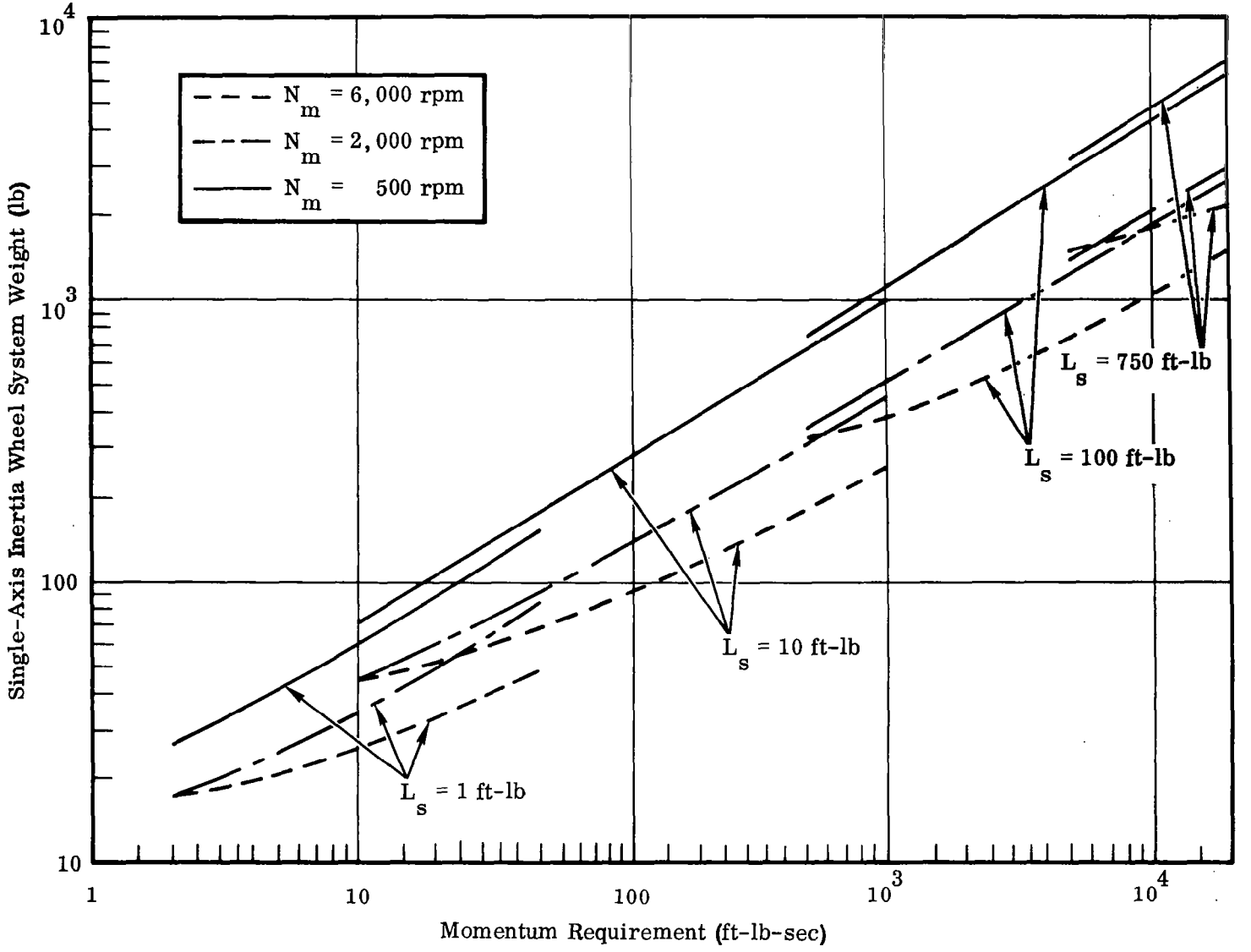

Figure 29. Inertia Wheel System Weight (Single Axis) as a Function of Momentum Capability — Class D Vehicles

The peak power per wheel required for maneuvering and resetting for the three vehicle classes is given in Figures 30, 31, and 32. In the cases where the peak input power requirement is less than 100 watts, an a-c servo motor is employed to produce the reaction torque. In these instances, a power inverter is required to furnish an alternating current. A d-c shunt motor is used in the cases where the input power exceeds 100 watts. Also to be included in the inertia wheel power requirement is the power dissipated by the electronics. This value is set at one watt.

The symbols used in Figs. 27-32 have the following meanings.

L_s = stall torque of motor

N_s = synchronous speed of motor

N_m = maximum speed of motor

Gyroscopic Control (Gyrotorquer)

The weight of the gyro control system is obtained by adding the weight of the electronics to the weight of the control packages employed. The weight of electronics is not proportionate to gyro size and the values used for the three-gyro, four-gyro, and six-gyro control systems were six pounds, eight pounds and 12 pounds respectively. The weights of the various gyro control systems were then determined as functions of momentum capability. These results are given in Fig. 33. The total continuous power required for the three-, four- and six-gyro control configurations is given in Fig. 34 as functions of required momentum. The values given are the sums of the power required to maintain a constant gyro spin velocity plus the power dissipated in the electronics. These power requirements must be supplied by an alternating current (115 volt, 400 Hz, three-phase inputs have been used for current systems) source. Therefore, a power inverter will be required by the system.

In Figs. 33 and 34, N_g denotes the gyro spin velocity.

Mass Expulsion Control

Mass expulsion differs from the other Class B, C, and D control systems described to this point. It is a momentum-elimination device in that angular momentum is transferred from within the vehicle to the external universe. Those systems previously discussed were momentum-storage devices in that the angular momentum was merely transferred from one rotating, rigid body to another within the satellite. Three types of reaction-jet control systems are considered in this area. These are cold gas systems, which employ the kinetic energy of the stored gas to produce the restoring force, and monopropellant and hypergolic systems, which utilize chemical energy. As most of the recent development effort in this field has been devoted to hypergolic systems, these are given the greatest emphasis.

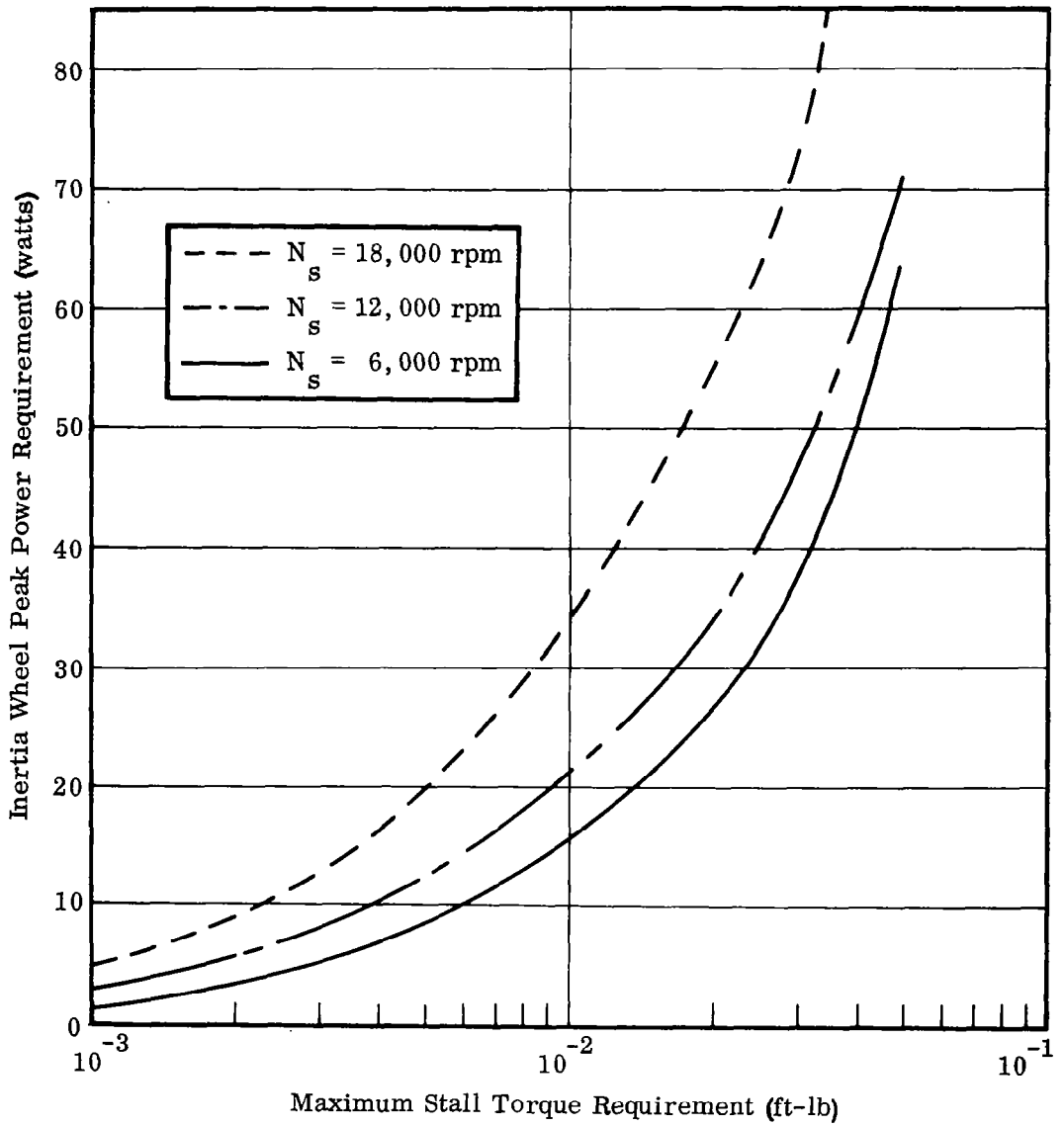

Figure 30. Inertia Wheel Peak Power Requirement (Single Axis) as a Function of Momentum Capability — Class B Vehicles

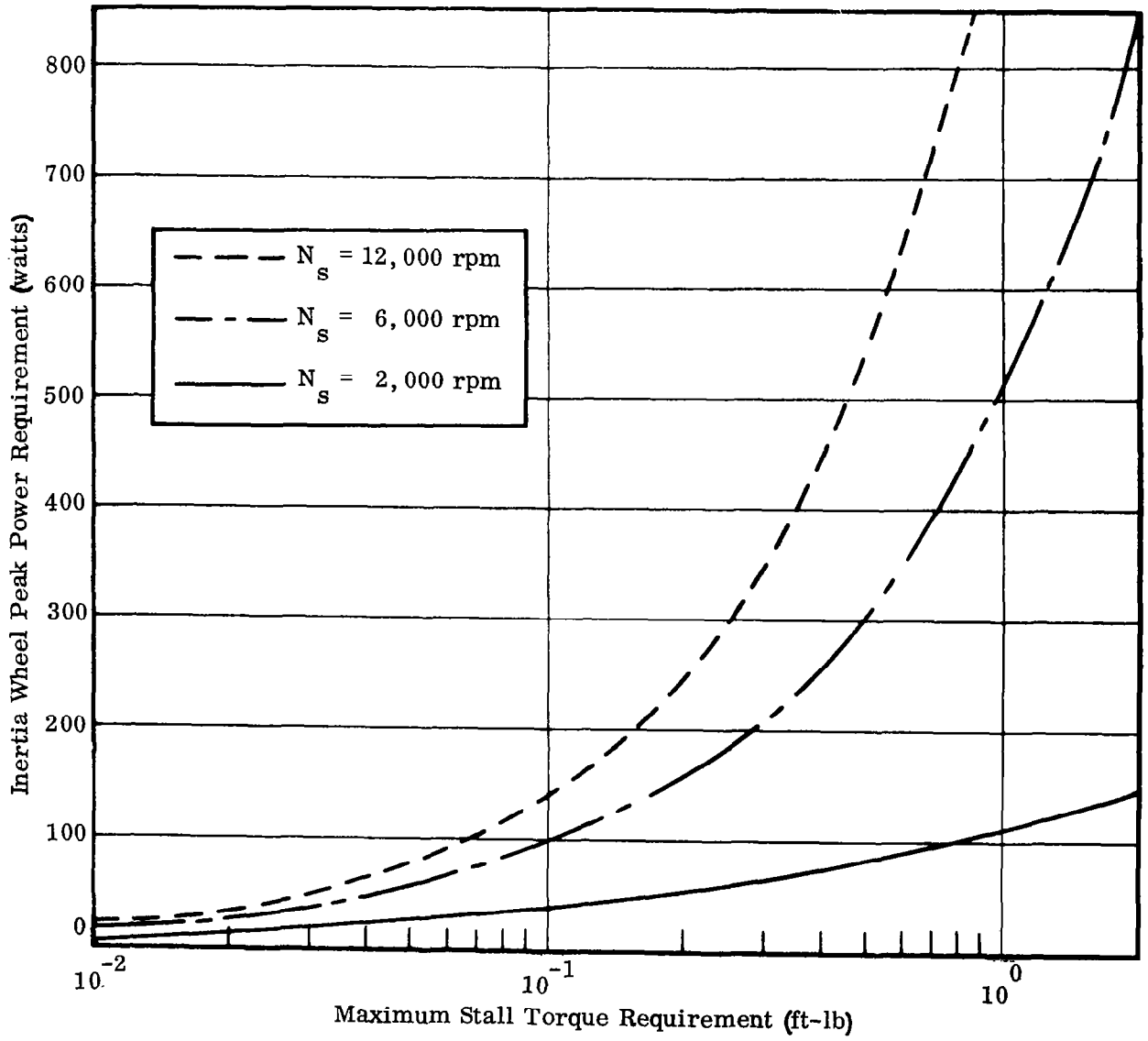

Figure 31. Inertia Wheel Peak Power Requirement (Single Axis) as a Function of Momentum Capability — Class C Vehicles

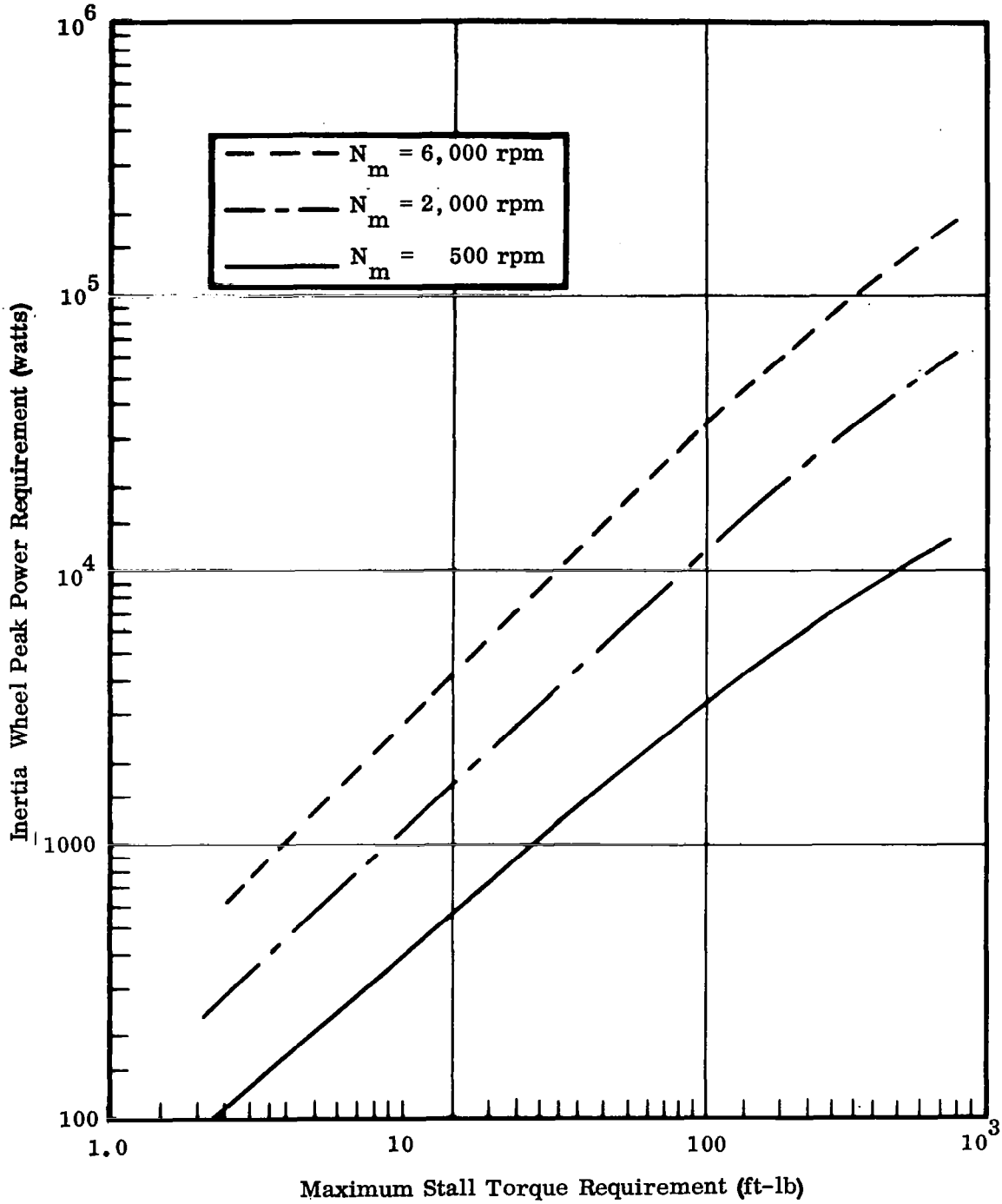

Figure 32. Inertia Wheel Peak Power Requirements (Single Axis) as a Function of Momentum Capability — Class D Vehicles

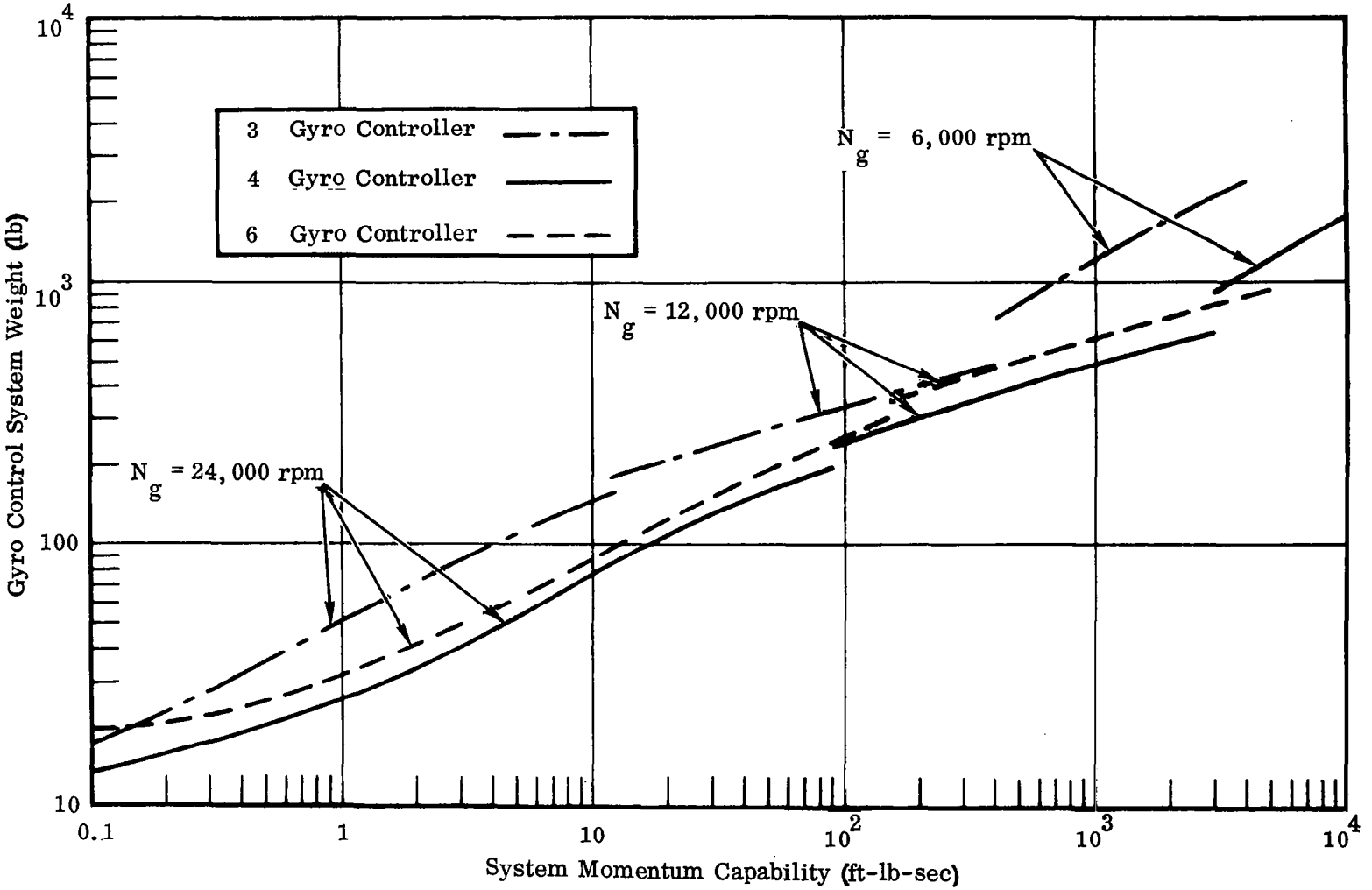

Figure 33. Gyro Control System Weight as a Function of System Momentum Capability

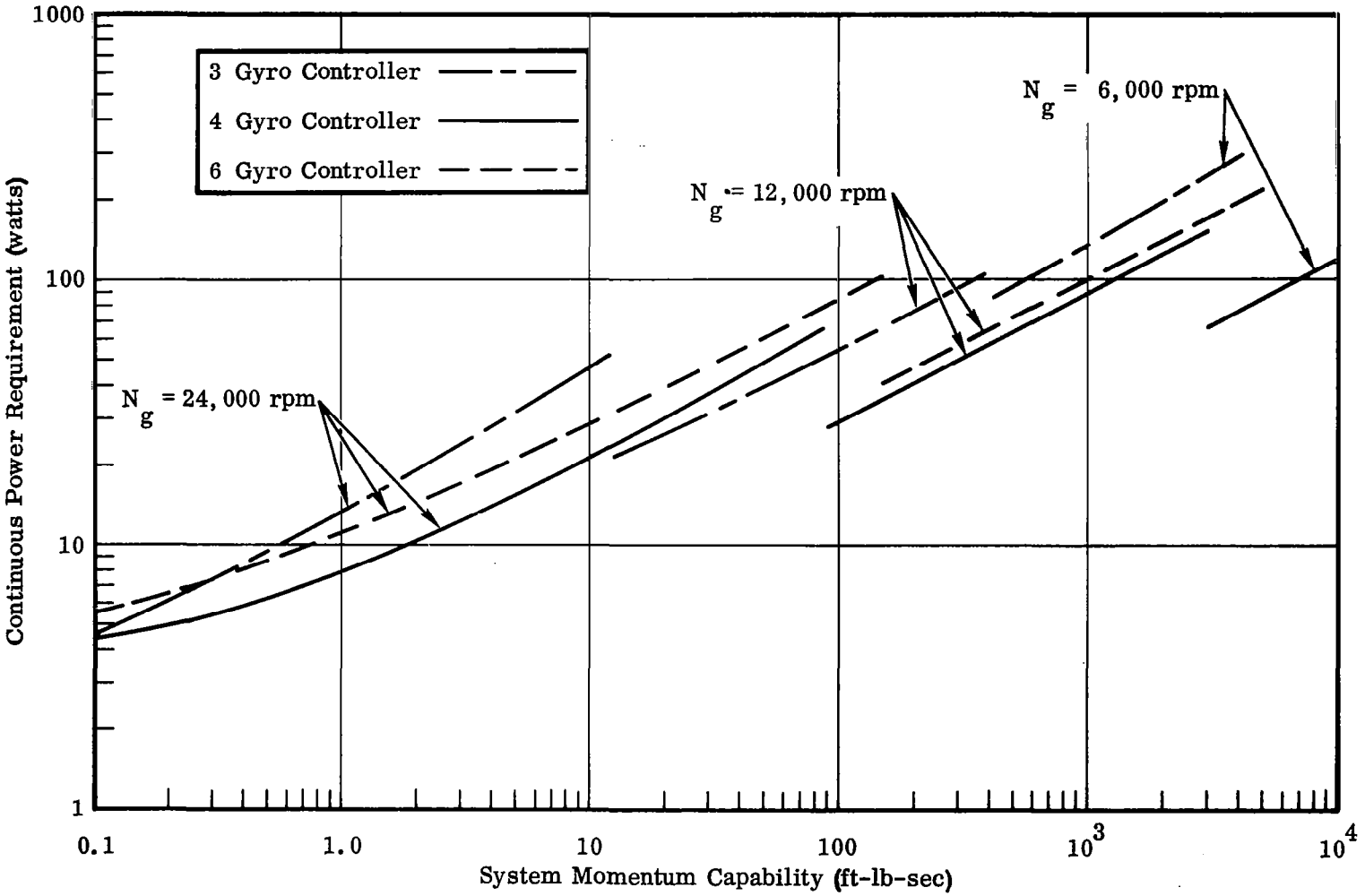

Figure 34. Continuous Gyro Control Power as a Function of System Momentum Capability

As mass-expulsion systems are momentum-elimination devices, the momentum required to perform the various mission functions must be determined. Momentum can be transferred into total impulse by dividing by the lever arm of the reaction force. The resulting control system weight then can be obtained for the three systems by making minor adjustments in the total impulse, due to system inefficiencies, and interpolation of the value given in Figures 35 and 36. These figures exhibit the weights of typical cold-gas, monopropellant, and bipropellant systems as functions of the total impulse requirement. The cold-gas system, due to its low storage density as compared to the liquid propellants, tends to be the most efficient system only for total impulse values under 1000 pound-seconds. The monopropellant system is most efficient from about 1000 pound-seconds to 5000 pound-seconds and the bipropellant system, due to its larger specific impulse, is the most efficient system for total impulse requirements exceeding 5000 pound-seconds. These areas of maximum efficiency are evident in the figures.

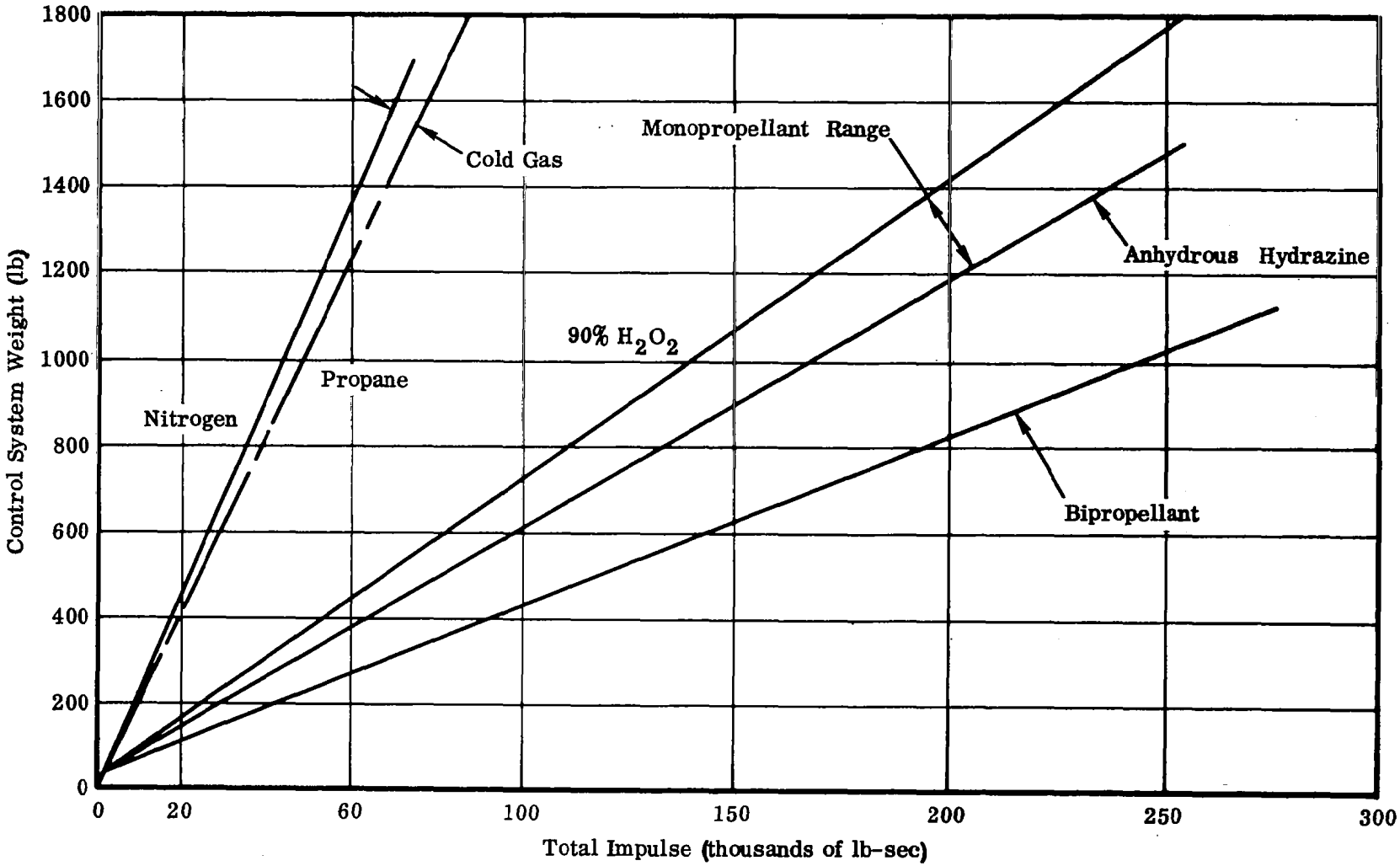

Figure 35. Control System Weight Versus Impulse Reaction Jet System

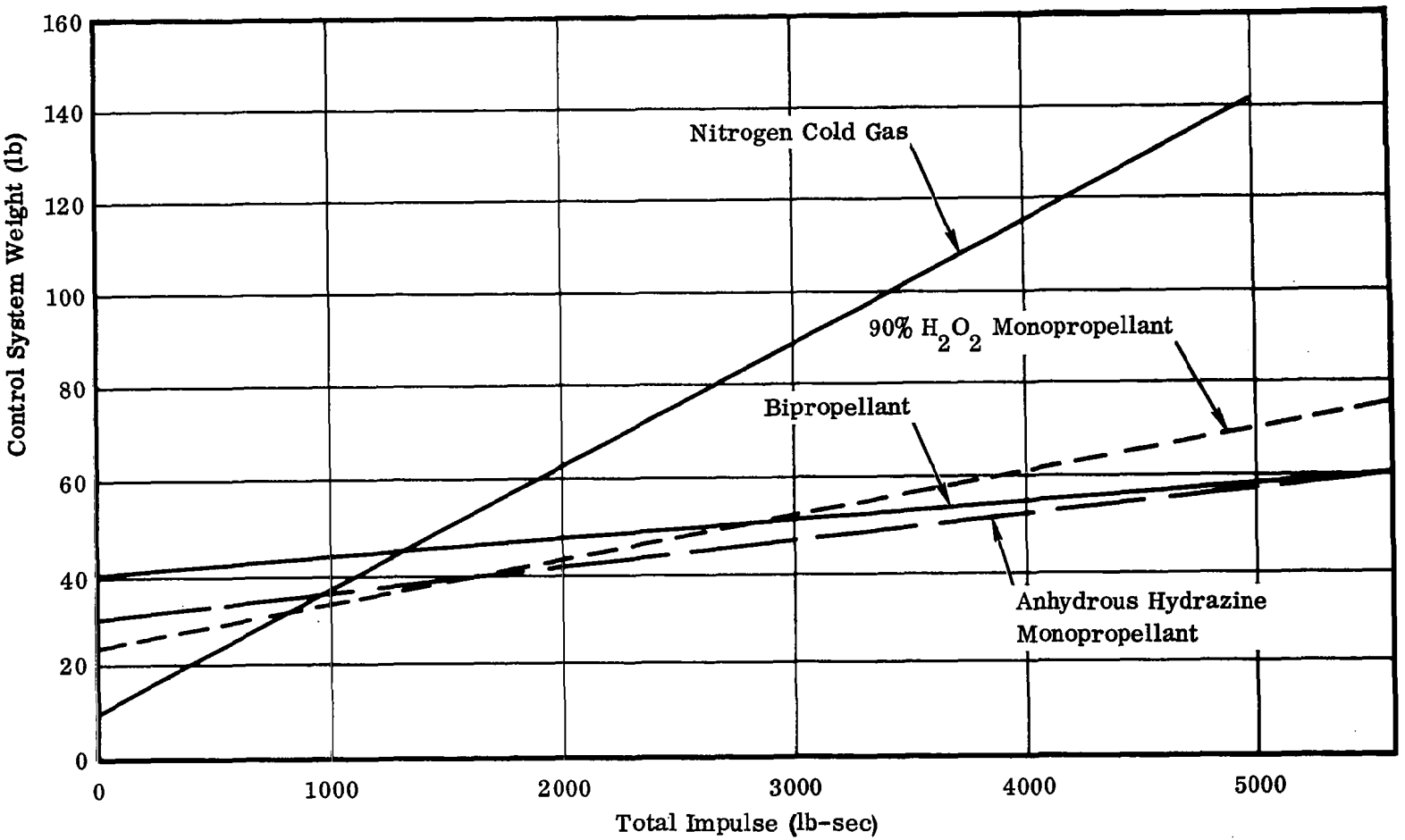

Figure 36. Control System Weight Versus Total Impulse Reaction Jet System

4. REFERENCES

1. Roberson, R. E. "Attitude Control of Satellites and Space Vehicles," Advances in Space Sciences, Vol. 2, Academic Press Inc. , New York, 1960

2. Thomson, W. T. "Passive Attitude Control of Satellite Vehicles," Chap. 7 in Guidance and Control of Aerospace Vehicles (Leondes ed), McGraw-Hill Book Co., New York, 1963

3. Adams, J. J. Study of an Active Control System for a Spinning Body, NASA TN D-905, 1961

4. Goldstein, H. Classical Mechanics, Addison Wesley Inc., Cambridge, Mass., 1950

5. Kurzhals, P.R., and Keckler, C.R. Spin Dynamics of Manned Space Stations, NASA TR R-155, 1963

6. Kennedy, H. B. "Attitude Control of Space Vehicles Using Gyro Precession Torques," Ballistic Missile and Aerospace Technology, Academic Press Inc., New York, 1961

7. Thomson, W. T. and Fung, W. C. "Instability of Spinning Space Stations Due to Crew Motion," AIAA Journ., Vol. 3, No. 6, 1965, p. 1082-1087

8. Taylor, R. S. "A Passive Pendulum Wobble Damping System for the NASA 21-Man Rotating Space Station," AIAA Symposium on Structural Dynamics and Aeroelasticity, Boston, Mass., 1965

9. Greensite, A. "The Attitude Control Problem for Flexible Satellites," Proc. SAE/NASA Aerospace Vehicle Flight Control Conf., Los Angeles, 1965, p. 161

10. Abzug, M. J. "Active Satellite Attitude Control," Chap. 8 in Guidance and Control of Aerospace Vehicles (Leondes ed.), McGraw-Hill Book Co., New York, 1963

11. Adams, J. and Chilton, R. A Weight Comparison of Several Attitude Controls for Satellites, NASA Memo 12-30-58L, Feb. 1959

12. Hsu, J. C., Lim, Y.S., and Meyer, A.U. — "On Active Attitude Control of Satellites," IEEE Transactions on Military Electronics, April 1965, p. 107-115

13. White, J.S. and Hansen, Q.M. — Study of Systems Using Inertia Wheels for Precise Attitude Control of a Satellite, NASA TN D-691, April 1961

14. Vaeth, J.E. — "Flywheel Control of Space Vehicles," IRE Conv. Record, New York, 1960, p. 91-103

15. Froelich, R.W. and Patapoff, H. — "Reaction Wheel Attitude Control for Space Vehicles," Proc. National Automatic Control Conf., Dallas, Texas, 1959, p. 139-149

16 Gevarter, W.B. — "Attitude Control of a Flexible Spinning Toroidal Manned Space Station," AIAA/JACC Guid. and Contr. Conf., Seattle, Wash., 1966, p.88-96

17. Dertouzos, M.L. and Roberge, J.K. — "High Capacity Reaction Wheel Attitude Control," IEEE Transaction on Application and Industry, March 1964, p. 99-104

18. Haeussermann, W. — "A Comparison of Actuation Methods for Attitude Control of Space Vehicles," Proceedings Manned Space Station Symposium, New York, 1960, p. 267-274

19. Wiggins, L.E. — "Relative Magnitudes of the Space Environment Torques on a Satellite," AIAA Journal, Vol. 2, No. 4, 1964, p. 770-771

20. Havill, J.R. and Ratcliff, J. W. — A Twin-Gyro Attitude Control System for Space Vehicles, NASA TN D-2419, August 1964

21. Suddath, J.H. — A Theoretical Study of the Angular Motions of Spinning Bodies in Space, NASA TR R-83, 1961

22. Fenster, S., Mott, J., and Parmet, I. — "Inertial and Celestial Sensing Methods," in Methods for Control of Satellites and Space Vehicles, Vol. I, WADD Tech. Report 60-643, July 1960

23. Nichol, K. C. — Research and Investigation on Satellite Attitude Control, Wright Patterson AFB Report No. AFFDL-TR-64-168, June 1965

24. Gillespie, W., Eide, D. G., and Churgin, A. B. — Some Notes on Attitude Control of Earth Satellite Vehicles, NASA TN D-40, Dec. 1959

25. Chobotov, V. — Equations of Motion for a Gravity Gradient Stabilized Satellite Subject to Ambient Perturbing Forces and Torques, Air Force Space Systems Div., Report No. TDR-269(4540-70)-2, May, 1964

26. Harding, C. F. — "Manned Vehicles as Solids with Translating Particles," Journal of Spacecraft and Rockets, Vol. 2, No. 3, 1965, p. 465-467

27. Rayleigh, J. — The Theory of Sound, 1894, republished by Dover, New York, 1945

28. Love, A.E.H. — A Trestise on the Mathematical Theory of Elasticity, Dover Publications, New York, 1944

29. Courant, R. and Hilbert, D. — Methods of Mathematical Physics, Vol. 1, Interscience Publishers, New York, 1953

30. Timoshenko, S. and Woinowsky-Krieger — Theory of Plates and Shells, McGraw-Hill Book Co., New York, 1959

31. Freeman, H. — Stability and Physical Realizability Considerations in the Synthesis of Multipole Control Systems, Trans. AIEE, Pt. 2, No. 35, March, 1958

32. Kavanagh, R. J. — Multivariable Control System Synthesis, Trans. AIEE Pt. 2, No. 39, Nov. 1958

33. Loebel, M. — "Several Linear Stabilization and Reorientation Control System Configurations for a Rotating Manned Orbital Space Station," Guidance and Control -II, Progress in Astronautics and Aeronautics, Vol. 13, Academic Press, New York, 1963

34. Wells, R. C., Sicko, J. S. and Courtney, F. M. — Gyroscopic Low Power Attitude Control for Space Vehicles, ASD-TDR-62-50, September 1962. Wright Patterson Air Force Base, Ohio

35. Hughes, W. G. — "Satellite Dynamics," Advances in Space Technology (Nayler, ed.), Newnes Lt'd., London, 1962

36. Cantor, C. "Fine Sun Tracker for Advanced Orbiting Solar Observatory," East Coast Conference on Aerospace and Naval Electronics, Baltimore, 1963

37. Lozins, N. G. "Pointing in Space," Space/Aeronautics, August, 1966 p. 76-83

38. Hatcher, N. M. "Spacecraft Attitude Sensors — Where We Stand Today," Astronautics and Aeronautics, December, 1966, p. 58-67

39. Roberson, R. E. "Gyroscopic Sensing of Satellite Yaw," Proceedings of 1st Congress on Automatic Control, Moscow, June, 1960

40. anon. "Soviets Cite Progress in Controlling Satellites," Missiles and Rockets, 3 November 1958, p. 52

41. Butz, J. S. Jr., "Nose Cone Tests Pay Space Lab Bonus," Aviation Week, 19 October 1959, 54, 55, 57, 59, 61, 63, 65

42. Nelson, J. H. "A New Absolute Instrument — The Proton Vector Magnetometer," J. Geophys, Res., 63, 1958, 880-881

43. DeBolt, H. E. "Magnetometer System for Orientation in Space," Electronics, April 8, 1960, 55-58

44. Ergin, E. I. and Wheeler, P. C. "Magnetic Attitude Control of a Spinning Satellite," J. Spacecraft and Rockets, Vol. 2, No. 6, 1965, p. 846-850

45. Whitford, A. E. and Kron, G. E. "Photoelectric Guiding of Astronomical Telescopes," Review of Scientific Instruments Vol. 8, 1937, p. 78

46. Cook, J. M. and Fleisig, R. "OAO Initial Stabilization and Control," Astronautics and Aerospace Engineering, September 1963, p. 88-95

47. Greensite, A. Design Criteria for Control of Space Vehicles, Vol. II-Part 1, Linear Systems, General Dynamics/Convair Report GDC-DDE66-019, 25 April 1966

48. Greensite, A. Design Criteria for Control of Space Vehicles, Vol II-Part 2, Nonlinear Systems, General Dynamics/Convair Report GDC-DDE65-056, 1 September 1965

49. Greensite, A. — Design Criteria for Control of Space Vehicles, Vol III-Part 7, Optimization Methods, General Dynamics/Convair Report GDC-DDE66-026, 5 July 1966

50. Kamm, L. J. — "Magnetometer: A Satellite Orientation Device," ARS Journal, June 1961

51. Roberson, R. E., et. al. — Methods for the Control of Satellites and Space Vehicles, WADD Tech. Report No. 60-643, July 1960

52. Esnault-Pelterie, R. — L'Astronautique, p. 130, A. Lahure, Paris, 1930

53. White, J. S. and Hansen, Q. M. — Study of a Satellite Attitude Control System Using Integrating Gyros as Torque Sources, NASA TN D-1073, September 1961

54. Kamm, L. J. — "Vertistat: An Improved Satellite Orientation Device," ARS Journal, June 1962, p. 911-913

55. Sohn, R. L. — "Attitude Stabilization by Means of Solar Radiation Pressure," ARS Journal, 1959, p. 371-373

56. Horsfall, R. B. — Stellar Inertial Navigation, IRE Trans. on Aerospace and Naval Electronics, June 1958, p. 106-114

57. Lunde, B. K. — "Horizon Sensing for Attitude Determination," Torques, and Attitude Sensing in Earth Satellites, (Singer, ed.) Academic Press, New York, 1964

58. Newton, R. R. — "Damping of a Gravitationally Stabilized Satellite," AIAA Journal, Vol. 2, No. 1, 1964, p. 20-25

59. Zajac, E. E. — "Damping of a Gravitationally Oriented Two-Body Satellite," ARS Journal, 1962, p. 1871-1875

60. Wadleigh, K. H., Galloway, A.J. and Mathur, P. N. — "Spinning Vehicle Nutation Damper," Journal of Spacecraft and Rockets, Vol. 1, No. 6, 1964, p. 588-592

61. Alper, J. R. — "Analysis of Pendulum Damper for Satellite Wobble Damping," Journal Spacecraft and Rockets, Vol. 2, No. 1, 1965, p. 50-54

62. Paul, B., West, J. W., and Yu, E. Y. "A Passive Gravitational Attitude Control System for Satellites," Bell System Technical Journal, September 1963, p. 2195-2239

63. Fletcher, H. J., Rongved, L., and Yu, E. Y. "Dynamic Analysis of a Two-Body Gravitationally Oriented Satellite," Bell System Technical Journal, September 1963, p. 2239-2266

64. Paul, B. "Planar Librations of an Extensible Dumbbell Satellite," AIAA Journal, Vol. 1, No. 2, 1963, p. 411-418

65. Roberson, R. E. "Gravitational Torque on a Satellite Vehicle, Journal Franklin Institute, Vol. 265, 1958, p. 13

66. Jensen, J., et.al. Design Guide to Orbital Flight, McGraw-Hill Book Co., New York, 1962, p. 752

67. Whipple, F. L. "The Meteoritic Risk to Space Vehicles," Vistas in Aeronautics, Permagon Press, New York, 1958

APPENDIX A

ANGULAR MOMENTUM OF A ROTOR IN A ROTATING BODY

The situation to be analyzed is shown schematically in Fig. A1. The spin axis of a rotor is fixed in a gimbal which is assumed to have three degrees of freedom with respect to a body coordinate system ($\bar{i}_b$, $\bar{j}_b$, $\bar{k}_b$). A gimbal coordinate system ($\bar{i}_G$, $\bar{j}_G$, $\bar{k}_G$) is rigidly attached to the gimbal, and a gyro coordinate system ($\bar{i}_g$, $\bar{j}_g$, $\bar{k}_g$) is fixed to the spinning rotor. The spin axis of the rotor, k_g, is at all times coincident with the gimbal axis, k_G. Furthermore, the gimbal and gyro coordinate frames have a common origin, Q, which is also the mass center of the gimbal and rotor, respectively.

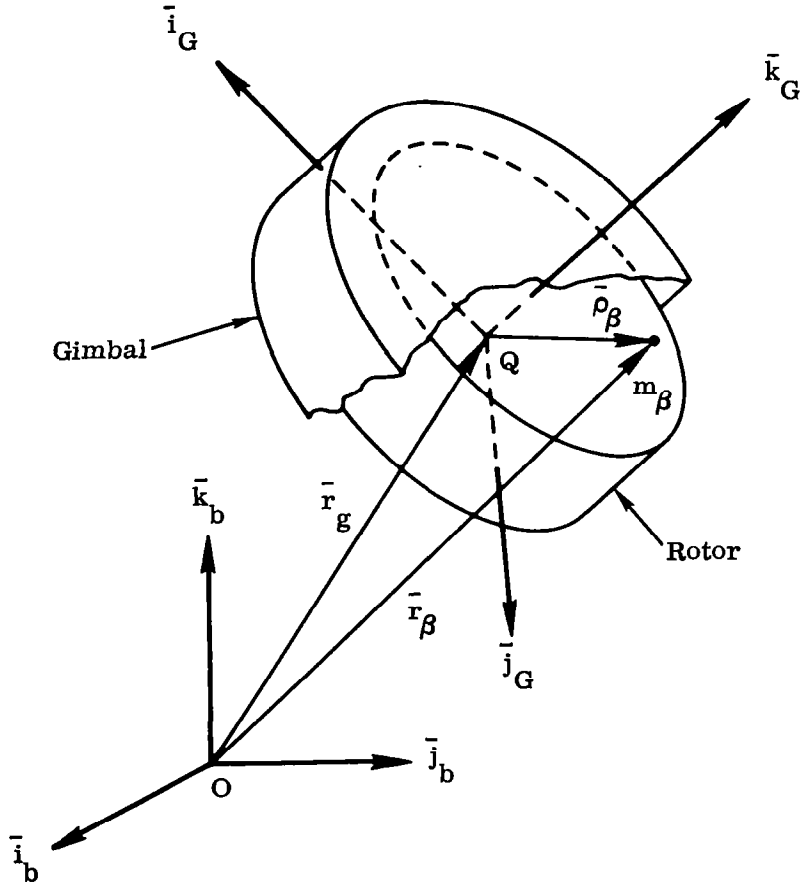

Figure A1. Geometry of Rotor and Gimbal

We seek to determine the angular momentum of the rotor about point O. For simplicity, we assume that the mass of the gimbal is negligible compared with that of the rotor, and that the axes of the gyro coordinate frame are also the principal inertial axes of the rotor. Then, by definition, the angular momentum of the rotor about point O is given by

$$\bar{H}_g = \sum_\beta \bar{r}_\beta \times m_\beta \bar{v}_\beta \tag{A1}$$

where m_β is a generic mass particle within the rotor and $\bar{v}_\beta$ is the velocity of m_β with respect to inertial space.

Now

$$\bar{v}_\beta = \frac{d}{dt} (\bar{r}_o + \bar{r}_\beta) \tag{A2}$$

where $\bar{r}_o$ is a vector from the origin of an inertial reference frame to the point O. Furthermore, since

$$\bar{r}_\beta = \bar{r}_g + \bar{\rho}_\beta \tag{A3}$$

we see that

$$\bar{v}_\beta = \bar{v}_o + \frac{d\bar{r}_g}{dt} + \frac{d\bar{\rho}_\beta}{dt} \tag{A4}$$

where $\bar{v}_o = \frac{d}{dt} \bar{r}_o$ is the velocity of point O with respect to inertial space.

Evaluating the second and third terms on the right hand side of (A4), we find

$$\frac{d}{dt} \bar{r}_g = \left(\frac{\delta \bar{r}_g}{\delta t}\right)_b + (\bar{\omega}_b + \bar{\omega}_r) \times \bar{r}_g \tag{A5}$$

$$\frac{d}{dt} \bar{\rho}_\beta = \left(\frac{\delta}{\delta t} \bar{\rho}_\beta\right)_g + (\bar{\omega}_g + \bar{\omega}_G + \bar{\omega}_b + \bar{\omega}_r) \times \bar{\rho}_\beta \tag{A6}$$

where $\bar{\omega}_b$ and $\bar{\omega}_r$ have the meaning defined in Subsection 3.1, and $\bar{\omega}_g$ is the angular velocity of the gyro frame with respect to the gimbal frame. The angular velocity of the gimbal frame with respect to the body frame is denoted by $\bar{\omega}_G$.

Combining Eqs. (A4) - (A6) and noting that

$$\left(\frac{\delta}{\delta t}\,\bar{r}_g\right)_b = \left(\frac{\delta}{\delta t}\,\bar{\rho}_\beta\right)_g = 0$$

since Q is fixed relative to the body frame and m_β is fixed relative to the gyro frame, we find

$$\bar{v}_\beta = \bar{v}_o + (\bar{\omega}_b + \bar{\omega}_r) \times \bar{r}_g + (\bar{\omega}_g + \bar{\omega}_G + \bar{\omega}_b + \bar{\omega}_r) \times \bar{\rho}_\beta \tag{A7}$$

Substituting (A7) in (A1), and making use of the fact that

$$\sum_\beta m_\beta \bar{\rho}_\beta = 0 \tag{A8}$$

since Q is the mass center of the rotor, we obtain

$$\bar{H}_g = m_g \bar{r}_g \times \left[\bar{v}_o + (\bar{\omega}_b \times \bar{\omega}_r) \times \bar{r}_g\right] + \sum_\beta m_\beta \bar{\rho}_\beta \times \left[(\bar{\omega}_g + \bar{\omega}_G + \bar{\omega}_b + \bar{\omega}_r) \times \bar{\rho}_\beta\right] \tag{A9}$$

where

$$m_g = \sum_\beta m_\beta$$

is the mass of the rotor (gyro).

Eq. (A9) may be written in the form

$$\bar{H}_g = m_g \bar{r}_g \times \left[\bar{v}_o + (\bar{\omega}_b + \bar{\omega}_r) \times \bar{r}_g\right] + J \cdot (\bar{\omega}_g + \bar{\omega}_G + \bar{\omega}_b + \bar{\omega}_r) \tag{A10}$$

where J is the inertia dyadic of the rotor, viz.

$$J = A\,\bar{i}_g \bar{i}_g + A\,\bar{j}_g \bar{j}_g + C\,\bar{k}_g \bar{k}_g = A\,\bar{I}_G \bar{I}_G + A\,\bar{J}_G \bar{J}_G + C\,\bar{k}_G \bar{k}_G \tag{A11}$$

$$A = \sum_\beta m_\beta (y_\beta^2 + z_\beta^2) = \sum_\beta m_\beta (x_\beta^2 + z_\beta^2) \tag{A12}$$

$$C = \sum_{\beta} m_{\beta} (x_{\beta}^2 + y_{\beta}^2) \tag{A13}$$

$$\bar{\rho}_{\beta} = x_{\beta} \bar{I}_g + y_{\beta} \bar{J}_g + z_{\beta} \bar{k}_g \tag{A14}$$

Denoting the angular velocity of the rotor about its axis of rotation by Ω, we see that

$$\bar{\omega}_g = \Omega \bar{k}_g = \Omega \bar{k}_G \tag{A15}$$

For the special case where the rotor and vehicle mass centers are coincident, $\bar{r}_g = 0$, and

$$\bar{H}_g = J \cdot (\bar{\omega}_g + \bar{\omega}_G + \bar{\omega}_b + \bar{\omega}_r) \tag{A16}$$

APPENDIX B

VIBRATION FREQUENCIES AND MODE SHAPES FOR A THIN CIRCULAR PLATE

List of Symbols

a = radius of plate; ft.

D = $\frac{Eh^3}{12(1-\nu^2)}$ = plate stiffness, lb ft

E = Young's modulus, lb/ft^2

f = applied force, lb

h = thickness of plate, ft

$I_n(\ )$ = modified Bessel function of the first kind of order n

$J_n(\ )$ = Bessel function of the first kind of order n

m = mass per unit area, $slugs/ft^2$

$\mathfrak{M}_{nm}$ = generalized mass for the nm mode; slugs

Q_{nm} = generalized force for nm mode; lb

q_{nm} = generalized coordinate for the nm mode; ft

t = time; sec

u = displacement normal to plane of plate; ft

$Y_n(\ )$ = Bessel function of the second kind of order n

ρ, α = polar coordinates

∇^2 = Laplacian = $\frac{\partial^2}{\partial\rho^2} + \frac{1}{\rho}\frac{\partial}{\partial\rho} + \frac{1}{\rho^2}\frac{\partial^2}{\partial\alpha^2}$

ν = Poisson's ratio

ξ_{nm} = relative damping factor for the nm mode

σ_{nm} = radial slope of the nm mode; rad/ft

φ_{nm} = normalized mode shape of the nm mode

ψ_{nm} = tangential slope of the nm mode; rad/ft

ω_{nm} = natural frequency of the nm mode; rad/sec

The ensuing development follows very closely the analysis contained in Ref. 9. This is a somewhat expanded treatment of a problem first solved by Rayleigh [27] but whose main purpose is to cast the results in a form suitable for control system analysis.

The basic equation describing the motion of a flat plate is [27] (See Fig. B1).

$$\nabla^2 (D\nabla^2 u) + m(\rho, \alpha) \frac{\partial^2 u}{\partial t^2} = f(\rho, \alpha, t) \tag{B1}$$

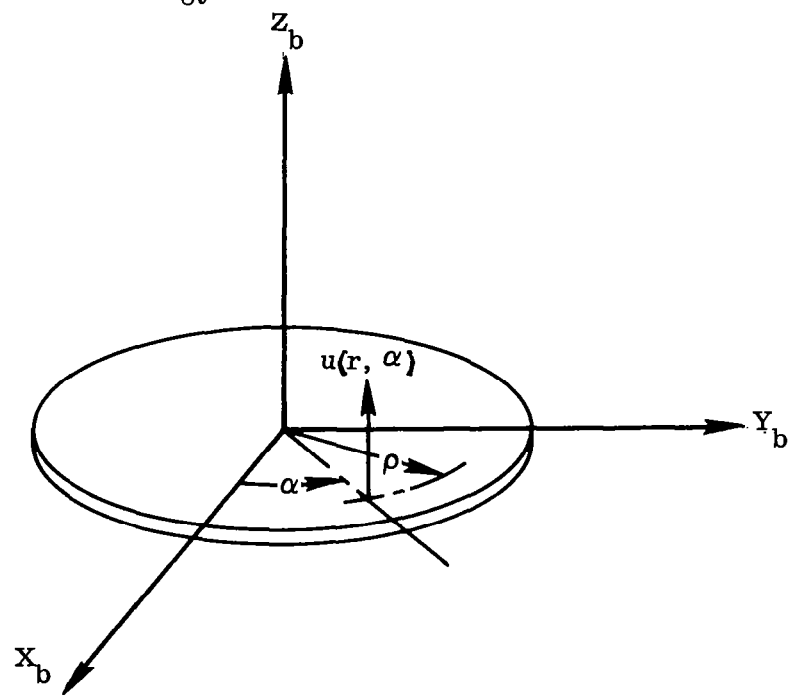

Figure B1. Geometry for Flat Plate Problem

To derive the free modes of vibration, we consider first the homogeneous form of this equation and, applying the usual separation of variables technique,

$$u = F(t)\, W(\rho, \alpha) \tag{B2}$$

arrive at

$$\frac{1}{m} \frac{\nabla^2 (D \nabla^2 u)}{W} = -\frac{1}{F} \frac{d^2 F}{dt^2} = \omega_{nm}^2$$

or

$$\frac{d^2 F}{dt^2} + \omega_{nm}^2 F = 0 \tag{B3}$$

$$\nabla^2 (D \nabla^2 W) - m \omega_{nm}^2 W = 0 \tag{B4}$$

It can be shown[29] that when suitable boundary conditions are prescribed

1. There exists a denumerably infinite sequence of eigenvalues, ω_{nm} and
2. for each eigenvalue, ω_{nm}, there exists an eigenfunction $W_{nm}(\rho, \alpha)$ which satisfies the relation

$$\int_0^{2\pi} \int_0^a m W_{nm} W_{pq} \rho \, d\rho \, d\alpha = 0 \tag{B5}$$

where $n \neq p$ or $m \neq q$; while

$$\int_0^{2\pi} \int_0^a m W_{nm}^2 \rho \, d\rho \, d\alpha = 1$$

The most general solution of the homogeneous form of Eq. (B1) is

$$u(\rho, \alpha, t) = \sum_{n=0}^{\infty} \sum_{m=0}^{\infty} F_{nm}(t)\, W_{nm}(\rho, \alpha) \tag{B6}$$

Assuming that the plate is circular and uniform such that m and D are constants, Eqs. (B3) and (B4) may be written as

$$\frac{d^2F}{dt^2} + \frac{k_{nm}^4}{c^2} F = 0 \tag{B7}$$

$$\nabla^4 W - k_{nm}^4 W = 0 \tag{B8}$$

where

$$c^2 = \frac{m}{D} \tag{B9}$$

and

$$\omega_{nm}^2 = \frac{k_{nm}^4}{c^2} \tag{B10}$$

Eq. (B8) may be written as

$$(\nabla^2 + k_{nm}^2)(\nabla^2 - k_{nm}^2) W = 0 \tag{B11}$$

The general solution of this equation is equal to the sum of the solutions to

$$(\nabla^2 + k_{nm}^2) W = 0 \tag{B12}$$

and

$$(\nabla^2 - k_{nm}^2) W = 0 \tag{B13}$$

Consider first Eq. (B12) which may be written in expanded form as follows

$$\frac{\partial^2 W}{\partial \rho^2} + \frac{1}{\rho}\frac{\partial W}{\partial \rho} - \frac{1}{\rho^2}\frac{\partial^2 W}{\partial \alpha^2} + k_{nm}^2 W = 0 \tag{B14}$$

If we assume a solution of the form

$$W^{(0)} = G_1(\rho)\, G_2(\alpha) \tag{B15}$$

and substitute back in (B14), we obtain

$$\frac{\rho^2}{G_1}\frac{d^2 G_1}{d\rho^2} - \frac{\rho}{G_1}\frac{dG_1}{d\rho} + k_{nm}\rho^2 = -\frac{1}{G_2}\frac{d^2 G_2}{d\alpha^2} = n^2 \tag{B16}$$

It follows that

$$\frac{d^2 G_1}{d\rho^2} + \frac{1}{\rho}\frac{dG_1}{d\rho} + \left(k_{nm}^2 - \frac{n^2}{\rho^2}\right) G_1 = 0 \tag{B17}$$

$$\frac{d^2 G_2}{d\alpha^2} + n^2 G_2 = 0 \tag{B18}$$

The respective solutions of the above equations are:

$$G_1(\rho) = A J_n(k_{nm}\rho) + C_1 Y_n(k_{nm}\rho) \tag{B19}$$

$$G_2(\alpha) = C_2 \cos n(\alpha + \epsilon) \tag{B20}$$

where A, C_1, C_2 and ϵ are arbitrary constants.

For Eq. (B13), a solution identical in form to (B19) and (B20) is obtained, but with k_{nm} replaced by ik_{nm}. Physical considerations dictate that the terms $Y_n(k_{nm}\rho)$ and $Y_n(i\,k_{nm}\rho)$ be discarded since each of these approaches infinity as ρ approaches zero. Consequently, the most general solution of Eq. (B11) may be written as:

$$\begin{aligned} W_{nm}(\rho,\alpha) &= \left[A J_n(k_{nm}\rho) + B I_n(k_{nm}\rho)\right]\left[C_2 \cos n(\alpha+\epsilon)\right] \\ &= R_n(\rho)\, V_n(\alpha) \end{aligned} \tag{B21}$$

Now since (ρ, α) and $(\rho, \alpha + 2\pi)$ represent the same point, it follows that n must be a positive integer or zero if W is to be single valued. Therefore, we need only consider n = 0, 1, 2, ---- .

The boundary conditions to be satisfied at the free edge are:[30]

$$\left(\frac{d^2}{d\rho^2} + \frac{\nu}{\rho}\frac{d}{d\rho} - \frac{n^2\nu}{\rho^2}\right) R_n = 0 \tag{B22}$$

$$\frac{d}{d\rho}\left(\frac{d^2}{d\rho^2} + \frac{1}{\rho}\frac{d}{d\rho} - \frac{n^2}{\rho^2}\right) R_n + \frac{n^2(\nu-1)}{\rho}\frac{d}{d\rho}\left(\frac{R_n}{\rho}\right) = 0 \tag{B23}$$

Eq. (B22) expresses the fact that, at a free edge, the bending moment in a radial direction is zero; while (B23) states that, at a free edge, the vertical shear is zero.

Substituting R_n from (B21) into the above equations, and making use of some standard relations for the Bessel functions, we obtain the equations:

$$\left[(\nu-1)\,(k_{nm}\,a\,J_n' - n^2\,J_n) - k_{nm}^2\,a^2\,J_n\right]A + \left[(\nu-1)\,(k_{nm}\,a\,I_n' - n^2\,I_n) + k_{nm}^2\,a^2\,I_n\right]B = 0 \tag{B24}$$

$$\left[n^2\,(\nu-1)\,(k_{nm}\,a\,J_n' - J_n) - k_{nm}^3\,a^3\,J_n'\right]A + \left[n^2\,(\nu-1)\,(k_{nm}\,a\,I_n' - I_n) + k_{nm}^3\,a^3\,I_n'\right]B = 0 \tag{B25}$$

Here

$$J_n \equiv J_n\,(k_{nm}\,a)$$

$$I_n \equiv I_n\,(k_{nm}\,a)$$

$$J' \equiv \frac{d}{d\,(k_{nm}\,\rho)}\,J_n\,(k_{nm}\,\rho)\Big|_{\rho\,=\,a}$$

$$I' \equiv \frac{d}{d\,(k_{nm}\,\rho)}\,I_n\,(k_{nm}\,\rho)\Big|_{\rho\,=\,a}$$

Equations (B24) and (B25) have the trivial solution A = B= 0. In order to yield a nontrivial solution, the determinant of the coefficients, A and B, must vanish. Setting this determinant equal to zero and simplifying, we obtain

$$2\,(\nu-1)\,k_{nm}^3\,a^3\,J_n'\,I_n + \left\{\left[n^2\,(\nu-1) - k_{nm}^2\,a^2\right]^2 - n^2\,(\nu-1)^2\right\}J_n'\,I_n - \left\{\left[n^2\,(\nu-1) + k_{nm}^2\,a^2\right]^2 - n^2\,(\nu-1)^2\right\}I_n'\,J_n + 2\,n^2\,k_{nm}\,a\,(\nu-1)\,J_n\,I_n = 0 \tag{B26}$$

For each value of n = 0, 1, 2, ---, there are an infinite number of values of k_{nm} which satisfy the above equation. With these k_{nm}, equations (B24) and (B25) are not independent (i.e., they cannot be solved for A and B separately). However, each such value of k_{nm} yields a value of the ratio B/A which we write as:

$$\Lambda_{nm} = B/A$$

to emphasize that it is a function of n and m.

Putting n = 0 in Eq. (B26) we find

$$2(\nu-1) J_0'(k_{0m}a) I_0'(k_{0m}a) - k_{0m}a \left[J_0(k_{0m}a) I_0'(k_{0m}a) - I_0(k_{0m}a) J_0'(k_{0m}a)\right] = 0 \qquad \text{(B27)}$$

The lowest value of k_{0m} which satisfies this equation is $k_{00} = 0$. Furthermore, putting n = 1 in Eq. (B26) we find that the lowest value of k_{1m} which satisfies the resulting equation is $k_{10} = 0$.

For n = 2, the lowest value of k_{2m} which satisfies Eq. (B26) is*

$$k_{20}a = 2.2915$$

For n = 0, the lowest non zero value of k_{om} which satisfies Eq. (B27) is

$$k_{01}a = 3.0127$$

While for n = 1, the lowest non zero value of k_{1m} which satisfies Eq. (B27) is

$$k_{11}a = 4.530$$

Note that $k_{00} = 0$ corresponds to a rigid body translation while $k_{10} = 0$ corresponds to a rigid body rotation.

Having calculated the quantities k_{nm} we may then find the Λ_{nm} (= B/A) from Eqs. (B24) and (B25). The mode shape, $W_{nm}(\rho, \alpha)$, of Eq. (B21) is now written as

$$W_{nm}(\rho, \alpha) = C_3 \left[J_n(k_{nm}\rho) + \Lambda_{nm} I_n(k_{nm}\rho)\right] \cos n(\alpha + \epsilon) \qquad \text{(B28)}$$

---

* Using $\nu = 1/3$

where C_3 and α are arbitrary constants. This merely reflects the fact that there is no preferred reference either radially or circumferentially. In other words, the expression for the mode shape gives relative rather than absolute displacements. The mode shapes are shown in Fig. B2.

For computational expediency, it is convenient to assign absolute values to the displacement, and this requires that we normalize in some fashion. This may be done in various ways. For present purposes, we write Eq. (B28) as

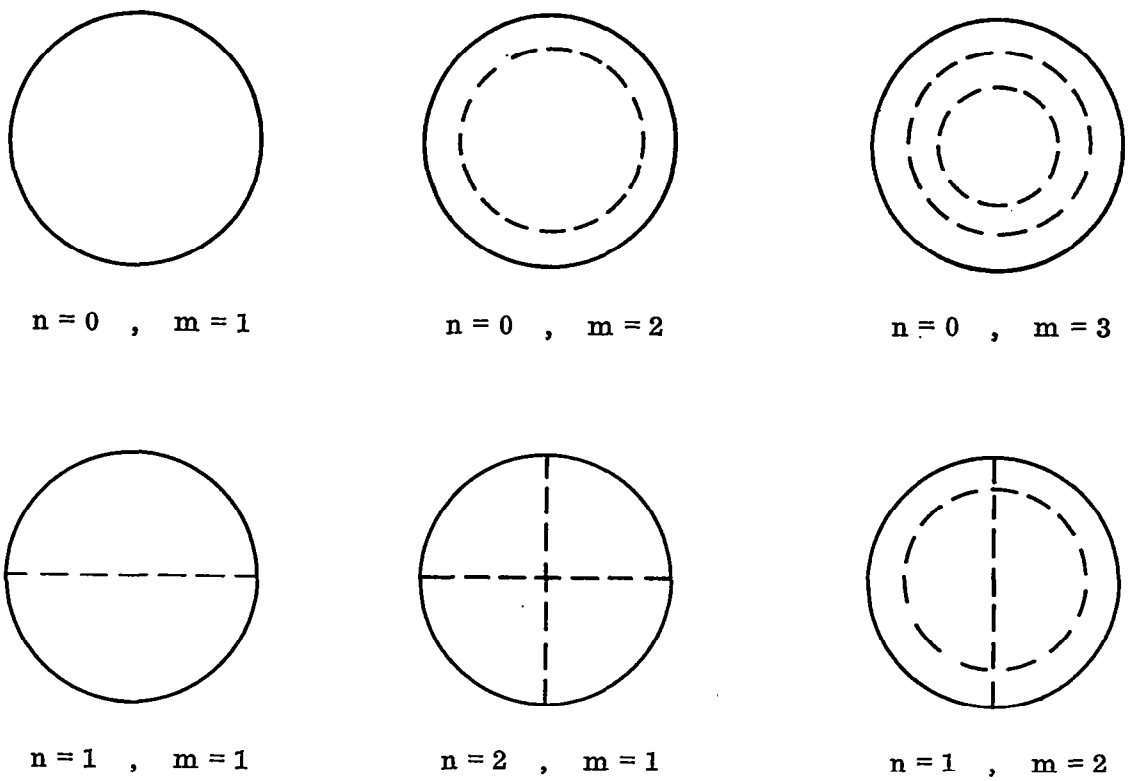

Note: The dotted lines indicate the lines of zero deflection.

Figure B2. Mode Shapes for Thin Circular Plate

$$W_{nm}(\rho, \alpha) = W^{(s)}_{nm}(\rho, \alpha) + W^{(c)}_{nm}(\rho, \alpha) \tag{B29}$$

where

$$W^{(s)}_{nm}(\rho, \alpha) = C_4 \left[J_n(k_{nm}\rho) + \Lambda_{nm} I_n(k_{nm}\rho)\right] \sin n\alpha \tag{B30}$$

$$W^{(c)}_{nm}(\rho, \alpha) = C_5 \left[J_n(k_{nm}\rho) + \Lambda_{nm} I_n(k_{nm}\rho)\right] \cos n\alpha \tag{B31}$$

and where C_4 and C_5 are constants.

The normalized modes are now defined as

$$\varphi^{(s)}_{nm}(\rho, \alpha) = \frac{W^{(s)}_{nm}(\rho, \alpha)}{W^{(s)}_{nm}\left[a, \frac{\pi}{2}(1 + 4n)\right]} \tag{B32}$$

$$\varphi^{(c)}_{nm}(\rho, \alpha) = \frac{W^{(c)}_{nm}(\rho, \alpha)}{W^{(c)}_{nm}(a, o)} \tag{B33}$$

We have therefore

$$\varphi^{(s)}_{nm}(\rho, \alpha) = \zeta_{nm}\left[J_n(k_{nm}\rho) + \Lambda_{nm} I_n(k_{nm}\rho)\right] \sin n\alpha \tag{B34}$$

$$\varphi^{(c)}_{nm}(\rho, \alpha) = \zeta_{nm}\left[J_n(k_{nm}\rho) + \Lambda_{nm} I_n(k_{nm}\rho)\right] \cos n\alpha \tag{B35}$$

where

$$\zeta_{nm} = \left[J_n(k_{nm}a) + \Lambda_{nm} I_n(k_{nm}a)\right]^{-1} \tag{B36}$$

It is easy to see that the normalized modes also satisfy the orthogonality relationships (B5)

It follows that the displacement $u(\rho, \alpha, t)$, given by Eq. (B6), may be expressed in the form

$$u(\rho, \alpha, t) = \sum_{n=0}^{\infty} \sum_{m=0}^{\infty} \left[q^{(s)}_{nm}(t)\, \varphi^{(s)}_{nm}(\rho, \alpha) + q^{(c)}_{nm}(t)\, \varphi^{(c)}_{nm}(\rho, \alpha)\right] \tag{B37}$$

where the generalized coordinates, $q_{nm}^{(s)}(t)$ and $q_{nm}^{(c)}(t)$ are given by

$$q_{nm}^{(s)}(t) = F_{nm}(t)\, W_{nm}^{(s)}\left[a, \frac{\pi}{2}(1+4n)\right] \tag{B38}$$

$$q_{nm}^{(c)}(t) = F_{nm}(t)\, W_{nm}^{(c)}(a, o) \tag{B39}$$

We now assume that the applied force distribution can be represented as

$$f(\rho, \alpha, t) = \sum_{n=o}^{\infty} \sum_{m=o}^{\infty} m \left[A_{nm}^{(s)}(t)\, \varphi_{nm}^{(s)}(\rho, \alpha) + A_{nm}^{(c)}(t)\, \varphi_{nm}^{(c)}(\rho, \alpha)\right] \tag{B40}$$

where the functions $A_{nm}^{(s)}(t)$ and $A_{nm}^{(c)}(t)$ are to be determined. Multiplying both sides of Eq. (B40) by $\varphi_{pq}^{(s)}(\rho,\alpha)$ and integrating over the whole plate, we have*

$$\int_o^{2\pi}\int_o^a \rho\, \varphi_{pq}^{(s)}\, f\, d\rho\, d\alpha = \sum_{n=o}^{\infty} \sum_{m=o}^{\infty} A_{nm}^{(s)}(t) \int_o^{2\pi}\int_o^a \rho\, m\, \varphi_{nm}^{(s)}\, \varphi_{pq}^{(s)}\, d\rho\, d\alpha \tag{B41}$$

Here we have made use of the fact that

$$\int_o^{2\pi}\int_o^a \rho\, m\, \varphi_{pq}^{(s)}\, \varphi_{nm}^{(c)}\, d\rho = 0 \tag{B42}$$

for all values of p, q, n, and m.

However, using the orthogonality property (B5), Eq. (B41) reduces to

$$\int_o^{2\pi}\int_o^a \rho\, \varphi_{pq}^{(s)}\, f\, d\rho\, d\alpha = A_{pq}(t) \int_o^{2\pi}\int_o^a \rho\, m \left[\varphi_{pq}^{(s)}\right]^2 d\rho\, d\alpha \tag{B43}$$

or

$$A_{nm}^{(s)}(t) = \frac{Q_{nm}^{(s)}}{\mathfrak{M}_{nm}^{(s)}} \tag{B44}$$

---

* We will drop the arguments of the function wherever convenient and where there is no loss of clarity.

where

$$Q_{nm}^{(s)} = \int_o^{2\pi}\int_o^a \rho\, \varphi_{nm}^{(s)}\, f\, d\rho\, d\alpha \tag{B45}$$

$$\mathfrak{m}_{nm}^{(s)} = \int_o^{2\pi}\int_o^a \rho\, m \left[\varphi_{nm}^{(s)}\right]^2 d\rho\, d\alpha \tag{B46}$$

Similarly, multiplying Eq. (B40) by $\varphi_{nm}^{(c)}(\rho, \alpha)$ and preceeding as above, we find

$$A_{nm}^{(c)}(t) = \frac{Q_{nm}^{(c)}}{\mathfrak{m}_{nm}^{(c)}} \tag{B47}$$

where

$$Q_{nm}^{(c)} = \int_o^{2\pi}\int_o^a \rho\, \varphi_{nm}^{(c)}\, f\, d\rho\, d\alpha \tag{B48}$$

$$\mathfrak{m}_{nm}^{(c)} = \int_o^{2\pi}\int_o^a \rho\, m \left[\varphi_{nm}^{(c)}\right]^2 d\rho\, d\alpha \tag{B49}$$

Substituting (B44 - (B49) in Eq. (B40), we have

$$f(\rho, \alpha, t) = \sum_{n=o}^{\infty}\sum_{m=o}^{\infty} m\left[\frac{Q_{nm}^{(s)}}{\mathfrak{m}_{nm}^{(s)}}\varphi_{nm}^{(s)} + \frac{Q_{nm}^{(c)}}{\mathfrak{m}_{nm}^{(c)}}\varphi_{nm}^{(c)}\right] \tag{B50}$$

Now if Eqs. (B37) and (B50) are substituted in Eq. (B1), with both sides of the resulting equation multiplied by $\varphi_{pq}^{(s)}(\rho, \alpha)$ and then integrated over the whole plate, the end result is

$$\sum_{n=o}^{\infty}\sum_{m=o}^{\infty}\int_o^{2\pi}\int_o^a \rho\left[\ddot{q}_{nm}^{(s)}\, m\, \varphi_{pq}^{(s)}\, \varphi_{nm}^{(s)} + q_{nm}^{(s)}\, \varphi_{pq}^{(s)}\, \nabla^2\left(D\nabla^2\varphi_{nm}^{(s)}\right)\right] d\rho\, d\alpha$$

$$= \sum_{n=o}^{\infty}\sum_{m=o}^{\infty}\int_o^{2\pi}\int_o^a \rho\, \frac{Q_{nm}^{(s)}}{\mathfrak{m}_{nm}^{(s)}}\, m\, \varphi_{pq}^{(s)}\, \varphi_{nm}^{(s)}\, d\rho\, d\alpha$$

Here we have made use of the orthogonality property (B42).

But from (B4) and (B32)

$$\nabla^2 (D \nabla^2 \varphi^{(s)}_{nm}) = m \omega^2_{nm} \varphi^{(s)}_{nm}$$

Substituting this in the preceding equation and making use of the orthogonality property (B5) we have finally

$$\ddot{q}^{(s)}_{nm} + \omega^2_{nm} q^{(s)}_{nm} = \frac{Q^{(s)}_{nm}}{\mathcal{M}^{(s)}_{nm}} \tag{B51}$$

If we repeat the above procedure but multiply by $\varphi^{(c)}_{pq}(\rho, \alpha)$ instead of $\varphi^{(s)}_{pq}(\rho, \alpha)$ as before, the end result obtained is

$$\ddot{q}^{(c)}_{nm} + \omega^2_{nm} q^{(c)}_{nm} = \frac{Q^{(c)}_{nm}}{\mathcal{M}^{(c)}_{nm}} \tag{B52}$$

In control system applications, the following mode slopes are important:

Radial Slope:

$$\sigma^{(s)}_{nm}(\rho, \alpha) = \frac{\partial \varphi^{(s)}_{nm}(\rho, \alpha)}{\partial \rho} \tag{B53}$$

Circumferential Slope:

$$\psi^{(s)}_{nm}(\rho, \alpha) = \frac{1}{\rho} \frac{\partial \varphi^{(s)}_{nm}(\rho, \alpha)}{\partial \alpha} \tag{B54}$$

with similar expressions for $\sigma^{(c)}_{nm}$ and $\psi^{(c)}_{nm}$.

To illustrate the method of calculating some typical generalized forces, consider a pure moment, L, which acts at the point (α_p, ρ_p), and whose axis is in the plane of the plate normal to a radial line. To treat this case, we assume that we can represent the moment by two forces, a small distance, $\Delta\rho$, apart.

Here we have

$$L = P \Delta\rho$$

$$f = P\Big|_{\substack{\rho = \rho_p + \Delta\rho \\ \alpha = \alpha_p}} - P\Big|_{\substack{\rho = \rho_p \\ \alpha = \alpha_p}}$$

Consequently

$$Q^{(c)}_{nm} = \int_0^{2\pi}\int_0^{a} \rho\, f\, \varphi^{(c)}_{nm}\, d\rho\, d\alpha = P\Delta\rho\left[\frac{\varphi^{(c)}_{nm}(\alpha_p, \rho_p + \Delta\rho) - \varphi^{(c)}_{nm}(\alpha_p, \rho_p)}{\Delta\rho}\right]$$

$$= L\left.\frac{\partial\varphi^{(c)}_{nm}}{\partial\rho}\right|_{\substack{\rho = \rho_p \\ \alpha = \alpha_p}} = L\,\sigma^{(c)}_{nm}(\alpha_p, \rho_p) \qquad \text{(B55)}$$

Similarly, if the axis of the applied moment is parallel to a radial line at (α_p, ρ_p), we have

$$f = P\Big|_{\substack{\alpha = \alpha_p + \Delta\alpha \\ \rho = \rho_p}} - P\Big|_{\substack{\alpha = \alpha_p \\ \rho = \rho_p}}$$

$$Q^{(c)}_{nm} = \int_0^{2\pi}\int_0^{a} \rho\, \varphi^{(c)}_{nm}\, f\, d\rho\, d\alpha = \frac{P\rho_p\,\Delta\alpha\left[\varphi^{(c)}_{nm}(\alpha_p + \Delta\alpha, \rho_p) - \varphi^{(c)}_{nm}(\alpha_p, \rho_p)\right]}{\rho_p\,\Delta\alpha}$$

$$= \frac{L}{\rho_p}\left.\frac{\partial^{(c)}_{nm}}{\partial\alpha}\right|_{\substack{\rho = \rho_p \\ \alpha = \alpha_p}} = L\,\psi^{(c)}_{nm}(\rho_p, \alpha_p) \qquad \text{(B56)}$$

APPENDIX C

VIBRATION FREQUENCIES AND MODE SHAPES FOR A THIN TORUS

List of Symbols

a = radius of centroidal axis of torus; ft

c = radius of circular cross section of torus; ft

E = Young's modulus; lb/ft^2

f = applied force; lb

m = mass of torus per unit length of circumference; slugs/ft

$\mathfrak{m}_n$ = generalized mass for the n^{th} mode; slugs

Q_n = generalized force for n^{th} mode; lb

q_n = generalized coordinate for the n^{th} mode; ft

t = time; sec

u = displacement normal to plane of torus; ft

α = coordinate for generic point on torus; rad

β = angle of twist about centroidal line of cross section; rad

μ = modulus of rigidity; lb/ft^2

ν = Poisson's ratio

ξ_n = relative damping factor of n^{th} mode

σ_n = radial slope of n^{th} mode; rad/ft

φ_n = normalized mode shape of the n^{th} mode

ω_n = undamped natural frequency of the n^{th} mode; rad/sec

For the case of a thin* circular ring (torus) whose cross section is also circular (see Fig C1) the equation of motion for the flexural vibrations normal to the plane of the ring takes the form [28]

$$\frac{\partial P}{\partial \alpha} - ma \frac{\partial^2 u}{\partial t^2} = f(\alpha, t) \tag{C1}$$

* In the present context, thin means that the radius of the circular cross section is small compared with the radius of the centroidal line of the torus.

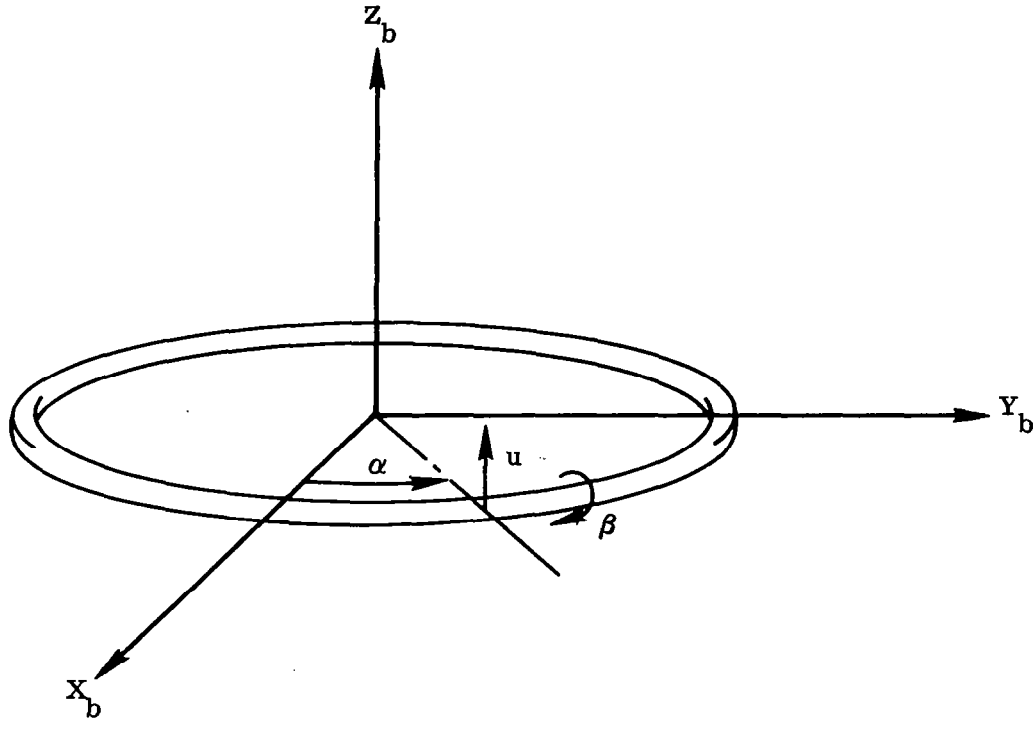

Figure C1. Geometry of Torus Problem

where

$$\frac{\partial G_1}{\partial \alpha} + G_2 - Pa = 0 \tag{C2}$$

$$\frac{\partial G_2}{\partial \alpha} - G_1 = 0 \tag{C3}$$

and

$$G_1 = \frac{1}{4} E\pi \frac{c^4}{a^2} \left(a\beta - \frac{\partial^2 u}{\partial \alpha^2} \right) \tag{C4}$$

$$G_2 = \frac{1}{2} \mu \frac{c^4}{a^2} \left(\frac{\partial u}{\partial \alpha} + a \frac{\partial \beta}{\partial \alpha} \right) \tag{C5}$$

After combining Eqs. (C1) and (C2), we obtain

$$\frac{\partial^4 u}{\partial \alpha^4} - \frac{2\mu}{E} \frac{\partial^2 u}{\partial \alpha^2} - a \left(1 + \frac{2\mu}{E}\right) \frac{\partial^2 \beta}{\partial \alpha^2} + \frac{4ma^4}{E\pi c^4} \frac{\partial^2 u}{\partial t^2} = 0 \tag{C6}$$

where we have assumed that f (α, t) is identically zero; i.e., we seek first the solution to the homogeneous form of Eq. (C1).

Following Love [28], we assume a solution of the form

$$u = V(\alpha)\, F(t) \tag{C7}$$

$$\beta = U(\alpha)\, F(t) \tag{C8}$$

such that

$$V(\alpha) = \lambda_v\, W(\alpha) \tag{C9}$$

$$U(\alpha) = \lambda_\beta\, W(\alpha) \tag{C10}$$

where λ_v and λ_β do not depend on α or t.

Substituting (C7) - (C10) in Eq. (C6), we obtain

$$\lambda_v \frac{W^{(iv)}}{W} - \left[\frac{2\mu\lambda_v}{E} + a\lambda_\beta \left(1 + \frac{2\mu}{E}\right)\right] \frac{W''}{W}$$

$$+ \frac{4\lambda_v ma^4}{E\pi c^4} \frac{\ddot{F}}{F} = 0 \tag{C11}$$

where the dots denote time derivatives and the prime indicates derivative with respect to α.

Since F depends only on t, and W depends only on α, Eq. (C11) implies that

$$\frac{E\pi c^4}{4ma^4} \frac{W^{(iv)}}{W} - \frac{E\pi c^4}{4ma^4} \left[\frac{2\mu}{E} + a\lambda \left(1 + \frac{2\mu}{E}\right)\right] \frac{W''}{W}$$

$$= - \frac{\ddot{F}}{F} = \omega^2 \tag{C12}$$

where

$$\lambda = \frac{\lambda_\beta}{\lambda_v} \tag{C13}$$

and ω^2 is a constant.

Consequently Eq. (C12) is equivalent to the following two equations

$$W^{(iv)} - \left[\frac{2\mu}{E} + a\lambda \left(1 + \frac{2\mu}{E}\right)\right] W'' - \frac{4ma^4\omega^2}{E\pi c^4} W = 0 \tag{C14}$$

$$\ddot{F} + \omega^2 F = 0 \tag{C15}$$

Assume now that

$$W(\alpha) = \cos(n\alpha + \epsilon) \tag{C16}$$

where n and ϵ are constants.

Substituting (C16) in (C14) leads to

$$n^4 + \left[\frac{2\mu}{E} + a\lambda \left(1 + \frac{2\mu}{E}\right)\right] n^2 - \frac{4ma^4\omega^2}{E\pi c^4} = 0 \tag{C17}$$

This is the relation which must be satisfied by ω in order that (C16) be a solution of Eq. (C14). The constant λ is unknown but it is easy to show that n must be an integer or zero:*

To obtain an additional relation for λ, we substitute (C4) - (C5) in Eq. (C3) obtaining

$$\frac{\mu\pi c^4}{2a^2}\left[\frac{\partial^2 u}{\partial\alpha^2} + \frac{a\partial^2\beta}{\partial\alpha^2}\right] - \frac{E\pi c^4}{4a^2}\left[a\beta - \frac{\partial^2 u}{\partial\alpha^2}\right] = 0 \tag{C18}$$

which after employing (C7) - (C10) and (C16) becomes

$$\lambda = -\frac{(1+\frac{2\mu}{E})\ n^2}{a\left(1+\frac{2\mu n^2}{E}\right)} \tag{C19}$$

Substituting this in Eq. (C17) and solving for ω, we find

$$\omega_n^2 = \frac{E\pi c^4 n^2 (n^2-1)^2}{4ma^4 (\frac{E}{2\mu} + n^2)} \tag{C20}$$

which by virtue of the standard relation

$$E = 2\mu\ (1+\nu) \tag{C21}$$

can be written as

$$\omega_n^2 = \frac{E\pi c^4 n^2 (n^2-1)^2}{4ma^4 (n^2+1+\nu)} \tag{C22}$$

There is thus a solution of the form (C7) and (C8) for each value of ω_n. The most general solution is given therefore by

$$u(\alpha, t) = \sum_{n=0}^{\infty} F_n(t)\, V_n(\alpha) \tag{C23}$$

---

* The argument is along the same lines as in Appendix A, namely, that W must be a single valued function of α.

$$\beta(\alpha, t) = \sum_{n=0}^{\infty} F_n(t)\, U_n(\alpha) \tag{C24}$$

Now by (C9) and (C16)

$$V_n(\alpha) = \lambda_v \cos(n\alpha + \epsilon)$$

This may be written as

$$V_n(\alpha) = (-\lambda_v \sin\epsilon)\sin n\alpha + (\lambda_v \cos\epsilon)\cos n\alpha$$

$$= C_1 \sin n\alpha + C_2 \cos n\alpha$$

$$\equiv V_n^{(s)}(\alpha) + V_n^{(c)}(\alpha) \tag{C25}$$

As in the case of the flat plate in Appendix B, the mode shape (C25) gives only relative displacement. We therefore define normalized modes as follows

$$\varphi_n^{(s)}(\alpha) = \frac{V_n^{(s)}(\alpha)}{V_n^{(s)}\left(\frac{\pi}{2} + 2\pi n\right)} = \sin n\alpha \tag{C26}$$

$$\varphi_n^{(c)}(\alpha) = \frac{V_n^{(c)}(\alpha)}{V_n^{(c)}(0)} = \cos n\alpha \tag{C27}$$

Similarly

$$U_n(\alpha) = \lambda_\beta \cos(n\alpha + \epsilon)$$

$$= (-\lambda_\beta \sin\epsilon)\sin n\alpha + (\lambda_\beta \cos\epsilon)\cos n\alpha$$

$$= (-\lambda\lambda_v \sin\epsilon)\sin n\alpha + (\lambda\lambda_v \cos\epsilon)\cos n\alpha$$

$$= \lambda\left[C_1 \sin n\alpha + C_2 \cos n\alpha\right]$$

$$= \lambda\left[V_n^{(s)}(\alpha) + V_n^{(c)}(\alpha)\right] \tag{C28}$$

If we now define generalized coordinates by

$$q_n^{(s)}(t) = F_n(t)\, V_n^{(s)}\left(\frac{\pi}{2} + 2\pi n\right) \tag{C29}$$

$$q_n^{(c)}(t) = F_n(t)\, V_n^{(c)}(0) \tag{C30}$$

We may express the solution (C23), (C24) as

$$u(\alpha, t) = \sum_{n=0}^{\infty} \left[q_n^{(s)}(t)\, \varphi_n^{(s)}(\alpha) + q_n^{(c)}(t)\, \varphi_n^{(c)}(\alpha)\right] \tag{C31}$$

$$\beta(\alpha, t) = \sum_{n=0}^{\infty} \lambda \left[q_n^{(s)}(t)\, \varphi_n^{(s)}(\alpha) + q_n^{(c)}(t)\, \varphi_n^{(c)}(\alpha)\right] \tag{C32}$$

In order to obtain a solution for the nonhomogeneous case, we assume that the applied force can be represented as

$$f(\alpha, t) = a \sum_{n=0}^{\infty} m \left[A_n^{(s)}(t)\, \varphi_n^{(s)}(\alpha) + A_n^{(c)}(t)\, \varphi_n^{(c)}(\alpha)\right] \tag{C33}$$

where the functions $A_n^{(s)}(t)$ and $A_n^{(c)}(t)$ are for the moment undetermined.

Multiplying both sides of this equation by $\varphi_p^{(s)}(\alpha)$ and integrating over the whole ring, we have

$$\int_0^{2\pi} \varphi_p^{(s)} f\, d\alpha = a \sum_{n=0}^{\infty} A_n^{(s)}(t) \int_0^{2\pi} m\, \varphi_p^{(s)}\, \varphi_n^{(s)}\, d\alpha$$

$$+ a \sum_{n=0}^{\infty} A_n^{(c)}(t) \int_0^{2\pi} m\, \varphi_p^{(s)}\, \varphi_n^{(c)}\, d\alpha \tag{C34}$$

However, the normalized modes are orthogonal; i.e.

$$\int_0^{2\pi} \varphi_p^{(s)}\, \varphi_q^{(s)}\, d\alpha = 0 \quad , \quad p \neq q \tag{C35}$$

$$\int_0^{2\pi} \varphi_p^{(s)} \, \varphi_q^{(c)} \, d\alpha = 0, \quad , \quad \text{all p and q} \tag{C36}$$

Therefore, Eq. (C34) may be written as

$$A_n^{(s)}(t) = \frac{Q_n^{(s)}}{\mathfrak{M}_n^{(s)}} \tag{C37}$$

where

$$Q_n^{(s)} = \int_0^{2\pi} \varphi_n^{(s)} \, f \, d\alpha \tag{C38}$$

is the generalized force, and

$$\mathfrak{M}_n^{(s)} = \int_0^{2\pi} a \, m \left[\varphi_n^{(s)}\right]^2 d\alpha \tag{C39}$$

is the generalized mass.

By multiplying both sides of Eq. (C33) by $\varphi_p^{(c)}(\alpha)$, instead of $\varphi_p^{(s)}(\alpha)$ as above, and proceeding in a similar manner, we find

$$A_n^{(c)}(t) = \frac{Q_n^{(c)}}{\mathfrak{M}_n^{(c)}} \tag{C40}$$

where

$$Q_n^{(s)} = \int_0^{2\pi} \varphi_n^{(c)} \, f \, d\alpha \tag{C41}$$

$$\mathfrak{M}_n^{(c)} = \int_0^{2\pi} a \, m \left[\varphi_n^{(c)}\right]^2 d\alpha \tag{C42}$$

Consequently, Eq. (C33) may be written as

$$f(\alpha, t) = \sum_{n=0}^{\infty} a\, m \left[\frac{Q_n^{(s)}}{m_n^{(s)}} \varphi_n^{(s)} + \frac{Q_n^{(c)}}{m_n^{(c)}} \varphi_n^{(c)} \right] \tag{C43}$$

The equation of motion for the nonhomogeneous case is obtained by substituting (C2), (C4), and (C5) in Eq. (C1). The result is

$$\frac{\partial^4 u}{\partial \alpha^2} - \frac{2\mu}{E} \frac{\partial^2 u}{\partial \alpha^2} - a\left(1 - \frac{2\mu}{E}\right) \frac{\partial^2 \beta}{\partial \alpha^2}$$

$$+ \frac{4ma^4}{E\pi c^4} \frac{\partial^2 u}{\partial t^2} = \frac{4a^3}{E\pi c^4} f(\alpha, t) \tag{C44}$$

After substituting the expressions for u, β, and f given by (C31), (C32), and (C43) respectively, multiplying both sides of the resulting equation by $\varphi_p^{(s)}(\alpha)$ and integrating over the whole ring, we obtain

$$\frac{4ma^4}{E\pi c^4} \int_0^{2\pi} \sum_{n=0}^{\infty} \left[\ddot{q}_n^{(s)} \varphi_n^{(s)} + \ddot{q}_n^{(c)} \varphi_n^{(c)} \right] \varphi_p^{(s)}\, d\alpha$$

$$- \int_0^{2\pi} \sum_{n=0}^{\infty} q_n^{(s)} \left\{ \left[\varphi_n^{(s)}\right]^{(iv)} - \left[\frac{2\mu}{E} + a\lambda\left(1 - \frac{2\mu}{E}\right)\right] \left[\varphi_n^{(s)}\right]'' \right\} \varphi_p^{(s)}\, d\alpha$$

$$- \int_0^{2\pi} \sum_{n=0}^{\infty} q_n^{(c)} \left\{ \left[\varphi_n^{(c)}\right]^{(iv)} - \left[\frac{2\mu}{E} + a\lambda\left(1 - \frac{2\mu}{E}\right)\right] \left[\varphi_n^{(c)}\right]'' \right\} \varphi_p^{(s)}\, d\alpha$$

$$= \frac{4a^3}{E\pi c^4} \int_0^{2\pi} \sum_{n=0}^{\infty} a\, m \left[\frac{Q_n^{(s)}}{m_n^{(s)}} \varphi_n^{(s)} + \frac{Q_n^{(c)}}{m_n^{(c)}} \varphi_n^{(c)} \right] \varphi_p^{(s)}\, d\alpha \tag{C45}$$

However, both $\varphi_n^{(s)}$ and $\varphi_n^{(c)}$ satisfy Eq. (C14); viz.

$$\left[\varphi_n^{(s)}\right]^{(iv)} - \left[\frac{2\mu}{E} + a\lambda\left(1 - \frac{2\mu}{E}\right)\right] \left[\varphi_n^{(s)}\right]'' = \frac{4ma^4}{E\pi c^4} \omega_n^2 \varphi_n^{(s)} \tag{C46}$$

$$\left[\varphi_n^{(c)}\right]^{iv} - \left[\frac{2\mu}{E} + a\lambda\left(1 - \frac{2\mu}{E}\right)\right]\left[\varphi_n^{(c)}\right]'' = \frac{4ma^4}{E\pi c^4}\,\omega_n^2\,\varphi_n^{(c)} \tag{C47}$$

We note also that in addition to (C35) and (C36), the normalized modes satisfy

$$\int_0^{2\pi}\left[\varphi_n^{(s)}\right]^2 d\alpha = \int_0^{2\pi}\left[\varphi_n^{(c)}\right]^2 d\alpha = \pi \tag{C48}$$

$$\int_0^{2\pi}\varphi_p^{(c)}\,\varphi_q^{(c)}\,d\alpha = 0 \quad , \qquad p \neq q \tag{C49}$$

By virtue of (C35), (C36), and (C46) - (C49), Eq. (C45) reduces to

$$\ddot{q}_n^{(s)} + \omega_n^2\,q_n^{(s)} = \frac{Q_n^{(s)}}{m_n^{(s)}} \tag{C50}$$

Similarly, replacing $\varphi_p^{(s)}$ by $\varphi_p^{(c)}$ in (C45) and proceeding as above, we obtain

$$\ddot{q}_n^{(c)} + \omega_n^2\,q_n^{(c)} = \frac{Q_n^{(c)}}{m_n^{(c)}} \tag{C51}$$

From Eq. (C22), we see that $\omega_o = 0$ and $\omega_1 = 0$. These correspond to the rigid body translation and rotation respectively.

APPENDIX D

TRANSFER FUNCTION FOR MOTOR FLYWHEEL UNIT

A linearized dynamic analysis of a motor-flywheel combination for controlling satellite attitude is contained in Reference 13, which is repeated here for convenience. The complete schematic for control about one body axis of the satellite is shown in Figure D1. The symbols have the following meaning

B_e = back emf constant

B_f = viscous friction constant

B_m = magnetic torque constant due to earth's magnetic field

I = moment of inertia of satellite about control axis

C = moment of inertia of flywheel about spin axis

K_m = gain constant

s = Laplace operator

L_C = output torque

L_D = disturbance torque on satellite

L_{DW} = disturbance torque on motor and flywheel

ω_b = angular velocity of satellite relative to inertial space

ω_w = angular velocity of flywheel relative to inertial space

ω_{wb} = angular velocity of flywheel relative to satellite body

The externally applied wheel torque, L_{DW}, is due to such effects as gravity torques on an unbalanced wheel and is generally completely negligible. Furthermore, ω_b is generally much smaller than ω_w which means that ω_w is essentially equal to ω_{wb}. In this case, a simple computation yields the transfer function

$$\frac{L_C}{V_m} = \frac{K_m B_e}{(B_e + B_f + B_m)} \left(\frac{\frac{(B_m + Cs)}{Cs}}{B_e + B_f + B_m} + 1 \right) \tag{D1}$$

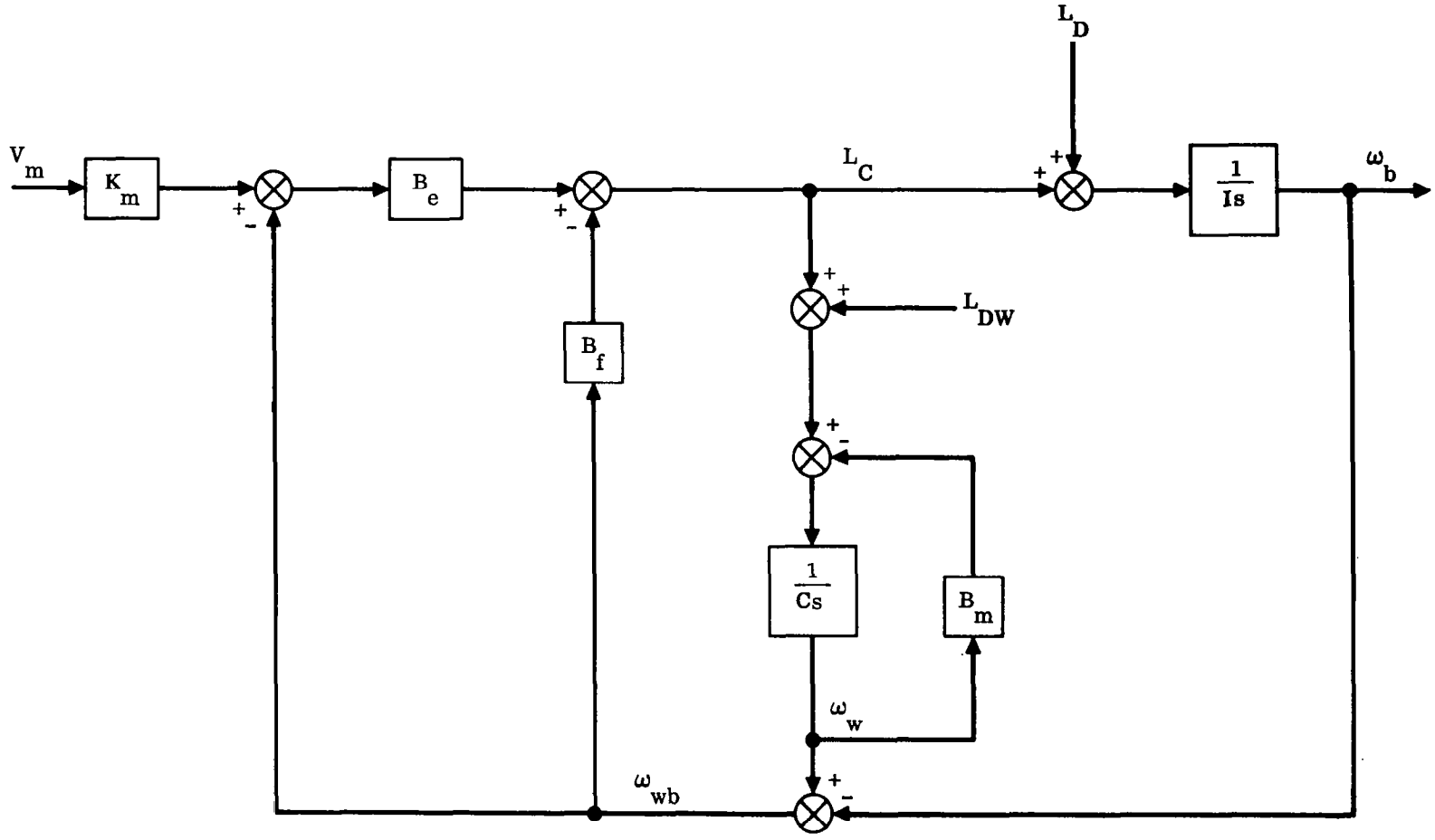

Figure D1. Schematic of Motor-Flywheel Unit

In most applications, the magnetic torque constant, B_m, and the viscous friction constant, B_f, are small compared with B_e. This permits Equation (D1) to be simplified to

$$\frac{L_C}{V_m} = \frac{K_m Cs}{\tau_m s + 1} \tag{D2}$$

where

$$\tau_m = \frac{C}{B_e} \tag{D3}$$

It is possible to obtain an alternate relation for the time constant, τ_m, in the following way. From Figure D1

$$L_C = K_m B_e V_m - B_e \omega_w \tag{D4}$$

The stall torque is obtained by setting $\omega_w = 0$ and $V_m = V_{m_{max}}$, viz.

$$L_{Cs} = K_m B_e V_{m_{max}} \tag{D5}$$

Also, by setting $L_C = 0$ with $V_m = V_{m_{max}}$ and $\omega_w = \omega_{w_{max}}$, we obtain the relation

$$B_e \omega_{w_{max}} = K_m B_e V_{m_{max}} \tag{D6}$$

After combing (D5) and (D6), we find

$$B_e = \frac{L_{Cs}}{\omega_{w_{max}}} \tag{D7}$$

Using this relation for B_e gives an alternate expression for τ_m as follows

$$\tau_m = \frac{C\omega_{w_{max}}}{L_{Cs}} \tag{D8}$$

APPENDIX E

ATTITUDE SENSORS FOR SATELLITES

One may conveniently categorize the attitude sensing methods for satellites as follows:

1. Celestial (star) tracking
2. Sun tracking
3. Horizon scanning
4. Ambient (gravity gradient, magnetic field)
5. Inertial (gyros, monitored stable platform)

Regarding inertial methods, the gyro-stabilized platform suggests itself as an immediate choice for an inertial reference. However, when long operational times are involved, gyro drift, even if extremely small by terrestrial standards, eventually causes intolerably high attitude errors to develop. An obvious remedy is to use the stabilized platform supplemented by an independent attitude reference such as a star tracker. The platform is then used to provide stability under relatively high frequency disturbances, while the star tracker prevents any long-term drift of the reference. When the vehicle itself is referred to an inertial reference, it would appear that one might just as well design the vehicle as a stabilized platform. In this case, one might eliminate gyros completely if the attitude reference signals could be processed to yield rate information. This idea is investigated in more detail later in the discussion.

A second role is the gyro's use as a gyrocompass for the detection of yaw deviations out of the orbital plane. In this case, it is assumed that independent control of the vehicle's vertical axis exists, creating the analog of the "finger of gravity" pointing toward the center of the earth which is experienced by terrestrial objects. Using the tendency of the vehicle vertical axis to keep its proper alignment, a gyro rotor can be so constrained relative to the vehicle frame that its spin axis tends to align itself normal to the orbital plane. It operates in much the same way as the gyrocompass on the earth, whose spin axis precesses into the plane of the local meridian. In this way the gyro provides a measurement of satellite yaw after the vertical is established by other means. Reference 39 contains a detailed discussion of this approach.

The third important case of inertial sensing is the use of rate gyroscopes to measure the angular velocity of the vehicle as resolved into body-fixed axes, the results being of value for damping attitude oscillations. The major problem here is

that the rate gyros pick up the entire angular velocity relative to inertial space, not merely the deviation velocities from the attitude reference frame, which are the quantities needed for damping in the equations of attitude motion. Thus, the motion of the reference frame somehow must be biased out of the gyro outputs, a procedure which presents formidable practical problems in general. Another practical question relates to the threshold angular velocity which can be detected. All that can be said here about this important topic is that for the very low angular rates normally of concern, the quality of the rate gyro must be commensurate with that of the very best available navigation gyros. Certainly any rate gyro of the quality used in flight control systems will be far from adequate.

This is not the only potential use of rate gyros, however. One can conceive a method in which the outputs of high-precision gyros attached to the vehicle frame are properly combined and integrated. From such signals the absolute change in attitude over a period of time can be determined. The method requires the knowledge of an initial orientation, of course, and the time duration must be short enough to keep the errors from gyro drift to within acceptable limits.

Among the ambient sensing techniques, the gravity gradient is the most prominent in determining the local vertical. This is treated in detail in Subsection 3.4.1.

The earth's magnetic field is a convenient orientation reference in terrestrial applications, and it is natural to attempt to use it for the same purpose in regions of space near the earth. Indeed, this is reported[40] to have been done in at least one satellite (Sputnik III). Moreover, magnetometers have been used for azimuth control of ballistic missile nose cones, which is a very similar task.[41]

There exists a body of literature on instrumentation for determining the vector magnetic field at a rocket or earth satellite.[42]

Another device motivated specifically by the attitude control problem is the light pump magnetometer.[43]

But of greater concern here than the instrument details is the ultimate precision with which such sensing can be done. It will be far less than the inherent precision of the instruments themselves because of such effects as magnetic storms, ionosphere currents, inhomogeneities of the earth's field, and magnetic variations of the vehicle itself. In addition, a method of this kind has inherent limitations in its spatial domain of applicability, since the field strength decreases with the inverse cube of distance. The field irregularities to be expected at some distance from the earth (the order of 10 earth radii) are pointed up by the results of Pioneer V experiments.

In the closer neighborhood of the earth where such irregularities may be less marked, an additional problem is that in order to infer orientation relative to most frames of reference using magnetic sensing, it would be necessary to know the vehicle position independently and use this information in the computation.

In short, attitude sensing based on the magnetic field does not appear to be operationally attractive except possibly to provide an after-the-fact record of orientation as a part of data-gathering instrumentation. It might suffice as an input for a relatively crude system for attitude control relative to some frames of reference. A method for maintaining the spin axis of a satellite normal to the plane of its orbit by utilizing the earth's magnetic field is described in Reference 44.

The class of sighting methods in which the periphery of a planetary disc is examined may be called "horizon scanning". The sensing device looks at a localized segment of the edge of the disc (the latter is interpreted as the line of maximum intensity gradient) and gives an output signal which is a function of (e.g. proportional to) the angular displacement between the edge and the axis of the instrument.

This concept can be mechanized and used in various ways. One situation is that in which a scanning instrument is free to rotate about an axis in the vehicle which is to be identified with the vertical direction. This could be visualized as a telescope barrel sweeping out the surface of a cone of which this is the axis, as shown in Figure E1. At the same time the line of sight undergoes a sweep motion normal to the generators of the cone, which carries it back and forth across the horizon, at least when the cone is close to the tangent cone to the nearby body from the instrument location. Physically this might be done by a rocking prism. A signal is generated with varying intensity as the line of sight passes from space to the illuminated disc, which can be differentiated to the point of maximum intensity gradient, i.e., the edge of the disc. This gives the angle θ shown in Figure E1 as a function of azimuth angle. Averaging θ then gives two components of angular displacement of the scanner cone axis away from the "vertical" represented by the normal to the plane of the "mean horizon".

As an alternative mechanization, the centerline of a narrow field of view is rotated in a plane which contains the nominal vehicle vertical axis, i.e., in a plane normal to one of the nominally horizontal body axes. A second identical scanner operates in a plane normal to the other nominally horizontal body axes. There is a broad pulse output from each detector during the time when the beam is looking at the illuminated body. The centers of these pulses are displaced from the vertical axis of the device by precisely the angle of attitude deviation in the scanner plane, and it is possible to reduce the determination of this angle to the measurement of the times at which the illumination pulse occurs.

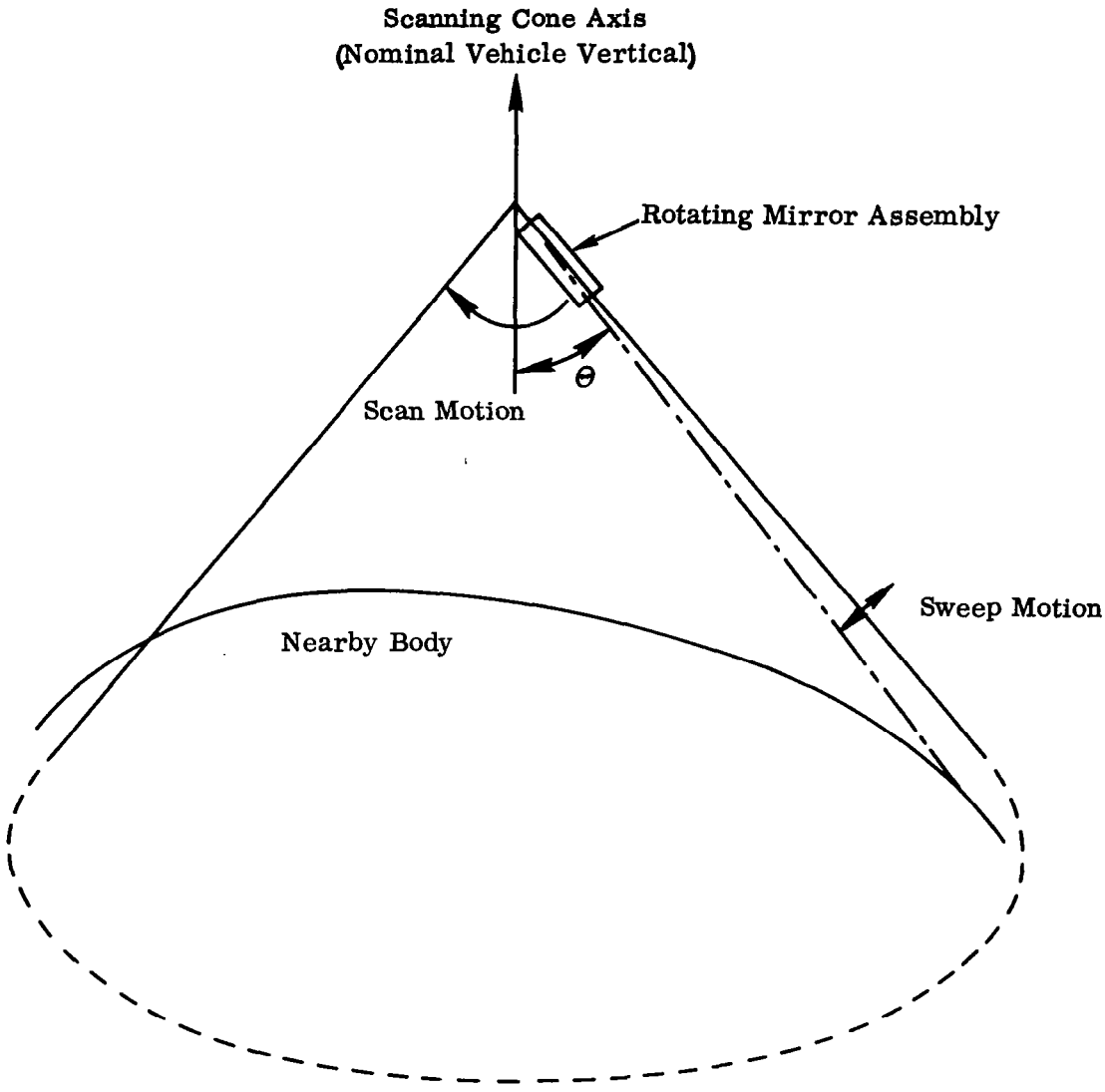

Figure E1. One Horizon Scanner Concept

Another type of horizon scanner is shown in Figure E2. This type operates by detecting the sharp discontinuity in infra-red radiation intensity which occurs when the line of sight crosses the outer edge of the tropopause.

A filter is used to remove visible and near infra-red radiation, leaving the detector sensitive mainly to radiation from atmospheric water vapor. The earth then appears effectively at a temperature between 200° and 220°K, according to whether it is day or night, and space appears at 4°K. Directly reflected solar radiation is not significant.

A small field of view is available to the detector which consists of a germanium objective (refractive index $\mu = 4$) with a thermistor detector mounted directly on it. The germanium objective acts both as lens and filter. The thermistor is very small, of the order of 0.5 mm or less, in order to have low heat capacity and therefore fast response. The mirror assembly is rotated to perform a conical scan. Step changes in output are obtained when the scan crosses the earth's horizon; the bisector of the scan angles at which the steps occur determines the rotational attitude of the satellite about the scanner axis, with respect to the local vertical plane which passes through this axis. Two such scanners completely determine the local vertical.

Accuracies of 1 deg have been obtained, and there seems to be no reason why, with careful design, it should not be possible to approach about 0.2 deg, this limit

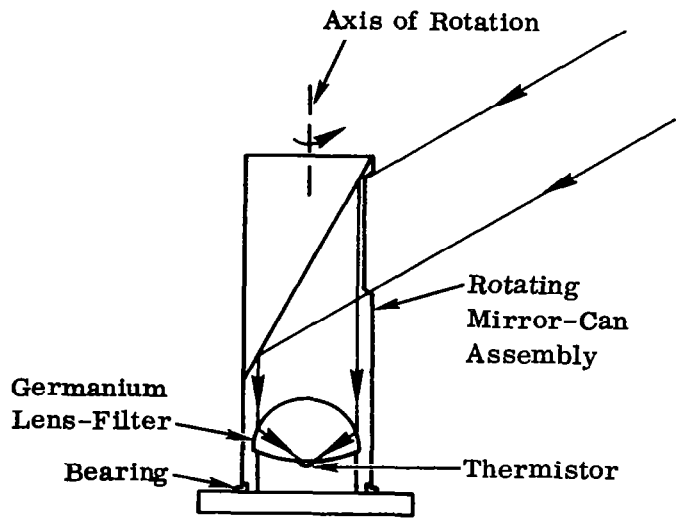

Figure E2. Alternate Horizon Scanner

being set by the resolution of the outer edge of the tropopause.

The determination of satellite attitude by sun and star tracking are conceptually very similar.

The analysis and design of a fine sun tracker for the Advanced Orbiting Solar Observatory are discussed in Reference 36. The tracker provides accurate pointing information in pitch and yaw, permitting precise static and dynamic orientation of the observatory with respect to the sun's apparent disc, in accordance with ground commands. The tracker uses a servo-driven optical slab in each axis to offset the optical null by the required amount. The error signal thus developed in a pair of matched silicon photo-voltaic cells is fed to the observatory control system, to produce the desired orientation in that axis.

It is claimed that this device is capable of achieving a 2 arc-second rms pointing accuracy.

Figure E3 is a block diagram of the sun tracker system. The digital command system in the tracker converts the ground command into an optical positional reference for the AOSO, by means of the tracker servo drive. This commanded rotation of the optics then produces a positional error signal via the optics and photo-detector

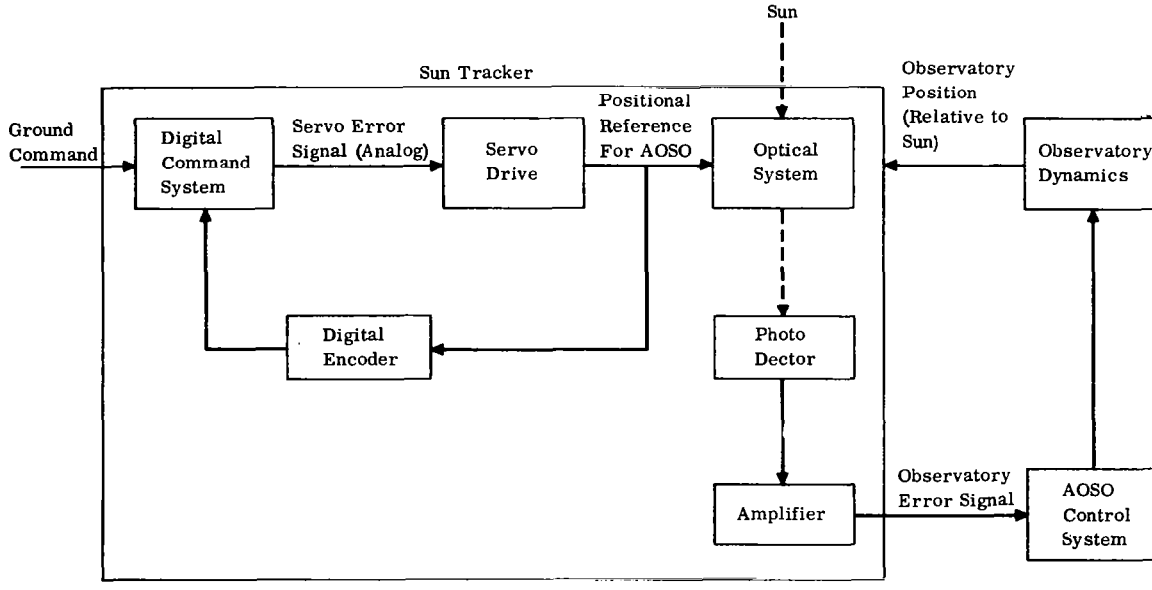

Figure E3. Sun Tracker System

which is amplified and fed to the AOSO control system. The latter drives the observatory until the photo-detector signal is nulled. At this point, the observatory position will correspond with the commanded rotation of the optics and hence, with the ground command as well.

In Figure E4 is shown a schematic diagram of the sun tracker optical system for each of the pitch and yaw axes. An optical slab of thickness d and index of refraction n is located midway between the photo-detector and the slit at the front of the tracker, where the sun's rays are admitted. The slab is rotated through an angle β, corresponding to the command signal, by means of the tracker servo drive.

The rays of the sun are refracted through the slab and form a narrow beam on the photo-detector surface. When the center of this beam is off the null line of the detector, an error signal is generated which is amplified and fed to the observatory control system. The latter then drives the observatory until the observatory position (sun angle, α) is such as to cause a null at the photo-detector. Under this condition, the sun angle, α, is a precise function of slab angle, β, and hence of the ground command as well.

A block diagram of the tracker servo drive is shown in Figure E5. The digital-to-analog converter output is amplified and fed to a d-c torquer motor which is

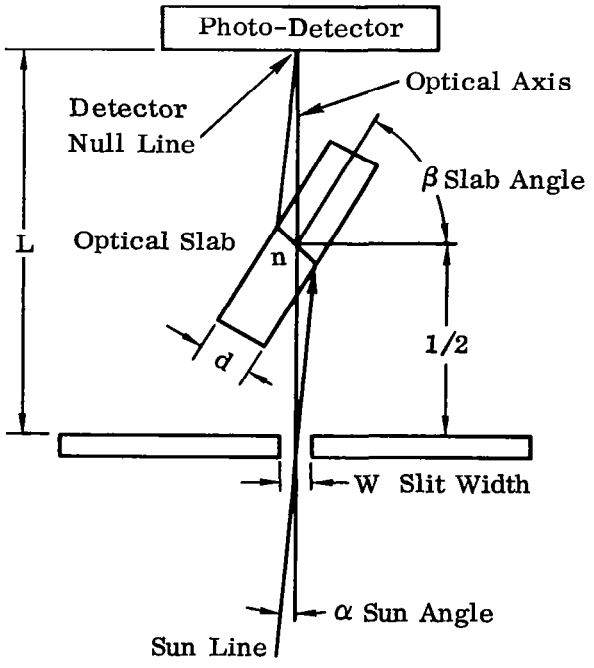

Figure E4. Optical System for Sun Tracker

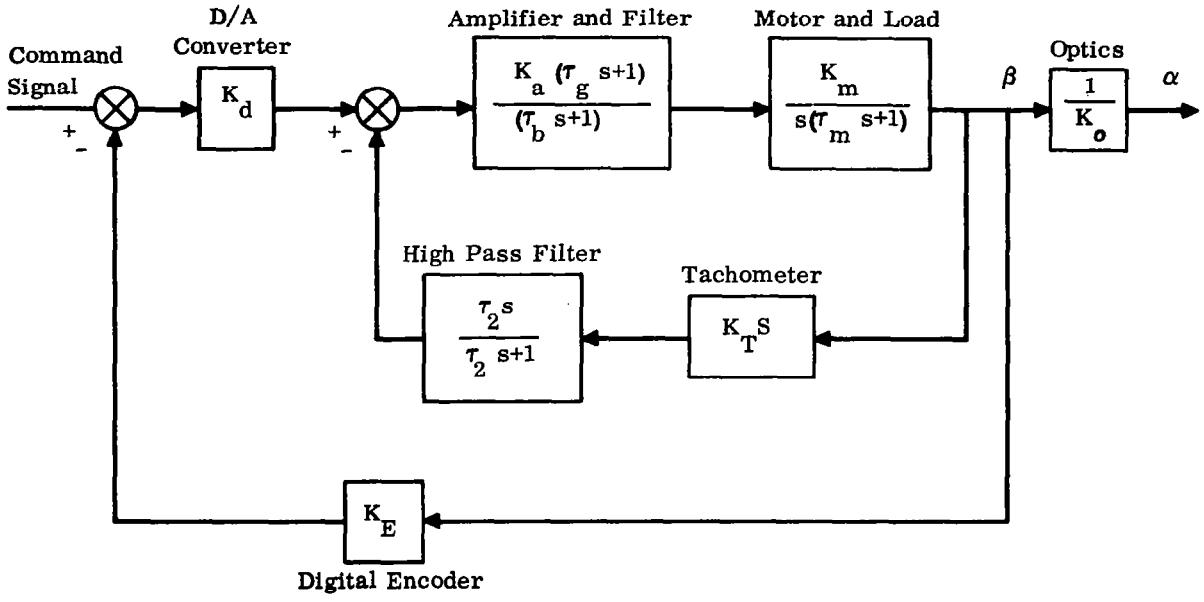

Figure E5. Tracker Servo Drive

directly coupled to the optical slab. Also directly coupled to the slab is a d-c tachometer. The tachometer signal is amplified, fed through a high-pass filter, and then subtracted from the digital-to-analog converter output, to provide the necessary servo system stabilization. At servo equilibrium the slab angle, β, and hence the commanded sun angle, α, correspond to the digital command.

Details of the design analysis may be found in Reference 36.

Historically, the first attempts to track stars automatically were aimed at relieving astronomers of the task of guiding an astronomical telescope during long periods of photographic observation. A simple means of doing this is depicted in Figure E6.

The detector is vehicle-mounted and consists of a one half silvered mirror set at a 45-deg angle. In the null position, the focused image is separated equally with one half of the light going through the transparent portion of the mirror and illuminating phototube A, the other one half is reflected at right angles by the silvered surface to phototube B. The phototubes are connected in series with the output signal taken at the junction between tubes. The tubes are selected for equal gains.

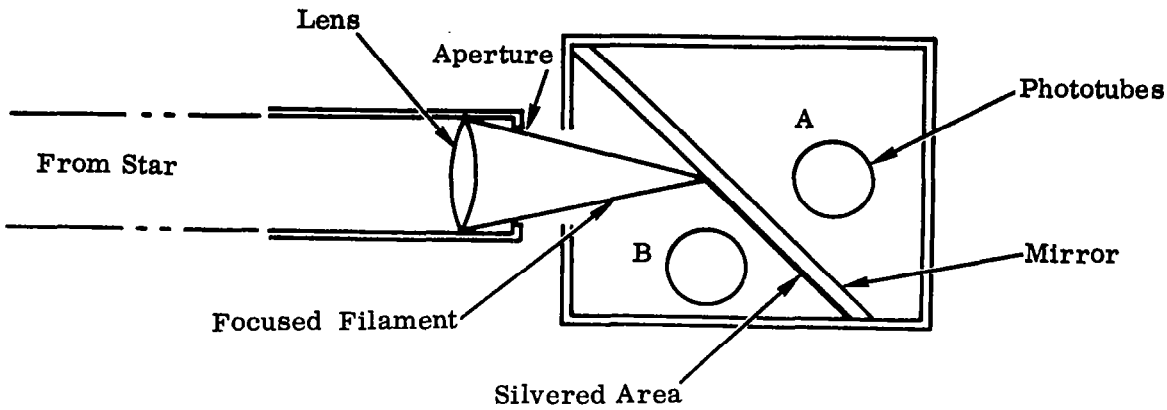

Figure E6. Star Tracker Optical System

When starlight is centered, the vehicle is at the null position and equal light falls on each phototube. The current in each tube will be equal and, therefore, there is no current output. If the light is displaced, one tube receives more light and draws a larger current so that the output becomes a measure of the star displacement. Typically, the output current is linear in the range 0.1 to 0.3 microamp and represents 20 seconds of arc displacement.

The main difficulty with this scheme is that the phototubes may be nonuniform in sensitivity with time and conditions of operation. Thus the accuracy of such a device would depend on the behavior of the separate phototubes and would be relatively unreliable for long operating times.

A more practical scheme, due to Whitford and Kron,[45] employs a frequency-modulated, disk-scanning system, the principle of which is illustrated in Figure E7. As the lens is rotated eccentrically about an axis passing through the center of the disk, the star image describes a circular track over the disk. The disk is composed of alternate opaque and transparent sectors, so that a frequency-modulated signal is output from the photosensitive surface behind the disk. The amplitude and phase of the demodulated signal provide two-axis information on the orientation of the tracker.

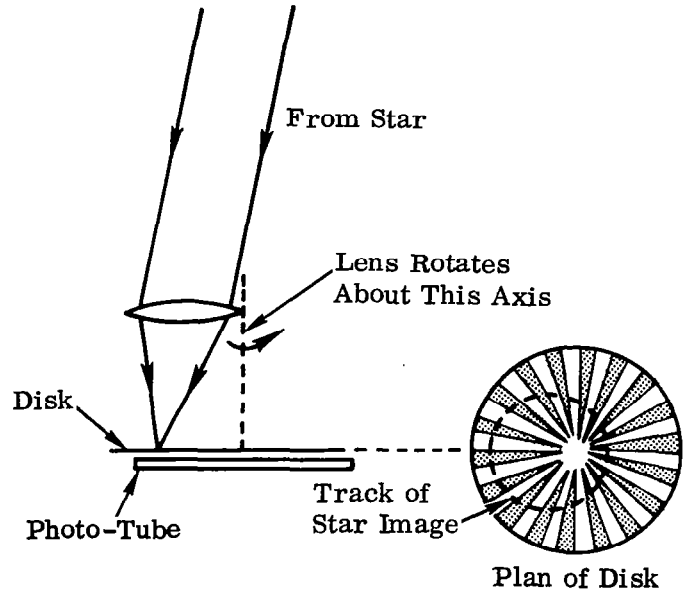

Figure E7. Frequency-Modulated, Disk-Scanning Star Tracker

The discussions above represent merely a brief survey of available methods and techniques in attitude sensing. A fairly comprehensive summary of the state of the art in 1960 is contained in Reference 22. More recent developments are presented in References 37 and 38, and application to a specific system (the OAO) is given in Reference 46.

For purposes of control system analysis, we may envision a two-channel sun (or star) tracker whose sensitive axes are permanently aligned parallel with the vehicle body axes, Y_b and Z_b. It is assumed that the X_b axis is to be aligned with the line of sight (LOS) to a specified star. We may then take a reference coordinate frame which is parallel to inertial space and whose origin coincides with the origin of the body reference frame. A measure of the angle between the unit vectors $\bar{i}_b$ and $\bar{i}_r$ is then given by m and n, the direction cosines between the line from the vehicle to the specified celestial object (sun or star) and the Y_b and Z_b axes respectively. A tracker mounted in the manner described above will then have as outputs two signals which are proportional to m and n. For analytical simplicity, this proportionality factor may be lumped with the gain of the control system. The problem is how to process the signals m and n for purposes of attitude control.

Normally, as in the case of an orbiting astronomical observatory, the satellite does not rotate with respect to inertial space. In other situations (i.e., a manned space station) the vehicle will have a spin about (say) the X_b axis for purposes of artificial gravity. Nevertheless, in this case it is required to point the X_b axis to the sun in order to charge the solar panels. Accuracy requirements will of course be different for the two cases, but conceptually the analysis is similar. Processing the tracker signals is more complicated in the spinning case, and for purposes of greater generality we will analyze this condition. The analysis of the non-spinning vehicle will then be a simple special case.

Let $\bar{i}_r$ be along the line of sight to the desired celestial reference, which for concreteness we assume is the sun. Then if the body frame is displaced relative to the reference frame, the relevant direction cosines may be determined as follows. Considering the vector

$$\bar{\rho} = \bar{i}_r$$

$$= x_b \bar{i}_b + y_b \bar{j}_b + z_b \bar{k}_b \tag{E1}$$

we see that the projections of $\bar{i}_r$ on the body axes are (x_b, y_b, z_b), which via Equation (1) are found to be

$$x_b = \cos\theta \cos\psi \equiv \ell \tag{E2}$$

$$y_b = \sin\varphi \sin\theta \cos\psi - \cos\varphi \sin\psi \equiv m \tag{E3}$$

$$z_b = \cos\varphi \sin\theta \cos\psi + \sin\varphi \sin\psi \equiv n \tag{E4}$$

and for small θ and ψ reduce to

$$x_b = 1 = \ell \tag{E5}$$

$$y_b = \theta \sin\varphi - \psi \cos\varphi = m \tag{E6}$$

$$z_b = \theta \cos\varphi + \psi \sin\varphi = n \tag{E7}$$

The output signals from the sun tracker are precisely m and m.* These may be simply related to the body rates through the Euler angles as follows. Assuming that $\dot{\varphi} = p_o \equiv$ constant, and zero initial conditions, we find from Equations (9) and (10)

*Actually, as noted earlier, these output signals are proportional to m and n. The factor of proportionality is assumed to be lumped with the control system gain.

$$\dot{\theta} = q \cos \varphi - r \sin \varphi$$

$$= q \cos p_o t - r \sin p_o t \tag{E8}$$

$$\dot{\psi} = q \sin \varphi + r \cos \varphi$$

$$= q \sin p_o t + r \cos p_o t \tag{E9}$$

Now by differentiating (E6) and (E7) and making use of Equations (6) and (7), we obtain

$$\dot{m} = \theta \dot{\varphi} \cos \varphi + \dot{\theta} \sin \varphi + \psi \dot{\varphi} \sin \varphi - \dot{\psi} \cos \varphi$$

$$= \dot{\varphi} (\theta \cos \varphi + \psi \sin \varphi) - (\dot{\psi} \cos \varphi - \dot{\theta} \sin \varphi)$$

$$= p_o n - r \tag{E10}$$

and

$$\dot{n} = -\theta \dot{\varphi} \sin \varphi + \dot{\theta} \cos \varphi + \psi \dot{\varphi} \cos \varphi + \dot{\psi} \sin \varphi$$

$$= \dot{\varphi} (\psi \cos \varphi - \theta \sin \varphi) + (\dot{\theta} \cos \varphi + \dot{\psi} \sin \varphi)$$

$$= - p_o m + q \tag{E11}$$

The last two relations show that body rate signals (for purposes of stabilization) may be obtained as a linear combination of the sun tracker output signals and their derivatives. Suitable control laws could take the form

$$L_{cy} = K_p m + K_v q \tag{E12}$$

$$L_{cz} = K_p n + K_v r \tag{E13}$$

It is sometimes convenient to work directly in terms of the angle between the X_b and X_r axes, which represents the angular deviation of the body from the desired line of sight. Referring to Figure E8, we see that

$$|\bar{i}_r \times \bar{i}_b| = \sin \gamma \approx \gamma \tag{E14}$$

However

$$\bar{i}_r \times \bar{i}_b = (m\bar{j}_b + n\bar{k}_b) \times \bar{i}_b$$

$$= n\bar{j}_b - m\bar{k}_b \tag{E15}$$

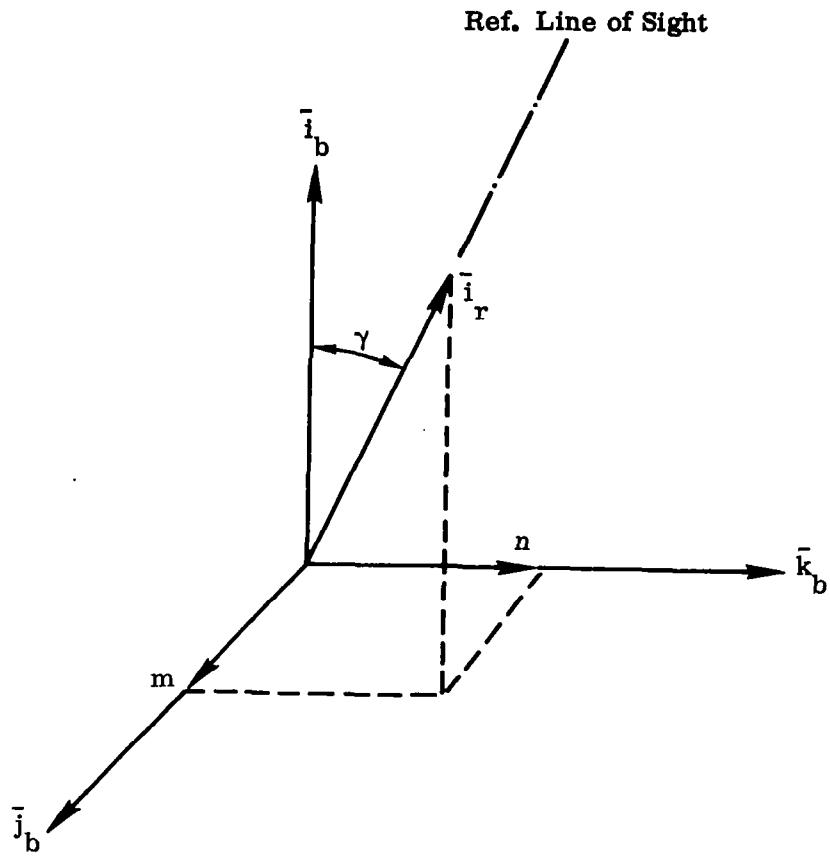

Figure E8. Angular Deviation of Body From Desired Line of Sight

Thus, using Equation (E6) and (E7), the attitude deviation angle, γ, may be expressed in complex notation as

$$\begin{aligned}\gamma &= \theta \cos\varphi + \psi \sin\varphi - i\,(\theta \sin\varphi - \psi \cos\varphi) \\ &= (\theta + i\psi)\, e^{-i\varphi} \\ &= \gamma_y + i\gamma_z \end{aligned} \qquad \text{(E16)}$$

where $i^2 = -1$.

The motion of a spinning body under no torque may be described in terms of this attitude deviation angle. From Equations (101) and (102)

$$\dot{q} - ar = 0 \tag{E17}$$

$$i\dot{r} + iaq = 0 \tag{E18}$$

Adding these equations gives

$$(\dot{q} + i\dot{r}) \quad ia \quad (q + ir) = 0 \tag{E19}$$

By differentiating (E16) we find

$$\dot{\gamma} = i\dot{\varphi}\gamma + (q + ir) \tag{20}$$

$$\ddot{\gamma} = i\dot{\varphi}\dot{\gamma} + (\dot{q} + i\dot{r}) \tag{E21}$$

After combining (E19) - (E21), we find that γ satisfies the equation

$$\ddot{\gamma} + i\,(\dot{\varphi} + a)\,\dot{\gamma} - a\dot{\varphi}\gamma = 0 \tag{E22}$$

Written as

$$[\,(s + i\dot{\varphi})\,(s + ia)]\,\gamma = 0$$

we see that in response to a unit impulse, γ takes the form

$$\gamma(t) = \frac{1}{(ia - i\dot{\varphi})}\,[e^{-i\dot{\varphi}t} - e^{-iat}]$$

$$= \frac{1}{(a - \dot{\varphi})}\,[(\sin at - \sin\dot{\varphi}t) + i\,(\cos at - \cos\dot{\varphi}t)]$$

which shows that the real and imaginary components of γ execute undamped harmonic oscillations which are a linear combination of modes with frequencies a and $\dot{\varphi}$.

Since the real and imaginary components of γ are given directly by the sun tracker output signals, some authors express the control system format in these terms.*

*Cf. Ref. 16

"The aeronautical and space activities of the United States shall be conducted so as to contribute . . . to the expansion of human knowledge of phenomena in the atmosphere and space. The Administration shall provide for the widest practicable and appropriate dissemination of information concerning its activities and the results thereof."

—NATIONAL AERONAUTICS AND SPACE ACT OF 1958

NASA SCIENTIFIC AND TECHNICAL PUBLICATIONS

TECHNICAL REPORTS: Scientific and technical information considered important, complete, and a lasting contribution to existing knowledge.

TECHNICAL NOTES: Information less broad in scope but nevertheless of importance as a contribution to existing knowledge.

TECHNICAL MEMORANDUMS: Information receiving limited distribution because of preliminary data, security classification, or other reasons.

CONTRACTOR REPORTS: Scientific and technical information generated under a NASA contract or grant and considered an important contribution to existing knowledge.

TECHNICAL TRANSLATIONS: Information published in a foreign language considered to merit NASA distribution in English.

SPECIAL PUBLICATIONS: Information derived from or of value to NASA activities. Publications include conference proceedings, monographs, data compilations, handbooks, sourcebooks, and special bibliographies.

TECHNOLOGY UTILIZATION PUBLICATIONS: Information on technology used by NASA that may be of particular interest in commercial and other non-aerospace applications. Publications include Tech Briefs, Technology Utilization Reports and Notes, and Technology Surveys.

Details on the availability of these publications may be obtained from:

SCIENTIFIC AND TECHNICAL INFORMATION DIVISION

NATIONAL AERONAUTICS AND SPACE ADMINISTRATION

Washington, D.C. 20546